AD-A106 417 TORONTO UNIV DOWNSVIEW (ONTARIO) INST FOR AEROSPACE --ETC F/G 14/2
BEYOND THREE DECADES OF CONTINUOUS RESEARCH AT UTIAS ON SHOCK T--ETC(U)
JUL 81 I I GLASS AFOSR-77-3309
UNCLASSIFIED UTIAS-45 AFOSR-TR-81-0743 NL

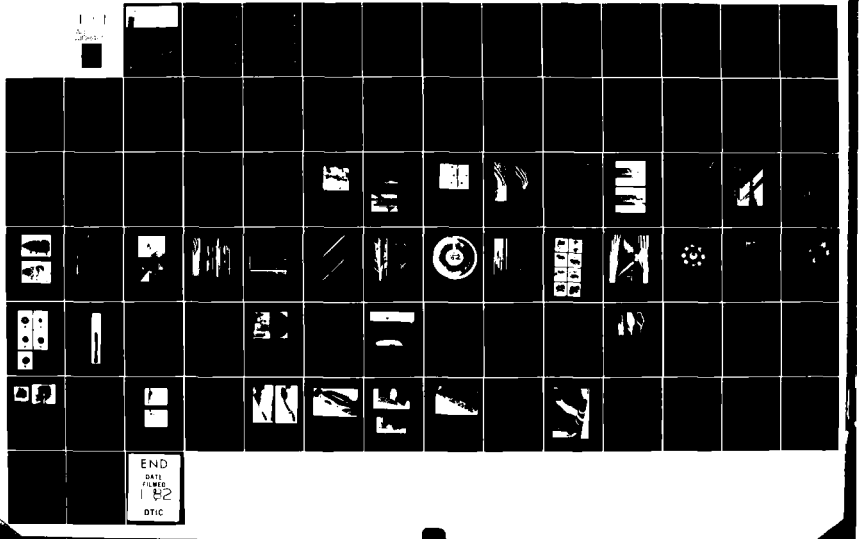

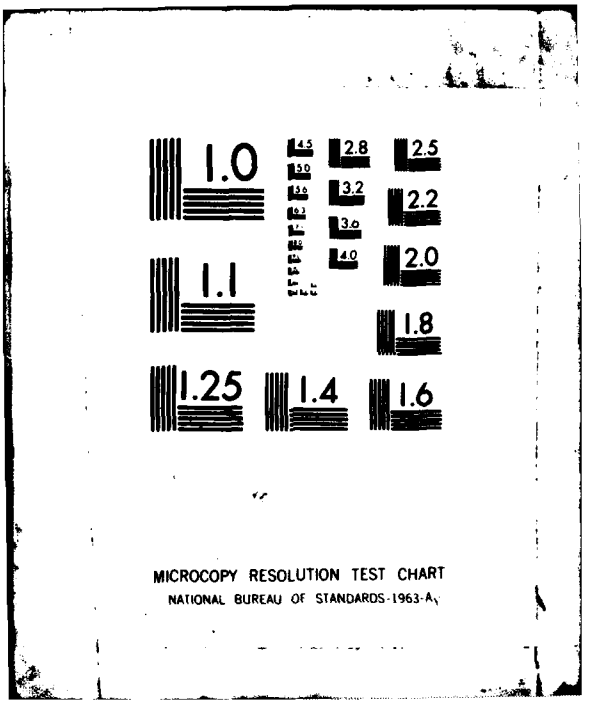
1.0
1.1
1.25
1.4
1.6
1.8
2.0
2.2
2.5
2.8
3.2
3.6
4.0
4.5
5.0
5.6
MICROCOPY RESOLUTION TEST CHART
NATIONAL BUREAU OF STANDARDS-1963-A

INSTITUTE FOR AEROSPACE STUDIES

UNIVERSITY OF TORONTO

AFOSR-TR- 81-0783

LEVEL II

BEYOND THREE DECADES OF CONTINUOUS RESEARCH AT UTIAS ON SHOCK TUBES AND WAVES

AFOSR-77-3303

(12)

by

I. I. Glass

(12)

July, 1981

UTIAS Review No. 45
CN ISSN 0082-5247

178920

UNCLASSIFIED
SECURITY CLASSIFICATION OF THIS PAGE (When Data Entered)

REPORT DOCUMENTATION PAGE	READ INSTRUCTIONS BEFORE COMPLETING FORM
1. REPORT NUMBER: AFOSR-TR- 81 -0783	2. GOVT ACCESSION NO.: AD-A108417
3. RECIPIENT'S CATALOG NUMBER	
4. TITLE (and Subtitle): BEYOND THREE DECADES OF CONTINUOUS RESEARCH AT UTIAS ON SHOCK TUBES AND WAVES	5. TYPE OF REPORT & PERIOD COVERED: Interim
	6. PERFORMING ORG. REPORT NUMBER: UTIAS Review No. 45
7. AUTHOR(s): I. I. Glass	8. CONTRACT OR GRANT NUMBER(s): AFOSR 77-3303
9. PERFORMING ORGANIZATION NAME AND ADDRESS: University of Toronto, Institute for Aerospace Studies, 4925 Dufferin St., Downsview, Ontario, Canada, M3H 5T6	10. PROGRAM ELEMENT, PROJECT, TASK AREA & WORK UNIT NUMBERS: 61102F 2307/A1
11. CONTROLLING OFFICE NAME AND ADDRESS: Air Force Office of Scientific Research/NA Bldg. 410, Bolling Air Force Base, DC 20332	12. REPORT DATE: July, 1981
	13. NUMBER OF PAGES: Approx. 65
14. MONITORING AGENCY NAME & ADDRESS(if different from Controlling Office)	15. SECURITY CLASS. (of this report): UNCLASSIFIED
	15a. DECLASSIFICATION/DOWNGRADING SCHEDULE

16. DISTRIBUTION STATEMENT (of this Report)

Approved for public release; distribution unlimited.

17. DISTRIBUTION STATEMENT (of the abstract entered in Block 20, if different from Report)

18. SUPPLEMENTARY NOTES

19. KEY WORDS (Continue on reverse side if necessary and identify by block number)

1. Shock tubes
2. Shock-wave dynamics
3. Implosion dynamics
4. Hypervelocity launchers
5. Rarefaction waves
6. Condensation and nucleation
7. Wave interactions
8. Ionizing shock-wave structure and boundary layers
9. Sonic-boom effects

Continued on reverse

20. ABSTRACT (Continue on reverse side if necessary and identify by block number)

Analytical and experimental research on nonstationary shock waves, rarefaction waves and contact surfaces has been conducted continuously at UTIAS since its inception in 1948. Some unique facilities were used to study the properties of planar, cylindrical and spherical shock waves and their interactions. Investigations were also performed on shock-wave structure and boundary layers

cont'd

Continued on reverse

DD FORM 1 JAN 73 1473 EDITION OF 1 NOV 65 IS OBSOLETE

UNCLASSIFIED
SECURITY CLASSIFICATION OF THIS PAGE (When Data Entered)

19. Key words - continued.

10. Oblique-shock-wave reflections
11. Shock waves in dusty gases
12. Thermonuclear fusion
13. Numerical methods
14. Optical techniques

20. Abstract - continued.

in ionizing argon, water-vapour condensation in rarefaction waves, magneto-gasdynamic flows, and the regions of regular and various types of Mach reflections of oblique shock waves. Explosively-driven implosions have been employed as drivers for projectile launchers and shock tubes, and as a means of producing industrial-type diamonds from graphite, and fusion plasmas in deuterium. The effects of sonic-boom on humans, animals and structures have also formed an important part of the investigations. More recently, interest has focussed on shock waves in dusty gases, the viscous and vibrational structure of weak spherical blast waves in air, and oblique shock-wave reflections. In all of these studies instrumentation and computational methods have played a very important role. A brief survey of this work is given with some perspectives on future research.

A

Qualified requestors may obtain additional copies from the Defense Documentation Center, all others should apply to the National Technical Information Service.

Conditions of Reproduction:

Reproduction, translation, publication, use and disposal in whole or in part by or for the United States Government is permitted.

Approved for public release; distribution unlimited.

AIR FORCE OFFICE OF SCIENTIFIC RESEARCH (AFSC)
NOTICE OF TRANSMITTAL TO DDC
This technical report has been reviewed and is
approved for public release IAW AFR 190-12.
Distribution is unlimited.
MATTHEW J. KERPER
Chief, Technical Information Division

BEYOND THREE DECADES OF CONTINUOUS RESEARCH AT UTIAS

ON SHOCK TUBES AND WAVES

by

I. I. Glass

This is the Paul Vieille Lecture presented at the
13th International Symposium on Shock Tubes and Waves
July 6-9, 1981
Niagara Falls, U.S.A.

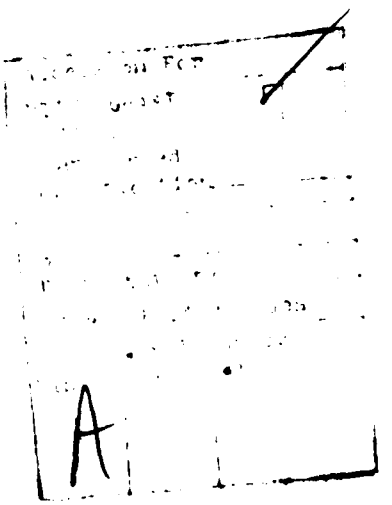

July, 1981

UTIAS Review No. 45
CN ISSN 0082-5247

Acknowledgements

This paper is dedicated to my students and colleagues everywhere who have made it all possible. In particular, I thank Dr. J. J. Gottlieb and Dr. J. P. Sislian for reading the manuscript, and their helpful discussions.

I am grateful to the Executive Committee for the honour of choosing me as the Paul Vieille Lecturer. This lecture was initiated when I was Chairman of the Seventh Symposium, Toronto, 1969. It is gratifying to see it established now as a tradition in memory of the first known researcher on shock tubes and waves, whose paper appeared in Comptes Rendus in 1899 (and in the original and translation in the Proceedings of the Seventh Symposium).

The financial support received over the years from many Canadian (DRB, NRC, NSERC, EMR) and U.S. (AFOSR, NASA, ONR, ARO) government agencies and Canadian (AC, P&W) industry is acknowledged with thanks.

Summary

Analytical and experimental research on nonstationary shock waves, rarefaction waves and contact surfaces has been conducted continuously at UTIAS since its inception in 1948. Some unique facilities were used to study the properties of planar, cylindrical and spherical shock waves and their interactions. Investigations were also performed on shock-wave structure and boundary layers in ionizing argon, water-vapour condensation in rarefaction waves, magnetogasdynamic flows, and the regions of regular and various types of Mach reflections of oblique shock waves. Explosively-driven implosions have been employed as drivers for projectile launchers and shock tubes, and as a means of producing industrial-type diamonds from graphite, and fusion plasmas in deuterium. The effects of sonic-boom on humans, animals and structures have also formed an important part of the investigations. More recently, interest has focussed on shock waves in dusty gases, the viscous and vibrational structure of weak spherical blast waves in air, and oblique shock-wave reflections. In all of these studies instrumentation and computational methods have played a very important role. A brief survey of this work is given with some perspectives on future research.

CONTENTS

		Page
	Acknowledgements	ii
	Summary	iii
1.	INTRODUCTION	1
2.	THE FIRST DECADE, 1948-1958	1
3.	THE SECOND DECADE, 1958-1968	4
4.	THE THIRD DECADE, 1968-1978	7
5.	THE FOURTH DECADE, 1978-	10
6.	CONCLUSIONS	12
	REFERENCES	13
	FIGURES	

1. INTRODUCTION

The actual research on shock tubes and supersonic wind tunnels was initiated by Dr. G. N. Patterson when he envisioned and planned the then Institute of Aerophysics in 1948, even though it was not actually available until 1949, and opened officially in 1950 [1]. He became its Founder and first Director. His first three students in the shock-tube field, Bitondo [2,3,4], Glass [3,5] and Lobb [2,6,7], were initially guided by his analysis of shock-tube flows [8] for the design of their facilities and appropriate experiments.

Since this survey is confined to nonstationary flows, it will not be possible to include references to many other gasdynamic flows which were studied then and subsequently throughout the decades by members of the staff and students alike. Dr. Patterson's interests later centred on kinetic theory [9,10], and when I obtained my Ph.D. in 1950, I assumed responsibility for research and development in nonstationary flows. The present survey then deals with the analytical, numerical and experimental studies in this field from 1948 until the present day.

It should be noted at the outset that this survey is not meant to be exhaustive as far as references are concerned or in the details of the various researches. Here and there a reference from sources other than UTIAS will be called up to assist the reader. Consequently, I hope that many authors will forgive me if their names do not appear and the readers for the brevity of this presentation. The choice had to be arbitrary in order to fit the limitations of this review.

2. THE FIRST DECADE, 1948-1958

Analytical and experimental work in this decade centred mainly on one-dimensional flows in shock tubes induced by shock waves and rarefaction waves. The various interactions of these waves as well as those with contact surfaces were also of considerable interest. As shown in Figs. 1 to 4, it was soon realized that the diaphragm breaking process was far from ideal [2,7,11]. This had a serious effect on the flow quality behind the contact region (Figs. 1-4), which originated in the driver section of the shock tube, and was disturbed and made turbulent by the remaining jagged edges of the diaphragm. Consequently, the predicted high Mach number in this cold gas was not achieved [6,12]. On the other hand, the flow Mach number in the region compressed by the shock wave in the channel was in quite satisfactory agreement with analysis at the lower shock strengths [7,12].

As for the velocity of the shock wave, it was soon found that it attenuated [11,12,13] with distance from the diaphragm, increasing shock Mach number, and lowered channel pressures for a given shock-tube cross-section (Fig. 5). The attenuation increased with decreasing cross-sectional area. Some early analyses [14,15,16] showed that the sidewall boundary layers (Fig. 6) induced by the shock wave and rarefaction wave were responsible for the shock-wave attenuation. In addition, the boundary layer caused the contact surface to accelerate [11] (Fig. 7) so that the testing time in the hot region was limited and it was not possible to increase it by going to a

longer channel, as inviscid analysis predicted. This situation also caused flow gradients in the hot region, which meant that gasdynamicists, physicists and chemists had to take these deviations into account in analysing their test results for perfect and imperfect gases with vibrational, dissociational or ionizational excitations.

Subsequently, the shock tube became one of the most versatile and economical test facilities for universities, government, and commercial institutions alike. It soon evolved into several hybrids of shock tunnels, expansion tubes and multidiaphragm shock tubes designed to provide high-stagnation temperature and high-Mach number test conditions useful for re-entry heat-shield design of space capsules which were then under development.

At UTIAS however, some emphasis was placed on wave interactions such as the refraction of a shock wave at a contact surface [3,4,17] and through a gas layer (Fig. 8). This work also showed that a shock wave may be tailored through refraction such that only a Mach wave is reflected from the contact surface. This idea led to the reflected shock wave, tailored-interface, shock-tunnel operation, thereby providing a constant-pressure high-enthalpy reservoir of gas for expansion through supersonic or hypersonic nozzles [18,19] (Fig. 9). It was also surmised that a layer of gas, such as hydrogen or helium, might provide a protective barrier for attenuating blast waves. However, it was soon noted that the subsequent overtaking of the transmitted shock wave by the refracted shock wave would quickly diminish the attenuation [17,20] and increase the pressure ratio across the transmitted wave to nearly the original shock strength incident on the layer of helium.

It is worth noting that the overtaking of two shock waves provides the ideal shock-tube problem after their interaction, that is, a shock wave and a centred rarefaction wave which are separated by a perfect contact surface (Fig. 8). A near-perfect shock-tube problem can also appear at the refraction of a shock wave at an air/helium interface, as shown in Fig. 8, with a very well defined centred rarefaction wave. Breaking a diaphragm in a shock tube does not produce a centred wave. The tail of the wave is usually obscured in schlieren or shadow photographs, showing that sharp gradients are absent (Fig. 2). However, the head of the wave is always visible and provides a gasdynamic means of measuring very accurately the speed of sound in gases [21a]. It is worth noting that only the equilibrium sound speeds were measured from the first characteristic line, even in CO_2-carbon dioxide [21b], and SF_6-sulfurhexafluoride [21c], as it was not possible to produce an ideal centred wave where the frozen precursor might have been observed [see 52a] near the origin.

Additional interactions were studied, such as the head-on collision of shock waves [22] and of shock and rarefaction waves [22,23]. In the former case, again a perfect contact surface is formed (Fig. 10). The head-on collision of two shock waves also provides a means of studying reflected shock waves without wall-effects by using two shock waves of equal strength. Very high temperatures with real-gas effects can be obtained in this manner. If a wall is used for reflection, the tailored-interface technique mentioned above can be used to provide a gas with very high escape speed, which is also useful for molecular-beam studies.

One-dimensional refractions of rarefaction waves at contact surfaces [24,25] were also investigated analytically and experimentally using hot-wire anemometry and piezo-pressure gauges. This study showed that rarefaction-wave profiles did not agree with one-dimensional theory and were very much weaker than predicted for a given diaphragm pressure ratio, especially for stronger waves [25]. The so-called Riemann invariants were also not satisfied [12]. Nevertheless, the rarefaction waves as produced agreed reasonably well with the refraction analysis. It can be stated that the various one-dimensional wave interactions studied analytically were verified by experiment. However, in the case of strong shock waves, real-gas effects had to be considered to improve the agreement with analysis [22,12].

With the construction of a 23-cm diameter field of view Mach-Zehnder interferometer [26], many worthwhile problems could now be investigated where quantitative density distributions were important for an understanding of the flows involved. This made it possible to study the transition through a contact front developed in a supersonic nozzle [27]. It was shown that it had a density profile resembling a shock-wave transition. The spiral vortex [28] produced by the diffraction of a plane shock wave over a sharp plate was another interesting problem for optical study (Fig. 11), especially with the interferometer. It has since been investigated by other researchers in greater detail. The interactions of plane shock waves with plane wire screens [29] and plane and oblique perforated plates [30,31] was also a fruitful area of interest (Figs. 12-14). Transmitted and reflected shock waves were formed which were separated by the screen or plate and a contact region. If the flow through the screen or plate was choked then a second, upstream-facing, shock wave was formed near the screen or plate similar to the flow development in a nozzle (Fig. 9). Since the screen or perforated plate produces a new transmitted shock wave and contact region, it is possible to obtain density and pressure measurements behind the new shock wave from measurements of the shock speed and contact surface speed in the (x,t)-plane, using a rotating drum camera. This method is useful for perfect gases. However, for real gases, neither the pressure nor particle velocity is very sensitive to changes in initial pressure for a given shock speed. Consequently, this is not a precise method of measuring real-gas properties behind strong shock waves. There is little doubt that direct measurements of pressure, density and temperature are required in such cases.

The interaction of a plane strong shock wave with a steady magnetic field [32] is not unlike the interaction with a wire screen. If argon is used as the test gas for example, then it ionizes and the axial components of the ponderamotive force produced on the gas when it interacts with the magnetic field also gives rise to a transmitted and reflected shock separated by a contact surface. A secondary upstream-facing rarefaction wave can also occur. The wave systems are limited by the initial conditions such that all waves may not always occur. A current flow is also produced at right angles to the flow velocity and magnetic field vectors. In essence, this is the principle of all magnetogasdynamic electric-power generators.

It is also worth noting that some theoretical work on various aspects of the collision and penetration of two rarefaction waves [33], and the overtaking of shock waves by rarefaction waves [34], and vice versa [35],

was also completed. Although these are interesting problems, they were not investigated experimentally. In the case of the overtaking problems, simplifying assumptions were made by neglecting secondary characteristics resulting from the interaction. This would limit the analyses to weak rarefaction waves.

It may be concluded that the studies of diaphragm rupture, the actual wave system in a shock tube, the effects of sidewall boundary layers, various types of wave interactions or shock-wave collisions with screens, perforated plates or magnetic fields have taught us a great deal about one-dimensional nonstationary flows in shock tubes. The agreement with analyses has been quite satisfactory by and large. Researchers using such facilities can apply corrections to deviating flows, whether they be due to inviscid, viscous, or real-gas effects. However, there are still untested analyses that require experimental verification. In addition, there are unanswered questions about actual flows in rarefaction waves, in the cold-flow region, and the entire flow profiles from the head of the rarefaction wave to the shock wave as functions of time. Undoubtedly numerical methods could help in answering some of these questions supported by better experimental data. However, researchers probably have more interesting, pressing and challenging current problems to solve and would not be interested in the academic resolutions of old problems; yet this is not always the case, as some recent references indicate. A few examples will be of interest, such as the use of the shock tube for transonic-flow testing of airfoils at high Reynolds numbers [36], the collision of shock waves with screens and honeycombs [37], inviscid-flow and viscous boundary-layer interactions [38], and properties of rarefaction waves and compression waves [39a] and their induced boundary-layer flows [39b]. Many additional examples can be found in journals and Proceedings of the recent Shock Tube Symposia.

3. THE SECOND DECADE, 1958-1968

This period is marked by the extension of the investigations to spherical and cylindrical-shock and blast-wave phenomena in gases and underwater. (It should be noted that a fairly complete picture of what was known during this period about planar flows was summarized in the portion of the Handbook of Supersonic Aerodynamics on Shock Tubes [12], which was published in 1959. It soon became out of print. However, photocopies were to be found in many laboratories worldwide and to this day, for example, on a visit to China in 1980, it was ironic to hear it considered as the "bible" for shock-tube research — the term being used by older researchers trained in the West.) Rather simple-type glass diaphragms were utilized for this purpose. Nevertheless, the glass spheres had to be blown carefully by an expert glass blower. The cylindrical diaphragms had optical quality glass discs welded to both ends. The assembly was held between two glass plates to ensure cylindrical flow without end-effects [40].

Our first venture was to study the wave system generated by an exploding pressurized glass sphere [41]. It proved to be a very fruitful avenue of research. Wave-speed schlieren records of the radius-time (r,t)-plane (Fig. 15) soon showed some remarkable differences with planar shock-tube

flows and also similarities. The glass diaphragm-breaking process was similar to that of other diaphragm materials used in a shock tube. Namely, the high-pressure driver-gas was made eddying and turbulent by the glass fragments. Nevertheless, the blast wave soon became spherically symmetrical despite the protuberances in the contact front (Fig. 16). As predicted by analysis [42,43] the shock wave and the contact front decelerated and the rarefaction wave head moved at the constant sound speed. In addition, it was clearly shown, for the first time, how the second shock wave, formed at the tail of the rarefaction wave imploded on the origin and reflected. Although the reflected implosion could be seen as a second shock following the main blast wave after the contact front in chemical explosions, the implosion phase was always obscured by the dense gases. Similar results were obtained for cylindrical explosions [44] (Fig. 17).

Additional interesting applications involved the collision of spherical shock waves (Figs. 18,19) [45] and underwater explosions (Fig. 20). Unfortunately, glass diaphragms have a limited pressure range in which they can be broken. Consequently, it was not possible to study the spherical shock-wave collision problem experimentally over an adequate range. The underwater explosions were more successful from an analytical viewpoint. It was necessary to solve the hydrodynamic shock-tube problem [46] in order to apply the appropriate boundary conditions at the moment of rupture and then continue with the analysis. The agreement of the experiments with this analysis was very satisfactory [47].

Simultaneous with the foregoing studies, the groundwork was being laid for a number of important analytical and experimental investigations. The concept of using explosive-driven implosions as drivers for shock tubes and hypervelocity projectile launchers was taking shape [48-50]. Some of the analytical work was also being done during this period on the nonequilibrium expansion flows of dissociating and ionizing argon around a sharp corner [51,52]. This was in preparation for conducting several investigations on real-gas effects in the very excellent new shock-tube facility designed, instrumented and tested for this purpose [53]. Concurrently, investigations were performed on magnetohydrodynamic flow in the boundary layer of a shock tube [54]; in a hypersonic shock-tunnel test-section (generously donated by the Cornell Aeronautical Laboratory, Buffalo) which was coupled to an existing UTIAS shock tube [55,56]; and an initial ionization process in strong shock waves produced in hydrogen and helium in a unique electromagnetic-driven implosion shock tube [57].

It is of interest to look at some of the above projects in more detail. The explosive-driven-implosion research and development is of particular importance as it has continued until the present day. It was not only necessary to understand the spherical combustion and detonation processes [50], but also to develop a means of instantly and simultaneously detonating an explosive hemispherical shell in a safe and reusable facility. Some consultation with U.S. and Canadian explosive-research laboratories made it clear that the current thinking was that it was not possible to detonate a solid explosive with a gaseous detonation wave. However, we felt that not enough was known then (nor is it known now) about the physical processes involved in the microsecond regime during the initiation of a solid explosive and therefore the advice from experts was put aside. A small one-dimensional

facility was built to test the initiation of solid explosives by gaseous detonation waves [58]. Many explosives were tried (including some dangerous ones, like lead azide; I am grateful to Dr. R. E. Duff for persuading me by telephone to immediately desist from using such unpredictable and hazardous materials) and PETN was found to be an excellent safe secondary-explosive to be used for making hemispherical shells of explosives to be detonated by the gaseous detonation wave in stoichiometric hydrogen-oxygen mixtures in the reusable hemispherical driver [59]. The implosion on reflection at the geometric centre produced a hot high-pressure plasma useful for driving projectiles, intense shock waves, the creation of diamonds from graphite and producing fusion plasmas in deuterium. This work will be discussed subsequently in more detail.

The explosive-driven implosion chamber used as a driver for projectiles and shock tubes is shown in Fig. 21. A great deal of analytical, design and experimental work was done to predict and verify its performance [60-65]. Although plans were made to build a much larger launcher (from a 5 mm barrel to a 25 mm barrel; from a 100-mm radius hemispherical cavity to a 300-mm radius cavity; from a few hundred-gram PETN-shell to one of many kilograms), it was soon found on the smaller-scale model that there were no projectile materials available that could withstand the enormous plasma base pressures and temperatures developed after reflection of an implosion. Consequently, even though very high velocities (20 km/s) were predicted analytically, no more than 5.4 km/s was actually obtained for an 8-mm dia lexan projectile weighing 0.36 g [66]. It is possible that such problems would not have existed on the *projected full-scale* launcher. Nevertheless, the very high cost of producing such a large facility, coupled with several uncertainties such as projectile integrity, the large amounts of explosive to be used, consistent focussing of the implosions and safety aspects associated with a facility of this size discouraged its construction.

It is also worth noting that an alternative scheme for producing explosive-driven implosions was tried by directly initiating a 5-mm thick sheet explosive hemispherical shell by using 91 explosive detonators. This meant that all detonators had to fire within a jitter of two or three microseconds — a formidable task. The method did not prove successful and had to be abandoned [67].

In order to prepare for the interferometric studies of nonequilibrium corner-expansion flows of dissociating oxygen and nitrogen, as well as ionizing argon, it became necessary to determine the refractivities of the component gases in the mixtures [68-70]. This was done successfully with considerable accuracy in the 10 cm x 18 cm hypervelocity shock tube by means of the 23-cm dia Mach-Zehnder interferometer. Additional analytical work was also done on such flows with coupled vibrational-dissociational nonequilibrium [71]. An initial investigation on dissociating-oxygen corner-flow did not prove to be definitive in its comparison with analysis [72] and therefore would require additional study.

Some preliminary research was also done on oblique shock-wave reflections at a sharp compressive corner and shock-wave diffraction over a sharp expansive corner [73]. In subsequent years this area of investigation was to lead to some important studies with significant results.

Interest was also aroused by the possibility of flying a micrometeoroid-impact gauge designed by NASA on one of NASA's or Canada's rocket experiments. This area of research was at that time of much importance. The safety of astronauts and spacecraft under bombardment from micrometeoroid particles travelling at the escape velocity from earth (11 km/s) up to the escape velocity from the solar system (73 km/s) was still an unsettled question. The gauge was calibrated by dropping glass microspheres under gravity and in a shock-tube flow [74] seeded with the same glass spheres as well as one micron particles charged electrostatically [75] and accelerated to 7 km/s at the NASA Goddard Space Flight Center. This gauge was not flown on one of the rocket experiments owing to lack of funds and personnel.

4. THE THIRD DECADE, 1968-1978

This decade is marked by efforts to experimentally observe (Fig. 22) and measure actual and physical properties [76] of the focus of combustion and explosive-driven implosions and to compare them with analytical predictions [77]. Temperatures were measured spectroscopically for combustion runs only [76], and projectile base-pressures were inferred from microwave measurements of the projectile velocity in the launcher barrel [78]. Spectroscopic temperature and pressure measurements [79,80] were reasonably successful and were improved on subsequently.

An important step was taken to apply the explosive-driven implosions as drivers for shock tubes [81]. A 25-mm shock-tube channel was used instead of a launcher barrel [82]. This proved to be a very worthwhile method of producing very strong shock waves (20 km/s) in air [83] (Fig. 23). It also led to the explanation of some anomalous radiation effects in the shock fronts [84] (Fig. 24), which until then defied a reasonably physical interpretation. One of the reviewers of our paper in complimenting our work noted that this proper explanation had waited for several years and urged us to change our research note to a full paper. Although this was a very useful driver, far more impressive electrical drivers were developed at JPL [85] and NASA Ames [86]. This made it possible to obtain at JPL shock-wave velocities of 45 km/s, with little attenuation in a 15 cm dia channel with a 4-μs test-time. Concurrently, an explosive (Voitenko) driver developed at NASA Ames [87], using 30 kg of explosive (about 300-fold greater than the explosive-driven implosion shock tube at UTIAS) yielded velocities of 70-67 km/s in a 3 cm x 3.1-m long glass tube over a distance of 1 meter in one of the runs (about 3-fold greater than at UTIAS). These experiments had to be done at the Lawrence Radiation Laboratory explosive test site, where the facility was destroyed after each run (except for the instrumentation). This is probably the highest shock-wave velocity obtained, with a modest attenuation, and some test time useful for Jovian entry studies. It should be noted that all of these facilities used very low (0.05 torr $\sim$ 2 torr) channel gas pressures.

Another very important application of the UTIAS Explosive-Driven Implosion Driver was in the production of synthetic diamonds grom graphite. By placing graphite in a steel capsule and exposing it to a focussed-implosion and its reflection, thereby generating enormous pressures (megabar range) and temperatures (millions of degrees), the attenuated transmitted shock-wave

pressures and temperatures were sufficient to create the phase transition. Industrial-type diamonds of 10-20 μm were produced with a yield of about 5-10% of the original graphite [88]. Although such diamonds had been produced statically and dynamically before, this technique was quite novel and promising for the manufacture of new materials and in the application to problems in solid-state physics.

The process was transferred to 3M Canada Ltd., as it was felt that it could best be developed by an industrial firm with much experience in related areas. As a result a fairly large group was set up by 3M at UTIAS to further develop and extend the work on the production of industrial diamonds. The success of this initial work (diamonds were produced in the first experiment) [88], led to the concept of using the explosive-driven implosions to produce fusion plasmas and neutrons from deuterium-deuterium reactions. Further consideration will be given to the implosion research in the final section.

This period was also productive in analytical and experimental studies of ionizing-argon flows. Definitive interferometric investigations were made of the shock structure of ionizing argon and krypton at nominal shock Mach numbers of 13 and 16 [70,89,90]. It was found that the shock wave developed nonstationary oscillations (Fig. 25) at the higher Mach numbers (> 14). The oscillations were easily removed by adding small amounts of hydrogen ($\sim$ 0.5% of the initial pressure), with the consequent reduction of the overall transition length to about one-third of its pure-gas value. The total plasma density and electron density profiles for pure argon (Fig. 26) and with small amounts of hydrogen added as an impurity, agreed well with analysis. Two questions remain unanswered to this day: precisely why only a hydrogen impurity removes the oscillations and why the electron cascade-front, where equilibrium ionization occurs moves towards the translational front as it approached the wall (Fig. 27). Some analytical work has recently appeared, which attempts to explain this phenomenon [91].

At the same time the laminar shock-tube wall-boundary layer (Fig. 28) and the flat-plate boundary-layer flow (Fig. 29) in the quasi-steady region was studied in ionizing argon analytically and interferometrically for the same shock Mach numbers as the shock structure [92-95]. (It is worth noting that a wall-boundary-layer study at low shock Mach numbers in air had been done many years earlier [96] using the same Mach-Zehnder interferometer with a smaller rectangular shock tube.) It was shown that the wall boundary layer had a profound effect on the shock structure. The smaller the tube hydraulic-diameter the thinner was the shock structure (Fig. 30). This result is of importance when comparing experimentally-measured shock structure with analysis. The properties of both types of boundary layers were compared analytically and experimentally. There certainly are differences between them. A difficulty with any experimental technique is to probe the boundary layer near the wall. Nevertheless, total plasma density and electron-number densities were obtained up to 0.1 mm from the wall. The shock-structure wall-boundary-layer interaction did not appear to affect the flat-plate boundary layer too much at lower shock Mach numbers ($\sim$ 13). However at higher Mach numbers ($\sim$ 16) radiation losses induced nonuniformities at a given test-section station [45]. Additional analysis should be done on this aspect of the investigation.

Another important area of ionizing-argon flows was the investigation of a quasi-steady corner-expansion [97]. The results agreed reasonably well with an earlier analysis [52c], which was later extended to include radiation losses [98]. Apparently, radiation losses were not too important at the lower shock Mach numbers (where the experimental data was obtained) to affect the corner-expansion. As noted earlier, at higher shock Mach numbers, radiation effects are quite significant and would affect such flows. Further analytical work should be done to settle this question.

A number of analytical and experimental investigations were started on condensation of water vapour cooled by nonstationary rarefaction waves in a shock tube [99-101]. Although the initial work was started in the Fifties in order to see if indeed condensation shock waves do appear in rarefaction waves (Fig. 31), it was not until the Seventies that it was shown analytically (using the method of characteristics) that such waves must occur as a result of the release of the latent heat of condensation [99]. The experimental pressure profiles [101] could be explained on either the analytical basis of homogeneous [99] or heterogeneous [100] nucleation. Which model is correct will have to await a future experimental decision. Unfortunately, this interesting work had to be terminated owing to insufficient financial support. It is also worth noting that in the Seventies a number of excellent facilities such as the wave-interaction tube [11], the shock sphere [40] and a new hypersonic shock tunnel [102] had to be abandoned owing to lack of funding in these areas of research.

This period also saw a continuation of the research on oblique shock-wave reflections, which culminated in some significant results. The work initially dealt with a number of considerations of real-gas effects [103]. It was later extended to solve once and for all the problem of: given a sharp compressive corner of angle θ_w in a shock-tube channel at specified initial conditions, what type of reflection will occur when it is hit by a plane shock wave at a specified Mach number M_s? Investigators from a number of countries had tackled this problem since the Forties with only partial success. It was finally solved and verified interferometrically at UTIAS for diatomic [104] and monatomic gases [105]. It was shown that in the (M_s, θ_w)-plane four types of reflections (regular, single Mach, complex Mach and double Mach) can occur. The regions and their transition boundaries were determined analytically for perfect and imperfect gases including the effects of equilibrium vibration, dissociation and ionization. Recently, it was found that our interferometric results and the optical data from many other researchers agree best with a perfect-gas analysis as far as the various regions and their transition boundaries are concerned. However, real-gas effects become important immediately after the viscous shock waves. Consequently, some areas bounded by the incident, reflected and Mach-stem shock waves may be in nonequilibrium or may achieve equilibrium depending on the various relaxation times. Therefore, in analysing the flows, real-gas effects must be considered.

The experimental lines of constant-density (isopycnics) (Fig. 32) showed that despite the many developments in computational methods, all were not capable of accurately predicting the isopycnics of such nonstationary flows [106]. This is now being addressed by a number of computational centres with increasing accuracy [107,108]. Numerical data can now be compared with the available interferometric data for monatomic, diatomic [104-106] and triatomic [125] gases.

It can be expected that more novel and accurate computational methods will evolve in the near future. Such results would be of much assistance to the experimenter in interpreting his optical data not only in the laboratory but in field trials of spherical blast waves. Numerical time-dependent solutions for such problems are yet to be achieved. Once computer codes are verified experimentally, they can produce far more data on physical quantities than it is possible to measure.

In the late Sixties the supersonic transport (SST) became controversial for a number of reasons. Their possible injurious effects on humans, animals and structures were important considerations for Canada, if overflight laws were to be enacted based on facts. Therefore, a number of Canadian establishments and the University of Toronto contributed to the construction of two simulators: a travelling-wave sonic-boom facility and a loudspeaker-driven booth [109]. A great deal of research was conducted in the areas of psychoacoustics, human response, effects on animals, structural response and gas-dynamic analyses [110-117]. Basically, no effects on humans when subjected to sonic booms similar to SST's were observed as far as heart rate changes, temporary threshold shifts and while driving an arduous automobile course. The structural effects on "aged" panels also were found to be negligible. However, small animals like mice, guinea pigs, chinchillas and Rhesus monkeys did tend to suffer physical damage at the basal turn of the cochlea in the form of bleeding which was absorbed in time (or destroyed hair cells). Sonic-boom rise-time, overpressure-amplitude and frequency of exposure were all important factors affecting the bleeding. However, the scaling laws from small animals to humans are unknown. Nevertheless, caution should be exercised against excessive exposure to superbooms.

Since human-startle effects increase with decreasing sonic-boom rise-time [118], the question arose why actual sonic booms produced by SST's can be 100 to 1000-fold greater than predicted by planar shock wave analysis. Atmospheric turbulence [119], temperature gradients near the ground, microphone-response limitations and vibrational excitation [120] of the oxygen and nitrogen components of air were all blamed. Consequently, this problem was investigated experimentally using exploding sparks and wires [121]. It now appears that vibrational excitation of oxygen can give rise to extended shock-wave transitions at low overpressures (about one-tenth the usual sonic-boom value of 100 Pascals). Small-scale turbulence would not be significant. However, large eddies of the size of the aircraft might well give rise to rounded booms with large rise-times or spiked booms with short rise-times. Both types are observed during any overflight past an array of microphones at different altitudes or on the ground.

5. THE FOURTH DECADE, 1978-

Some of the problems discussed in the previous section are being continued and extended. New research is being initiated and conducted in new or forthcoming facilities. The following research areas are being pursued at the present time: implosion-wave dynamics, oblique shock-wave reflections, sonic-boom effects and the new areas of turbulent, swirling, combusting flows (although this does not deal with shock-tube flows, it deserves to be mentioned) and shock waves in dusty gases.

Three aspects of implosion-wave dynamics are of importance at this time. The spectroscopic measurements of temperature at an implosion focus, which is produced by combustion or with explosives, and the application of the Random-Choice Method [122] to analyse the experimental results. This topic will be presented as a separate paper at this symposium [123]. Consequently, it will not be dealt with here. The application of explosive-driven implosions to the production of industrial diamonds and other new materials is very active. An improved facility has been built for this purpose which eliminates a good deal of physical labour through mechanization (Fig. 33). The horizontal position of the flat face of the hemisphere during a run has greatly improved the frequency of excellent focussing. The measurement of physical quantities using manganin-wire pressure gauges, X-ray diffraction, electron diffraction and photomicrographs have all proved to be very useful (Fig. 34). A model is being developed to explain how dynamic transitions from graphite to diamond can take place in the submicrosecond regime [124]. Additional solid-state problems will be investigated in the oncoming years.

The use of explosive-driven implosions to produce fusion has not been easy mainly due to lack of financial support and trained personnel. Nevertheless, neutrons and γ-rays have been generated from D-D reactions at the focus in runs of 54-atm stoichiometric deuterium-oxygen ($2D_2 + O_2$) and about 100-g PETN explosive-shells (Fig. 35). Similar results have also been obtained by placing a small hemispherical capsule containing 1.2 atm of pure deuterium covered by a metal diaphragm at the implosion focus (similar to a Voitenko compressor [87]). Experts in the field were skeptical if we would obtain neutrons with so little explosive energy. Our prospects for improving this work and to measure the neutron flux and other radiation properties are not good without adequate financial support. Yet, our ideas have proved to be sound and they await further developments.

The research on oblique shock-wave reflections in monatomic and diatomic gases has been successfully applied to a triatomic gas such as carbon-dioxide [125], which is already substantially excited at room temperature. Yet, the numerous experiments all agree with the (M_s, θ_w)-plot for a perfect gas with $\gamma = 1.29$ (Figs. 36, 37). Consequently, the shock-wave-reflection process behaves as if the specific heats were frozen in front and immediately behind the shock waves. The flow regions bounded by the shock waves will be in nonequilibrium and if the flow times are long enough equilibrium will finally be attained. The results do not fit the complete vibrational-dissociational-equilibrium model nor any other partial equilibrium model [125]. The research is being continued in air. The early dissociation of oxygen with increasing shock strength compared to nitrogen adds some interesting aspects to this problem (Fig. 38). It is, of course, of most interest to experimenters conducting spherical-blast investigations in the field.

It has now been found that some small animals suffer significant hearing impairment (in the entire range or in some part of the high-frequency range) after the blood clots in the cochlea have been absorbed. Since their hearing range far exceeds that of man (mice hear up to 100 kHz), it is at present not known whether humans also suffer losses and for how long at high frequencies (< 20 kHz) when chronically exposed to sonic booms [126]. This question will be investigated in the near future.

It now appears that the excellent N-waves produced by exploding wires may not be able to exactly simulate SST sonic booms. The Random-Choice Method has been successfully applied to solve this problem by modelling the exploding wire or spark by a blast from a small pressurized sphere. Since this method does not introduce an artificial viscosity it is possible to solve the spherical shock-wave transition. It is thinner than the equivalent plane-wave profile solved by G. I. Taylor. Since this subject is also being presented as a separate paper [127] at this Symposium no further details will be given. The work on the structural response of a wood-plaster room subjected to sonic boom and its subsequent crack-propagation properties has been completed and is being presented as a separate paper at this Symposium [128]. The agreement between pressure and strain measurements and analysis was very good. The agreement of the finite-element crack-propagation analysis and (of necessity) one decisive experiment was very satisfactory. The problem of the pressures generated in two interconnecting rooms by a sonic boom is now being investigated analytically and experimentally.

The design of thermally efficient combustors with a minimum of pollutants for jet engines and home furnaces is a very important field of research in view of our dwindling fossil fuels. Such flows are usually turbulent, swirling and chemically reacting. It is a difficult problem to model analytically [129]. In order to verify such analysis, it is important to measure the turbulence quantities of the flow. This can be done using laser-Doppler velocimetry. It can also be applied to measure fuel-droplet size and distribution. Such a facility has now been developed and will shortly be applied to verify the analytical work [129]. Hypersonic combustion is another area of interest [130-132] and will be continued if financial support is made possible.

The structure of moving shock waves in dusty air is of considerable interest. For this purpose the analysis of a dusty-gas shock tube has been completely investigated using the Random-Choice Method [133]. The nonequilibrium-flow profiles from the head of the rarefaction wave to the frozen shock wave were computed, including the shock-front and contact-front transitions (Fig. 39). Working curves were determined for frozen and equilibrium shock transitions as functions of the initial conditions, dust concentration and diaphragm-pressure ratio. The regions where only dispersed shock waves eventually occur have also been found (Fig. 40). A new 7.6 cm x 20 cm shock tube is under construction to validate the analysis and to conduct many new experiments of current interest to the researcher in the laboratory or on field trials.

6. CONCLUSIONS

This brief survey of research on shock tubes and waves at UTIAS over the past 33 years has attempted to give some insight into a unique experience. It is doubtful if any other laboratory has been engaged in this ever-changing field, continuously, over such a lengthy period. A lot of good research and development work was done in a number of specially conceived facilities. It has led to the training of many Ph.D. and Masters graduates, visiting scientists and academics. Numerous UTIAS reports and journal papers were published. The present list of references is by no means complete. Our work over the years has attempted to add to and enlarge mankind's store of scientific and engineering knowledge. The outlook for the future is bright. There are excellent young people at UTIAS to take over and continue this important work on shock tubes and waves for many years to come.

REFERENCES

1. Patterson, G. N. — Pathway to Excellence, UTIAS, 1977.

2. Bitondo, D.; Lobb, R. K. — Design and Construction of a Shock Tube. UTIA Report No, 3, 1950.

3. Bitondo, D.; Glass, I. I.; Patterson, G. N. — One-Dimensional Theory of Absorption and Amplification of a Plane Shock Wave by a Gaseous Layer. UTIA Report No. 5, 1950.

4. Bitondo, D. — Experiments on the Amplification of a Plane Shock Wave. UTIA Report No. 7, 1950.

5. Glass, I. I. — Design of a Wave-Interaction Tube. UTIA Report No. 6, 1950.

6. Lobb, R. K. — On the Length of a Shock Tube. UTIA Report No. 4, 1950.

7. Lobb, R. K. — A Study of Supersonic Flows in a Shock Tube. UTIA Report No. 8, 1950.

8. Patterson, G. N. — Theory of the Shock Tube. NOL Memo 9903, White Oak, Md., 1948.

9. Patterson, G. N. — Molecular Flow of Gases. John Wiley & Sons, New York, 1956.

10. Patterson, G. N. — Introduction to the Molecular Theory of Gas Flows. UTIAS, 1971.

11a. Glass, I. I.; Martin, W. A.; Patterson, G. N. — A Theoretical and Experimental Study of the Shock Tube. UTIAS Report No. 2, 1953.

11b. Glass, I. I.; Patterson, G. N. — A Theoretical and Experimental Study of Shock-Tube Flows. J. Aero. Sci., 22, 2, pp. 73-100, 1955.

12. Glass, I. I.; Hall, J. G. — Handbook of Supersonic Aerodynamics, Section 18, Shock Tubes. Navord Report 1488 (Vol. 6), U.S. Government Printing Office, Washington, D.C., 1959.

13. Boyer, D. W. — Effects of Kinematic Viscosity and Wave Speed on Shock Wave Attenuation. UTIA Technical Report No. 8, 1956.

14. Mirels, H. — Attenuation in a Shock Tube due to Unsteady Boundary Layer Action. NACA TN 3278, 1956.

15. Trimpi, R. L.
Cohen, N. B.
An Integral Solution to the Flat Plate Laminar Boundary Layer Flow Existing Inside and After Expansion Waves and After Shock Waves Moving into Quiescent Fluid with Particular Application to the Complete Shock Tube Flow. NACA TN 3944, 1957.

16. Mirels, H.
Braun, W. H.
Nonuniformities in Shock-Tube Flow due to Unsteady Boundary Layer Action. NACA TN 4021, 1957.

17a. Ford, C. A.
Glass, I. I.
An Experimental Study of Shock Wave Refraction. UTIA Report No. 29, 1954.

17b. Ford, C. A.
Glass, I. I.
An Experimental Study of One-Dimensional Shock Wave Refraction. J. Aero. Sci. 23, 2, pp. 189-191, 1956.

18. Parks, E. K.
Supersonic Flow in a Shock Tube of Divergent Cross-Section. UTIA Report No. 18, 1952.

19. Bull, G. V.
Starting Process in an Intermittent Wind Tunnel. UTIA Report No. 12, 1951.

20. Bull, G. V.
Fowell, L. R.
Henshaw, D. H.
The Interaction of Two Similarly Facing Shock Waves. UTIA Report No. 25, 1953.

21a. Glass, I. I.
An Experimental Determination of the Speed of Sound in Gases from the Head of a Rarefaction Wave. UTIA Report No. 9, 1951.

21b. Glass, I. I.
On the Speed of Sound in Gases. J. Aero. Sci. 19, 4, p. 286, 1951.

21c. Glass, I. I.
Hall, J. G.
Determination of the Speed of Sound in Sulfur-hexafluoride in a Shock Tube. J. Chem. Phys. 27, 5, p. 1223, 1957.

22. Gould, D. G.
The Head-On Collision of Two Shock Waves and a Shock and Rarefaction Wave in One-Dimensional Flow. UTIA Report No. 17, 1952.

23. Nicholl, C. I. H.
The Head-On Collision of Shock and Rarefaction Waves. UTIA Report No. 10, 1951.

24. Billington, I. J.
Glass, I. I.
On the One-Dimensional Refraction of a Rarefaction Wave at a Contact Surface. UTIA Report No. 31, 1955.

25. Billington, I. J.
An Experimental Study of One-Dimensional Refraction of a Rarefaction Wave at a Contact Surface. UTIAS Report No. 32, 1955.

26. Hall, J. G. — The Design and Performance of a 9 Inch Plate Mach-Zehnder Interferometer. UTIA Report No. 27, 1954.

27. Hall, J. G. — The Transition Through a Contact Region. UTIA Report No. 26, 1954.

28. Waldron, H. F. — An Experimental Study of a Spiral Vortex Formed by Shock-Wave Diffraction. UTIA Technical Note No. 2, 1954.

29. Franks, W. J. — Interaction of a Shock Wave with a Wire Screen. UTIA Technical Note No. 13, 1957.

30. Friend, W. H. — The Interaction of a Plane Shock Wave with an Inclined Perforated Plate. UTIA Technical Note No. 25, 1958.

31. Waldron, H. F. — An Experimental Investigation of the Flow Properties Behind Strong Shock Waves in Nitrogen. UTIA Report No. 50, 1958.

32. de Leeuw, J. H. — The Interaction of a Plane Strong Shock Wave with a Steady Magnetic Field. UTIA Report No. 49, 1958.

33. Steketee, J. A. — On the Interaction of Rarefaction Waves in a Shock Tube. UTIA Review No. 4, 1952.

34. Glass, I. I.; Heuckroth, L. E.; Molder, S. — On the One-Dimensional Overtaking of a Shock Wave by a Rarefaction Wave. UTIA Technical Note No. 30, 1960; see also ARS J., pp. 1453-1454, 1961.

35. Bremner, G. F.; Dukowitz, J. K.; Glass, I. I. — On the One-Dimensional Overtaking of a Rarefaction Wave by a Shock Wave. UTIA Technical Note No. 33, 1960; see also ARS J., pp. 1455-1456, 1961.

36. Cook, W. J.; Presley, L. L.; Chapman, G. T. — Shock Tube as a Device for Testing Transonic Airfoils at High Reynolds Numbers. AIAA J., 17, 7, pp. 714-721, 1979.

37. Tong, K. O.; Knight, C. J.; Srivastava, B. K. — Interaction of Weak Shock Waves with Screens and Honeycombs. AIAA J., 18, 11, pp. 1298-1305, 1980.

38. Zeitoun, D.; Imbert, M. — Interaction Between the Unsteady Boundary Layer and Inviscid Hot Flow in a Shock Tube. AIAA J., 17, 8, pp. 821-827, 1979.

39a. Hall, J. G. — Studies of Transient Gas Boundary Layer Flows Generated by Unsteady Waves. Proceedings on Unsteady Aerodynamics, edited by R. B. Kinney University of Arizona, 1975.

39b. Amr, Y. M.; Hall, J. G. — Stability Limits and Transition Times of Wave-Induced Wall Boundary Layers. 13th Int. Symp. on Shock Tubes and Waves, July 6-9, 1981, Niagara Falls, New York.

40. Glass, I. I. — Aerodynamics of Blasts. UTIA Review No. 17, 1960; see also CASI J. 7, 3, pp. 109-135, 1961.

41. Glass, I. I.; Hall, J. G. — Shock Sphere - An Apparatus for Generating Spherical Flows. J. Appl. Phys. 28, 4, pp. 424-425, 1958.

42. Boyer, D. W.; Brode, H. L.; Glass, I. I.; Hall, J. G. — Blast from a Pressurized Sphere. UTIA Report No. 48, 1958.

43. Boyer, D. W. — Spherical Explosions and Implosions. UTIA Report No. 58, 1959.

44. Collins, R. — Some Methods of Generating Cylindrical Explosions. UTIA Technical Note No. 43, 1960.

45. Glass, I. I.; Heuckroth, L. E. — An Experimental Investigation of the Head-On Collision of Spherical Shock Waves. UTIA Report No. 59, 1960; see also Phys. Fluids, 2, 5, pp. 542-546, 1959.

46. Glass, I. I.; Heuckroth, L. E. — The Hydrodynamic Shock Tube. Phys. Fluids, 6, 4, pp. 543-547, 1963.

47. Heuckroth, L. E.; Glass, I. I. — Low-Energy Spherical Underwater Explosions. Phys. Fluids, 11, 10, pp. 2095-2107, 1968; see also UTIA Report No. 96, 1964.

48. Benoit, A. — An Experimental Investigation of Spherical Combustion for the UTIA Implosion-Driven Launcher. UTIA Technical Note No. 71, 1963.

49a. Benoit, A. — Thermodynamic and Composition Data for Constant Volume Combustion of Stoichiometric Mixtures of Hydrogen-Oxygen Diluted with Helium or Hydrogen. UTIAS Technical Note No. 85, 1964.

49b. Benoit, A. — Specific Heat Ratios and Isentropic Exponents for Constant Volume Combustion of Stoichiometric Mixtures of Hydrogen-Oxygen Diluted with Helium or Hydrogen. UTIAS Technical Note No. 102, 1966.

49c. Benoit, A. — Properties of Chapman-Jouguet Detonations in Stoichiometric Hydrogen-Oxygen Mixtures Diluted with Helium or Hydrogen. UTIAS Technical Note No. 104, 1967.

49d. Benoit, A. — Equilibrium Thermodynamic Data for the H_2-O_2-He Systems. UTIAS Technical Note No. 128, 1968.

50. Benoit, A.; Glass, I. I. — An Experimental Study of Spherical Combustion Waves in a Hemispherical Chamber. Combustion & Flame, 12, 2, pp. 521-533, 1968.

51. Glass, I. I.; Kawada, H. — Prandtl-Meyer Flows of Dissociated and Ionized Gases. UTIA Report No. 85, 1962.

52a. Glass, I. I.; Takano, A. — Nonequilibrium Flows of Dissociated Oxygen and Ionized Argon Around a Corner. Prog. Aero. Sci., 6, pp. 163-249, 1965.

52b. Glass, I. I.; Takano, A. — Nonequilibrium Expansion Flow of Dissociated Oxygen Around a Corner. UTIA Report No. 91, 1963.

52c. Glass, I. I.; Takano, A. — Nonequilibrium Expansion Flow of Ionized Argon Around a Corner. UTIAS Report No. 95, 1963.

53. Boyer, A. G. — Design, Instrumentation and Performance of the UTIAS 4 in x 7 in Hypersonic Shock Tube. UTIAS Report No. 99, 1964.

54. Dukowitz, J. K. — A Magnetohydrodynamic Flow in the Shock Tube Boundary Layer with Transverse Magnetic Field. UTIAS Report No. 115, 1966. (This work was supervised by Prof. J. H. de Leeuw.)

55. Chan, Y. Y.; Mason, R. P.; Reddy, N. M. — Instrumentation and Calibration of UTIAS 11 in x 15 in Hypersonic Shock Tunnel. UTIAS Technical Note No. 91, 1965.

56. Reddy, N. M. — The Use of Self-Calibrating Catalytic Probes to Measure Free-Stream Atom Concentration in a Hypersonic Flow. UTIAS Report No. 121, 1966.

57a. Belozerov, A. N. — Study of the Initial Ionization Process in a Strong Shock Wave. UTIAS Report No. 131, 1968. (This work was supervised by Prof. R. M. Measures.); see also Belozerov, A. N. and Measures, R. M., J. Fluid Mech., 36, pp. 695-720, 1969.

57b. Kalra, S. P.; Measures, R. M. — Approach to Ionization Equilibrium and Atomic Cross-Section Measurements in a Helium Shock Wave. Can. J. Phys., 51, 18, pp. 1956-1965, 1973. (This work was supervised by Prof. R. M. Measures.)

58. Makomaski, A. H. — Preliminary One-Dimensional Investigation of the Initiation of Low-Density PETN by Hydrogen-Oxygen Detonation Waves. UTIAS Technical Note No. 83, 1965.

59. Flagg, R. F.
Glass, I. I.
Explosive-Driven Spherical Implosion Waves. Phys. Fluids, 11, 10, pp. 2282-2284, 1968; see also Flagg, R. F., The Application of Implosion Wave Dynamics to a Hypervelocity Launcher. UTIAS Report No. 125, 1967.

60. Watson, J. D.
Implosion-Driven Hypervelocity Launcher Performance Using Gaseous Detonation Waves. UTIAS Technical Note No. 113, 1967.

61. Sevray, P.
Performance Analysis of UTIAS Implosion-Driven Hypervelocity Launcher. UTIAS Technical Note No. 121, 1968.

62. Flagg, R. F.
Mitchell, G. P.
An Optimization Study of the UTIAS Implosion-Driven Hypervelocity Launcher MK II. UTIAS Technical Note No. 130, 1968.

63. Garg, S. K.
Spherical Elastic-Plastic Waves in Solid Media. UTIAS Technical Note No. 32, 1969.

64. Czerwinski, W.
Structural Design and Development of UTIAS Implosion-Driven Launcher. UTIAS Report No. 153, 1970.

65. Macpherson, A. K.
A Preliminary Monte-Carlo Analysis of the Reflection of an Imploding Hemispherical Shock Wave Similar to that Generated in the UTIAS Implosion Driven Hypervelocity Launcher or Shock Tube. UTIAS Report No. 152, 1970.

66. Glass, I. I.
Appraisal of UTIAS Implosion-Driven Hypervelocity Launchers and Shock Tubes. Prog. Aero. Sci. 13, pp 223-291, 1972.

67. Kennedy, J. E.
Glass, I. I.
Multipoint Initiated Implosions from Hemispherical Shells of Sheet Explosive. UTIAS Technical Note No. 99, 1966.

68. Anderson, J. H. B.
Osborne, P. J. K.
Glass, I. I.
Gladstone-Dale Constants for the Oxygen Atom and Molecule. Phys. Fluids, 10, 8, p. 1848, 1967.

69. Wettlaufer, D. E.
Glass, I. I.
Specific Refractivities of Atomic Nitrogen and Oxygen. Phys. Fluids, 13, 11, pp. 2065-2066, 1972.

70. Bristow, M. P. F.
Glass, I. I.
Polarizability of Singly-Ionized Argon. Phys. Fluids, 2066-2067, 1972.

71. Tirumalesa, D. — Oxygen Corner-Expansion Flows with Coupled Vibrational and Dissociational Nonequilibrium. UTIAS Technical Note No. 120, 1967.

72. Drewry, J. E. — An Experimental Investigation of Nonequilibrium Corner Expansion Flows of Dissociated Oxygen. UTIAS Report No. 124, 1967.

73. Weynants, R. R. — An Experimental Investigation of Shock-Wave Diffraction Over Compressive and Expansive Corners. UTIAS Technical Note No. 126, 1968.

74. Gorjup, M.; Glass, I. I. — Laboratory Calibration of a Micrometeoroid Impact Gauge, CAS J., 13, 5, pp. 197-204, 1967.

75. Evans, R. L.; Glass, I. I. — Calibration of a Condenser Microphone Micro-Meteoroid Sensor. CAS J. 16, 9, pp. 375-379, 1970.

76. Roberts, D. E.; Glass, I. I. — A Spectroscopic Investigation of Combustion-Driven Spherical Implosion Waves. Phys. Fluids, 14, 8, 1662-1670, 1971; see also UTIAS Technical Note No. 140, 1969.

77. Elsenaar, A. — A Numerical Model for a Combustion-Driven Spherical Implosion Wave. UTIAS Report No. 144, 1969.

78. Elsenaar, A. — Microwave Measurements of Projectile Motion in the Barrel of the UTIAS Implosion-Driven Hypervelocity Launcher. UTIAS Technical Note No. 145, 1969.

79. Roig, R. A.; Glass, I. I. — A Spectroscopic Study of Combustion Driven Implosions. Phys. Fluids, 20, 10, pp. 1651-1656, 1977.

80. Vasudevan, B. — Pressure Measurements at the Focus of Combustion-Driven Implosions. UTIAS Technical Note No. 209, 1977.

81. Poinssot, J. C. — A Preliminary Investigation of a UTIAS Implosion-Driven Shock Tube. UTIAS Technical Note No. 136, 1969.

82a. Chan, S. K. — An Analytical and Experimental Study of an Implosion-Driven Shock Tube. UTIAS Report No. 191, 1973.

82b. Chan, S. K.; Capelli, G.; Graf, W. O. — Performance Trials of the Eight-Inch Diameter UTIAS Implosion Driven Hypervelocity Launchers MK II and MK III. UTIAS Technical Note No. 161, 1971.

83. Glass, I. I., Brode, H. L., Chan, S. K. — Strong Planar Shock Waves Generated by Explosively-Driven Spherical Implosions. AIAA J. 12, 3, pp. 367-374, 1974.

84. Chan, S. K., Glass, I. I. — Radiative Relaxation Behind High-Speed Shock Waves in Air. Phys. Fluids, 17, 4, pp. 688-690, 1974.

85. Menard, W. A. — A Higher Performance Electric-Arc-Driven Shock Tube. AIAA J., 9, 10, pp. 2096-2098, 1971.

86. Dannenberg, R. E. — Capabilities of Arc-Driven Shock Tubes. In Proceedings, 11th International Symposium on Shock Tubes and Waves, Edited by B. Ahlborn, A. Hertzberg and D. Russel, University of Washington Press, Seattle, pp. 416-431, 1977.

87. Compton, D. L., Cooper, D. M. — Duplication in a Shock Tube of Stagnation Region Conditions on a Jovian Atmosphere-Entry Probe. Proceedings, 9th International Shock Tube Symposium, Edited by D. Bershader and W. Griffith, Stanford University Press, Stanford, pp. 218-329, 1973.

88. Glass, I. I., Sharma, S. P. — Production of Diamonds from Graphite Using Explosive-Driven Implosions. AIAA J. 14, 3, pp. 402-404, 1976.

89. Glass, I. I., Liu, W. S. — Effects of Hydrogen Impurities on Shock Structure and Stability in Ionizing Monatomic Gases, Part 1. Argon. J. Fluid Mech. 84, Part 1, pp. 55-77, 1978.

90. Glass, I. I., Liu, W. S., Tang, F. C. — Effects of Hydrogen Impurities on Shock Structure and Stability in Ionizing Monatomic Gases, Part 2. Krypton. Can. J. Phys., 55(14), pp. 1269-1279, 1977.

91. Fowles, R. G. — Stimulated and Spontaneous Emission of Acoustic Waves from Shock Fronts. Phys. Fluids (to be published), 1981.

92. Liu, W. S., Whitten, B. T., Glass, I. I. — Ionizing Argon Boundary-Layers, Part 1. Quasi-Steady Flat-Plate Laminar Boundary-Layer Flows. J. Fluid Mech., 87, Part 4, pp. 609-640, 1978.

93. Liu, W. S., Glass, I. I. — Ionizing Argon Boundary Layers, Part 2. Shock-Tube Side-Wall Boundary-Layer Flows. J. Fluid Mech., 92, Part 3, pp. 459-496, 1979.

94. Liu, W. S., Takayama, K., Glass, I. I. — Coupled Interactions of Shock-Wave Structure with Laminar Boundary Layers in Ionizing Argon Flows. J. Fluid Mech. 96, Part 4, pp. 735-756, 1980.

95. Glass, I. I.
Liu, W. S.
Tang, F. C.
Radiation-Induced Shock-Tube Flow Nonuniformities in Ionizing Argon. Phys. Fluids, 23, 1, pp. 224-225, 1980.

96. Martin, W. A.
An Experimental Study of the Boundary Layer Behind a Moving Plane Shock Wave. UTIAS Report No. 47, 1957.

97. Igra, O.
Glass, I. I.
Corner Expansion Flow of Ionized Argon. In Dynamics of Ionized Gases. Edited by M. S. Lighthill et al, Tokyo University Press, pp. 449-460, 1973.

98. Igra, O.
Radiation Effects in a Nonequilibrium Corner-Expansion Flow of Ionizing Argon. Phys. Fluids, 23, 8, pp. 1513-1517.

99. Sislian, J. P.
Glass, I. I.
Condensation of Water Vapor in Rarefaction Waves: I. Homogeneous Nucleation. AIAA J., 14, 12, pp. 1731-1737, 1976.

100. Kotake, S.
Glass, I. I.
Condensation of Water Vapor in Rarefaction Waves: II. Heterogeneous Nucleation. AIAA J., 15, 2, pp. 215-221, 1977.

101. Glass, I. I.
Kalra, S. P.
Sislian, J. P.
Condensation of Water Vapor in Rarefaction Waves: III. Experimental Results. AIAA J., 15, 5, pp. 683-693, 1977.

102. Koziak, W. W.
Quantitative Laser Schlieren Measurements in an Expanding Hypersonic Laminar Boundary Layer. UTIAS Report No. 173, 1971. (Supervised by Dr. P. A. Sullivan, who built the new hypersonic shock tunnel.)

103. Law, C. K.
Glass, I. I.
Diffraction of Strong Shock-Waves by a Sharp Compressive Corner. CAS Trans., 4, pp. 2-12, 1971.

104. Ben-Dor, G.
Glass, I. I.
Domains and Boundaries of Non-Stationary Oblique Shock-Wave Reflexions, 1. Diatomic Gas. J. Fluid Mech., 92, Part 3, pp. 459-496, 1979.

105. Ben-Dor, G.
Glass, I. I.
Domains and Boundaries of Non-Stationary Shock-Wave Reflexions, 2. Monatomic Gas. J. Fluid Mech., 96, Part 4, 1980.

106. Ben-Dor, G.
Glass, I. I.
Nonstationary Oblique Shock-Wave Reflections, Actual Isopycnics and Numerical Experiments. AIAA J., 16, 11, pp. 1146-1153, 1978.

107. Book, D. L.
Boris, J. P.
Kuhl, A. L.
Oran, E. S.
Picone, J. M.
Zalesak, S. T.
Simulation of Complex Shock Reflections from Wedges in Inert and Reactive Gaseous Mixtures. NRL Memo Report 4333, 1980.

108.	Booen, M. W. Needham, C. E.	Two Dimensional Hull Code Simulation of Complex and Double Mach Reflections. Air Force Weapons Laboratory Technical Note NTE-TN-81-001, 1981. Also H. M. Glaz, NSWC, Private Comm. June 1981.
109.	Glass, I. I. Ribner, H. S. Gottlieb, J. J.	Canadian Sonic-Boom Simulation Facilities. CAS J., 18, 10, pp. 235-246, 1972.
110.	Carothers, R.	Initial Calibration and Physiological-Response Data for the Travelling-Wave Sonic-Boom Simulator. UTIAS Technical Note No. 180, 1972.
111.	Gottlieb, J. J. Glass, I. I.	Recent Developments in Sonic-Boom Simulation Using Shock Tubes. Can. J. Phys., 52, 3, pp. 207-218, 1973.
112.	Leigh, B. R. Tennyson, R. C. Glass, I. I.	Aged Plaster Panels Subjected to Sonic Booms. CAS J., 21, 9, pp. 352-360, Nov. 1975.
113.	Glass, I. I. Lips, K. W. Nowakiwsky, O. V. Reid, L. D.	Sonic-Boom-Startle Effects During Simulated and Actual Driving Tests. CAS J. 22, 2, pp. 70-88, 1976.
114.	Gottlieb, J. J.	Sonic Boom Research at UTIAS. CAS J., 20, 5, pp. 199-222, 1974.
115.	Gottlieb, J. J.	Simulation of a Travelling Sonic Boom in a Pyramidal Horn. Prog. Aero. Sci., 17, pp. 1-66, Pergamon Press, New York, 1976.
116.	Reinis, S.	Acute Changes in Inner Ears of Laboratory Animals by Simulated Sonic Booms. UTIAS Report No. 211, 1976.
117.	Wahba, N. N.	Pressure Inside a Room Subjected to Sonic Boom. UTIAS Technical Note No. 207, 1977.
118.	Niedzwiecki, A. Ribner, H. S.	Subjective Loudness of N-Wave Sonic Booms. J. Acoust. Soc. Amer., 64, 6, pp. 1617-1621, 1978.
119.	Tubb, P. E.	Measured Effects of Turbulence on the Rise Time of a Weak Shock. UTIAS M.A.Sc. Thesis, 1975 (supervised by Prof. H. S. Ribner).
120.	Johannesen, N. H. Hodgson, J. P.	The Physics of Weak Waves in Gases. Rep. Prog. Phys., 42, pp. 629-676, 1979.
121.	Holst-Jensen, O.	An Experimental Investigation of the Rise Times of Very Weak Shock Waves. UTIAS Technical Note No. 229, 1981.
122.	Saito, T. Glass, I. I.	Application of Random-Choice Method to Problems in Shock and Detonation-Wave Dynamics. UTIAS Report No. 240, 1979.

123. Saito, T.
Kudian, A. K.
Glass, I. I.
Temperature Measurements of an Implosion Focus. 13th Int. Symp. on Shock Tubes and Waves, July 6-9, 1981, Niagara Falls, New York.

124. Kleiman, K.
Application of Explosive Driven Implosions to Production of Diamonds and New Materials. Ph.D. Thesis in Progress (supervised by Prof. I. I. Glass and Prof. N. Salansky).

125a) Ando, S.
Glass, I. I.
Domains and Boundaries of Pseudostationary Oblique-Shock-Wave Reflections in Carbon Dioxide. 7th Int. Symp. on Military Appl. Blast Symp., July 13-17, Medicine Hat, Canada, 1981 (see also UTIAS TN No. 231, 1981).

125b) Deschambault, R. L.
UTIAS M.A.Sc. Thesis, in progress.

126. Reinis, S.
Featherstone, J. W.
Weiss, D. S.
The Effects of Sonic Booms on Hearing and Inner Ear Structure. Int. Symp. on Effects of Impulse Noise on Hearing. Aug. 25-27, 1980, Malmo, Sweden.

127. Honma, H.
Glass, I. I.
Tsumita, Y.
Holst-Jensen, O.
Weak Spherical Shock-Wave Transitions of N-Waves in Air with Vibrational Excitation. 13th Int. Symp. on Shock Tubes and Waves, July 6-9, 1981, Niagara Falls, New York.

128. Wahba, N. N.
Glass, I. I.
Tennyson, R. C.
Response of A Room Subjected to Simulated Sonic Booms. 13th Int. Symp. on Shock Tubes and Waves, July 6-9, 1981, Niagara Falls, New York.

129. Sislian, J. P.
Analysis of Swirling Jet Turbulent Mixing and Combustion. UTIAS Report No. 249, 1981.

130. Sislian, J. P.
Analysis of Turbulent Free-Jet Hydrogen-Air Diffusion Flames with Finite Chemical Reaction Rates. UTIAS Report No. 224, 1978 (also NASA CR Report 3024, 1978).

131. Sislian, J. P.
Equations of Motion and Two-Equation Turbulence Model for Plane or Axisymmetric Turbulent Flows in Body-Oriented Orthogonal Curvilinear Coordinates and Mass-Averaged Dependent Variables. UTIAS Report No. 225, 1978 (also NASA CR Report 3025, 1978).

132. Sislian, J. P.
Evans, J. S.
Glass, I. I.
Analysis of Turbulent Free-Jet Hydrogen-Air Diffusion Flames with Finite Chemical Reaction Rates. CAS J., 25, 1, pp. 61-75, 1979.

133. Miura, H.
Glass, I. I.
A Dusty-Gas Shock Tube. 7th Int. Symp. on Military Appl. Blast Symp., July 13-17, Medicine Hat, Canada, 1981.

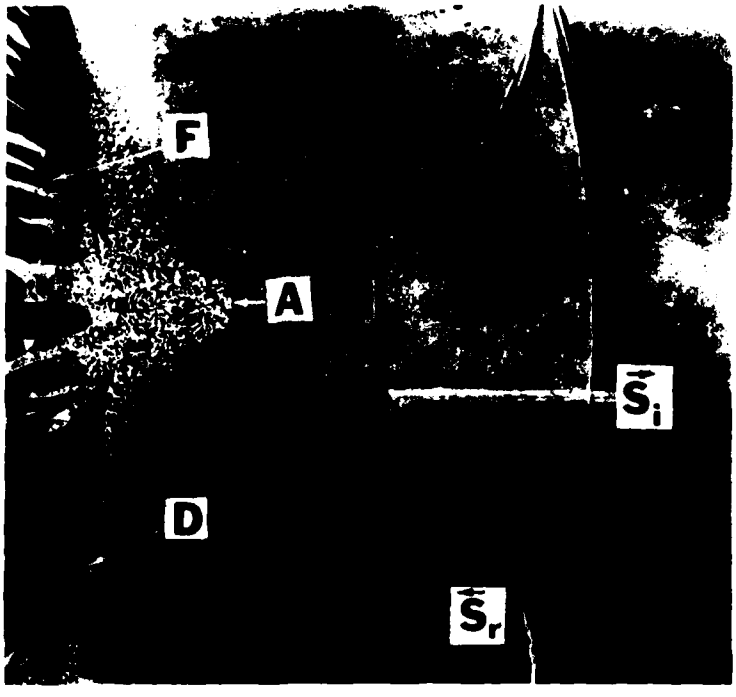

FIG. 1 SHOCK-TUBE DIAPHRAGM BREAKING PROCESS IN THE (x,y)-PLANE.

A shadowgram of the bursting of a "red-zip" cellophane diaphragm in the UTIAS 2 in x 7 in shock tube at an initial pressure ratio of 2 across the diaphragm. The bulging, ruptured diaphragm D, and the pressurized air A, escaping through the fragments F, appear on the left. The curved incident S_i, and reflecting S_r, compression and shock waves are seen on the right.

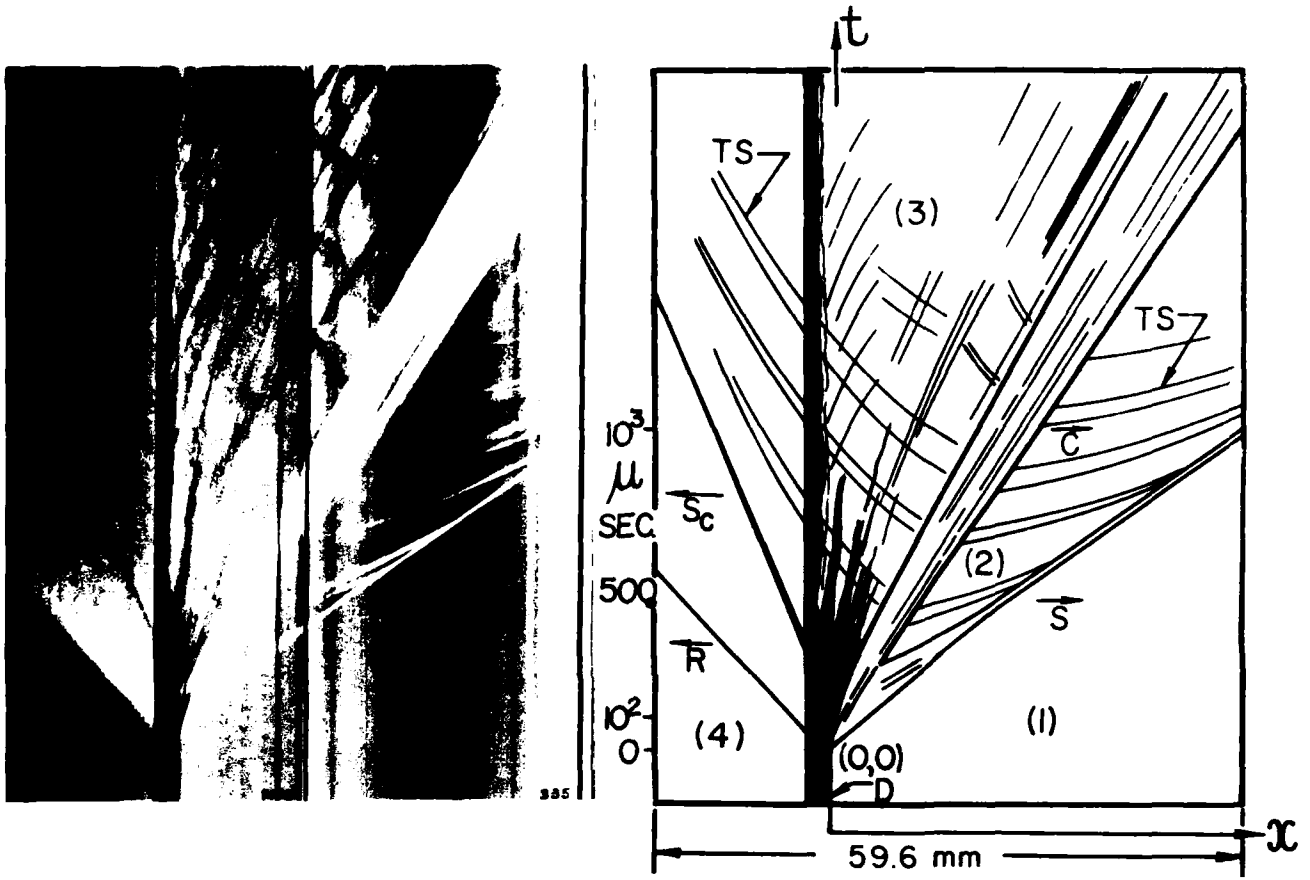

FIG. 2 SHOCK-TUBE DIAPHRAGM BREAKING PROCESS IN THE (x,t)-PLANE.

A schlieren record and explanatory sketch of the wave system in the distance-time plane produced in a shock tube from the instant the diaphragm ruptures, shows: R, rarefaction wave; S, shock wave; C, contact front; Sc, condensation shock wave; TS, transverse shock waves; D, bulging cellophane diaphragm; (1), air in low-pressure channel; (4), air in high-pressure chamber; pressure p_4 = 2.2 atm; p_1 = 0.44 atm, p_4/p_1 = 5.00, sound speeds in chamber and channel, a = 1132 fps, shock wave Mach number, M_s = 1.39; pressure rise ratio across shock wave p_2/p_1 = 2.1; flow Mach number of region (2) heated and compressed by shock wave M_2 = 0.50; flow Mach number in region (3) cooled and expanded by the rarefaction wave M_3 = 0.65.

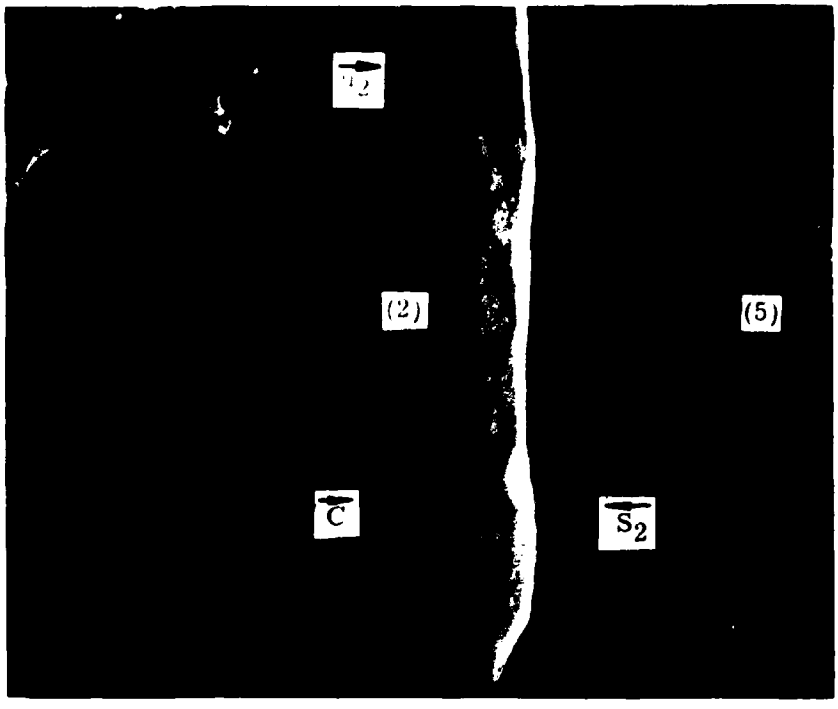

FIG. 3 COLLISION OF A REFLECTED SHOCK WAVE WITH A CONTACT REGION IN THE (x,y)-PLANE.

The reflected shock wave S_2 has penetrated the diffuse and eddying contac region C, and is no longer planar. The shock wave has also been disturbed by the boundary layer generated by the incident shock wave in state (2). Since the velocity in the boundary layer is lower than u_2, the shock wave there races ahead. The major portion of the contact region is just approaching the shock wave,and this region of the driver gas is state (3). The state behind S_2 is state (5), which is at rest. The schlieren photograph was taken in a 2 in x 7 in shock tube at a diaphragm pressure ratio of 100 with a channel pressure of 32 torr. The gas in the driver and channel sections was air, initially at room temperature.

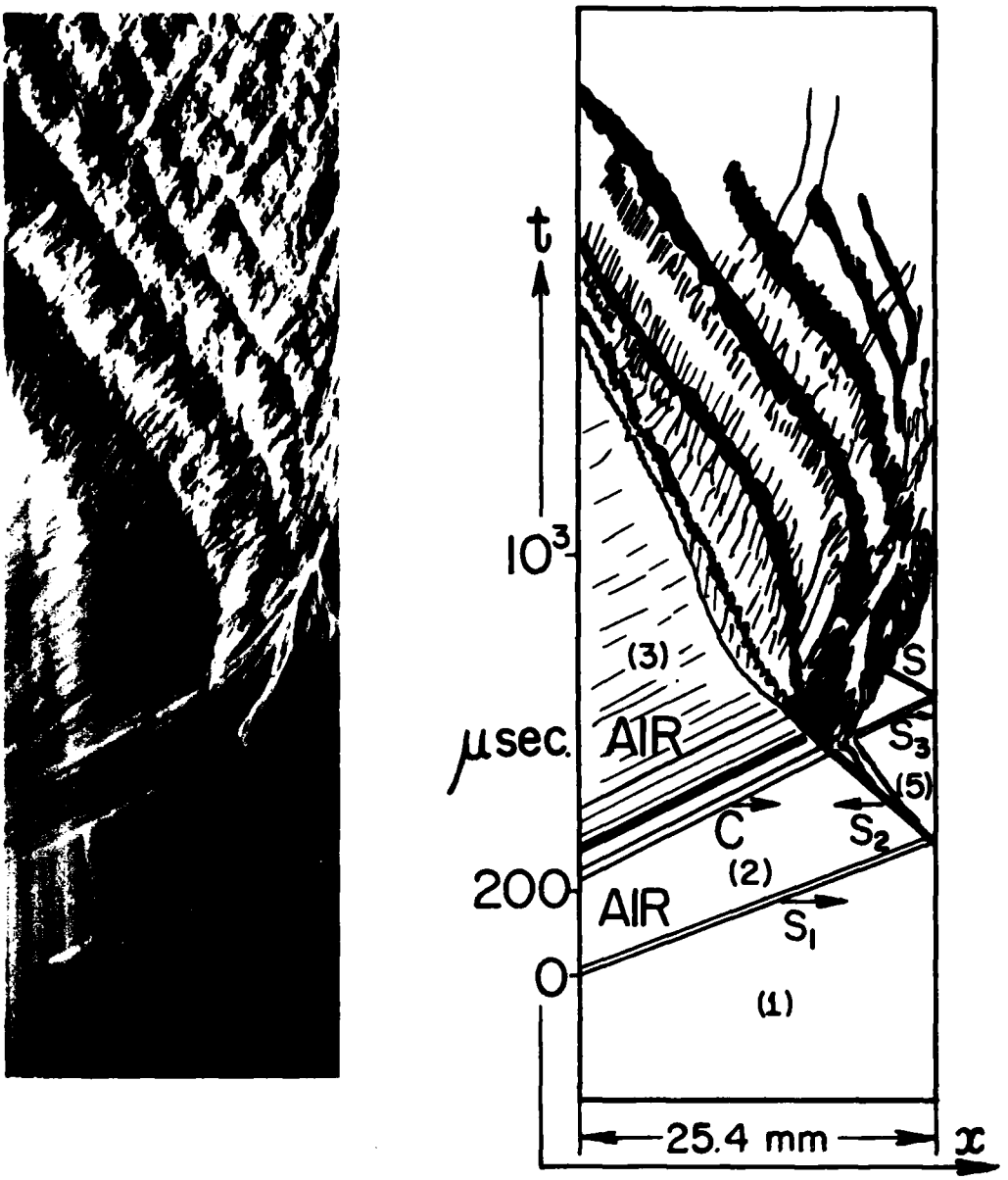

FIG. 4 COLLISION OF A REFLECTED SHOCK WAVE WITH A CONTACT REGION IN THE (x,')-PLANE.

The schlieren photograph which was taken in the 3 in x 3 in Wave-Interaction Tube, clearly shows the paths of the incident shock wave S_1, and the reflected shock wave S_2, as it collides with the contact region C and refracts to send back a reflected shock wave S_3. The passage of the refracted shock wave in state (3) gives rise to multiple bifurcated shock waves. The initial diaphragm pressure ratio P_{41} = 153, p_1 = 20 torr, a_1 = 347 m/s (1136 fps), M_s = 2.34, M_2 = 1.46, M_3 = 2.70, U_{21} = 1.76.

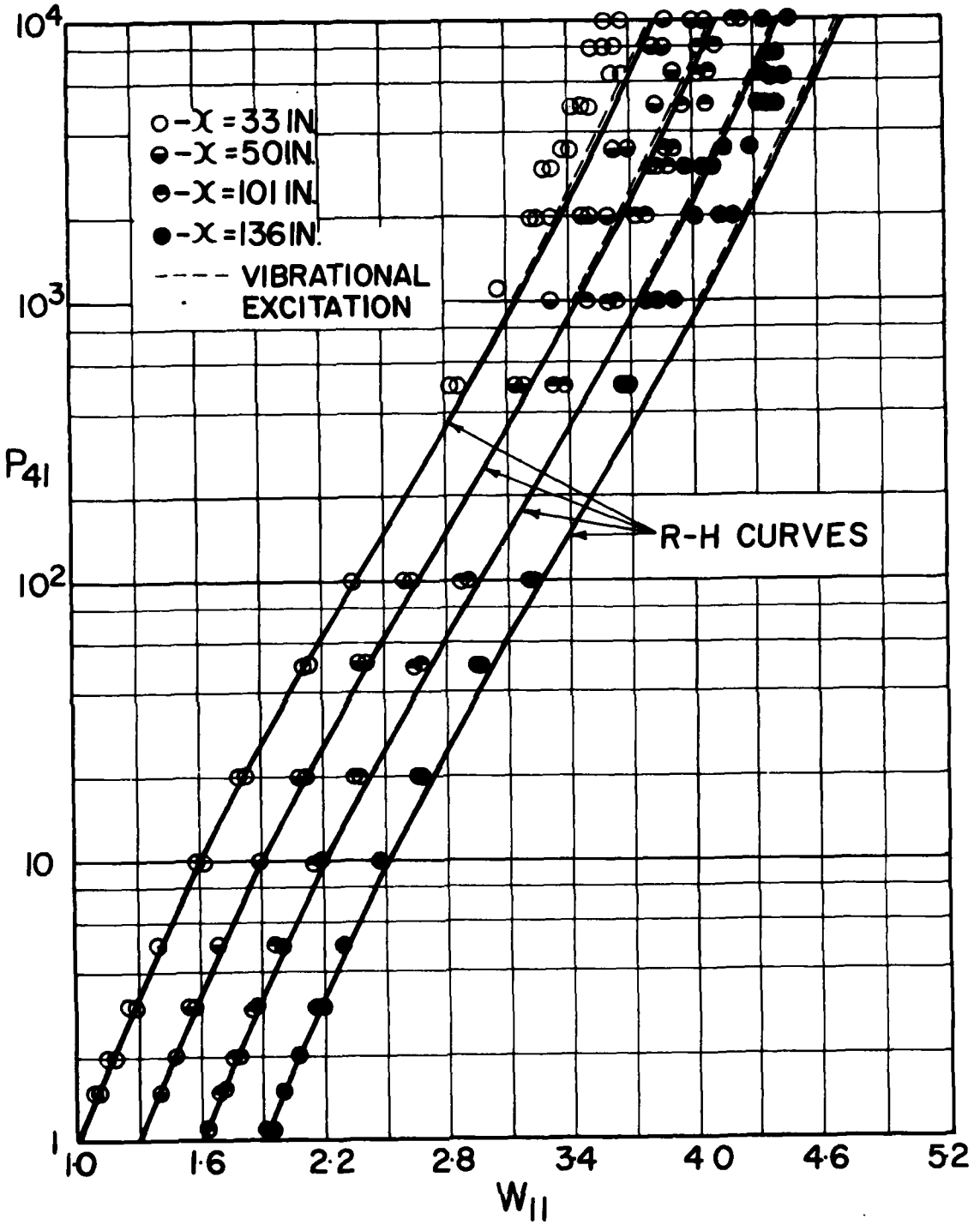

FIG. 5 SHOCK-WAVE ATTENUATION IN A 3 IN x 3 IN WAVE-INTERACTION TUBE.

The variation of the initial shock-wave Mach number M_s or W_{11}, in air, is shown as a function of diaphragm pressure ratio P_{41}, for various distances from the diaphragm from 33 in to 136 in (0.84m to 3.46m). Agreement with analysis is good up to diaphragm pressure ratios of about 10, and then progressive deviation occurs with P_{41} and distance as well as reduced initial pressure. In this case, P_{41} was increased by reducing p_1 for structural reasons. Consequently x and p_1 could not be separated.

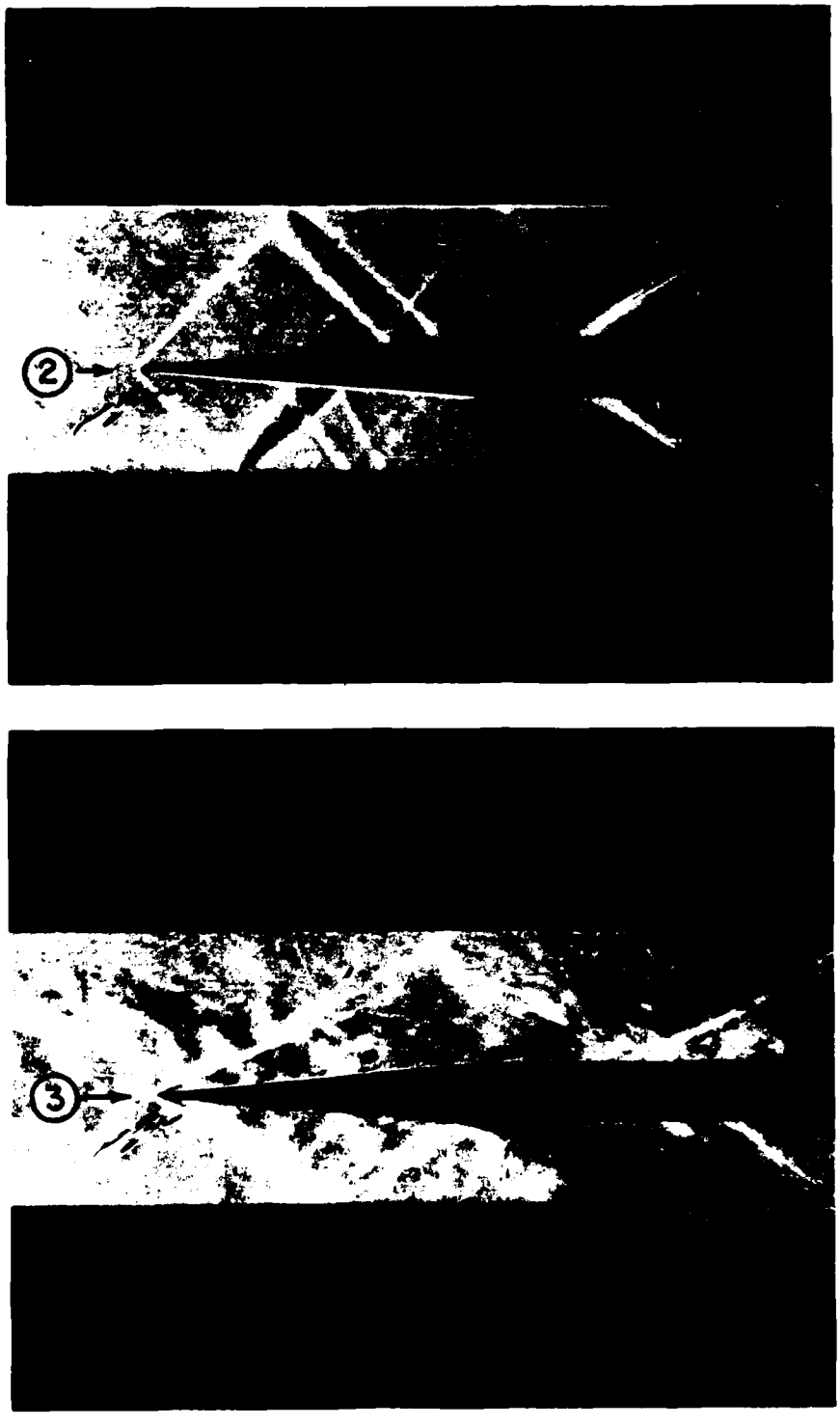

FIG. 6 OBLIQUE SHOCK-WAVE BOUNDARY-LAYER INTERACTIONS.

Schlieren photographs show the flows and boundary layers in the uniform regions in a 2 in x 7 in shock tube. The flow in hot state (2) over a two-dimensional 10-degree wedge shows that it is quite uniform at a Mach number M = 1.50. The flow in cold state (3) at a Mach number M = 2.4, is rough and eddying. A clear but complex interaction of the oblique shock wave with the wall boundary layer appears in state (2) but not in state (3). The latter region is not suitable for testing.

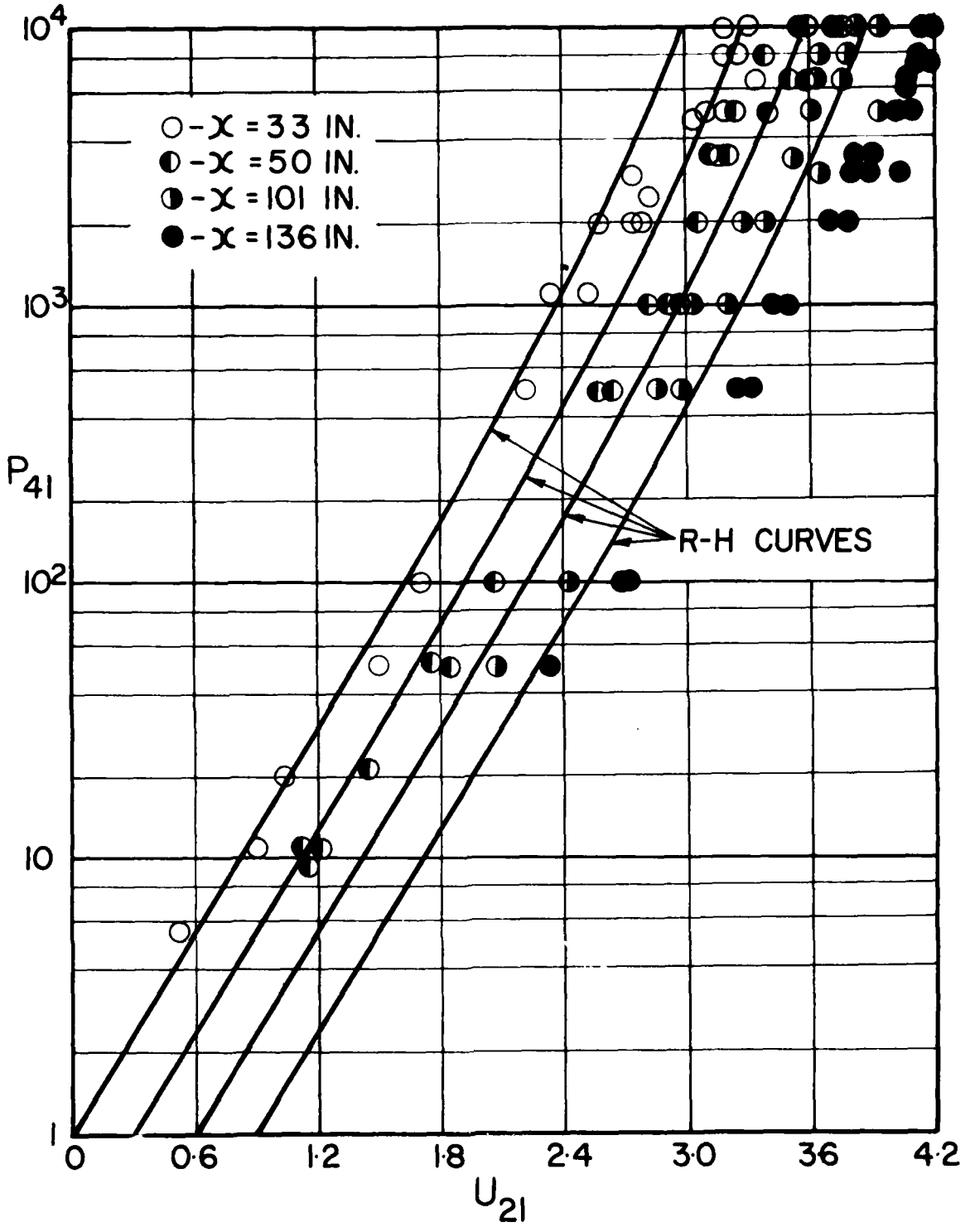

FIG. 7 CONTACT SURFACE ACCELERATION IN A 3 IN x 3 IN WAVE-INTERACTION TUBE.

The measurements were made from the velocity U_{21} of the first surface of the contact region in the (x,t)-plane. The acceleration of the contact surface with diaphragm pressure ratio P_{41} and distance x is clearly illustrated. As for shock attenuation, x and p were not separated in these data.

FIG. 8 REFRACTION OF A PLANE SHOCK WAVE IN AIR THROUGH A LAYER OF HELIUM.

(a) Composite photograph of two (x,t)-plane schlieren records showing the double refraction of a plane shock wave at a helium layer and the resulting subsequent overtaking of two shock waves moving in the same direction.

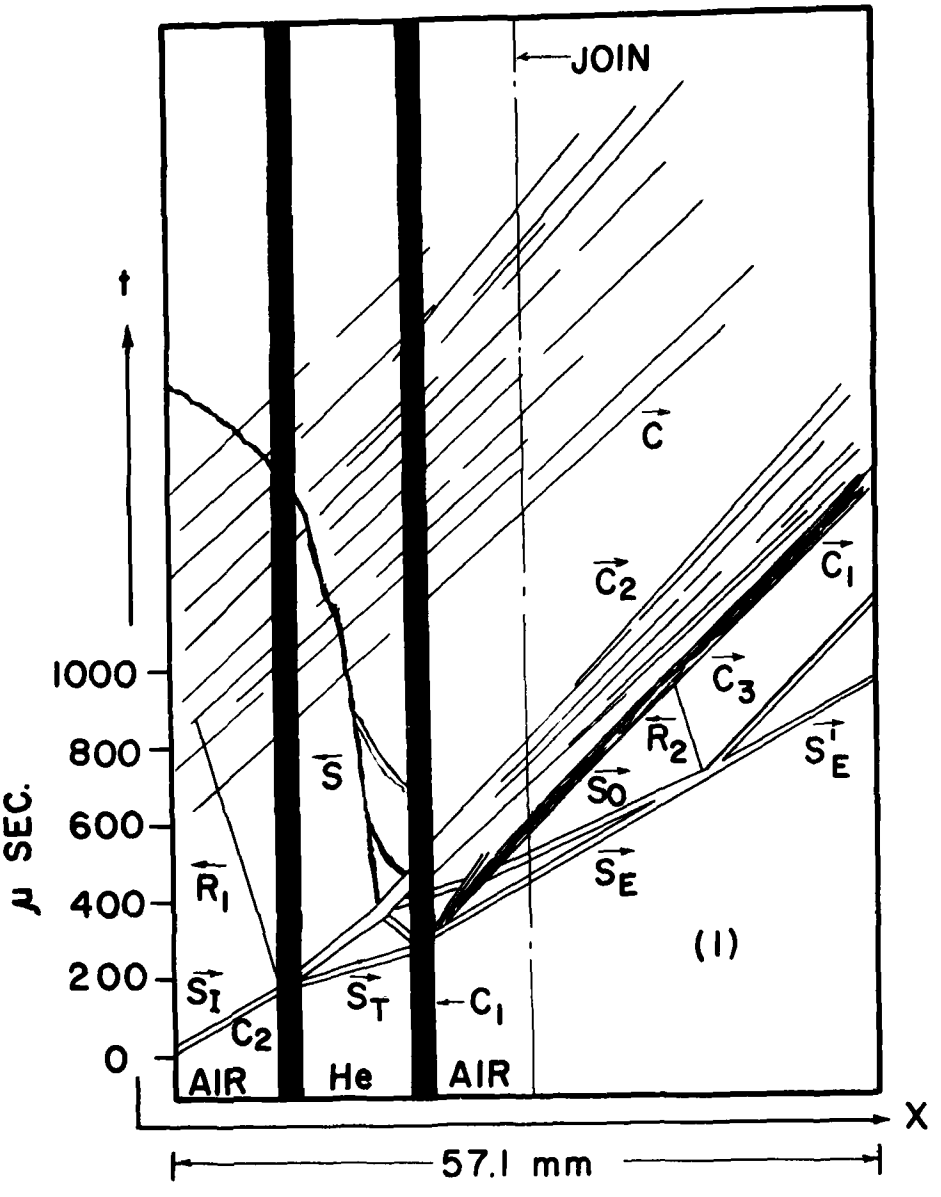

FIG. 8(b) Explanatory line diagram of (a). The gases are at rest and at atmospheric pressure initially. The incident shock wave S_I, in air, refracts into helium at the microfilm contact surface C_2, causing a transmitted shock wave S_T, and a reflected rarefaction wave R_1. The transmitted shock wave S_T refracts into air at the microfilm contact surface C_1, generating an emerging shock wave S_E, and a reflected shock wave S, which refracts at C_2, producing a reflected shock wave S_O, which overtakes S_E. This gives rise to the final shock wave S_E', a perfect contact surface C_3, and a very weak reflected rarefaction wave R_2. The initial refraction at C_2 causes shock S_I to attenuate in pressure ratio in the helium layer. The second refraction at C_1 amplifies the pressure ratio of S_E in air. However, owing to the nonlinear nature of the refractions S_E is weaker than S_I. The overtaking of S_O and S_E now amplify S_E' so that it is nearly the same strength as S_I. Note the rapid diffusion of the helium-air contact surfaces at C_1 and C_2 and the very stable contact surface C_3 in air, Mach numbers of S_I = 1.70°, S_E = 1.65° and S_E' = 1.69°, pressure ratio across R_2 = 0.97.

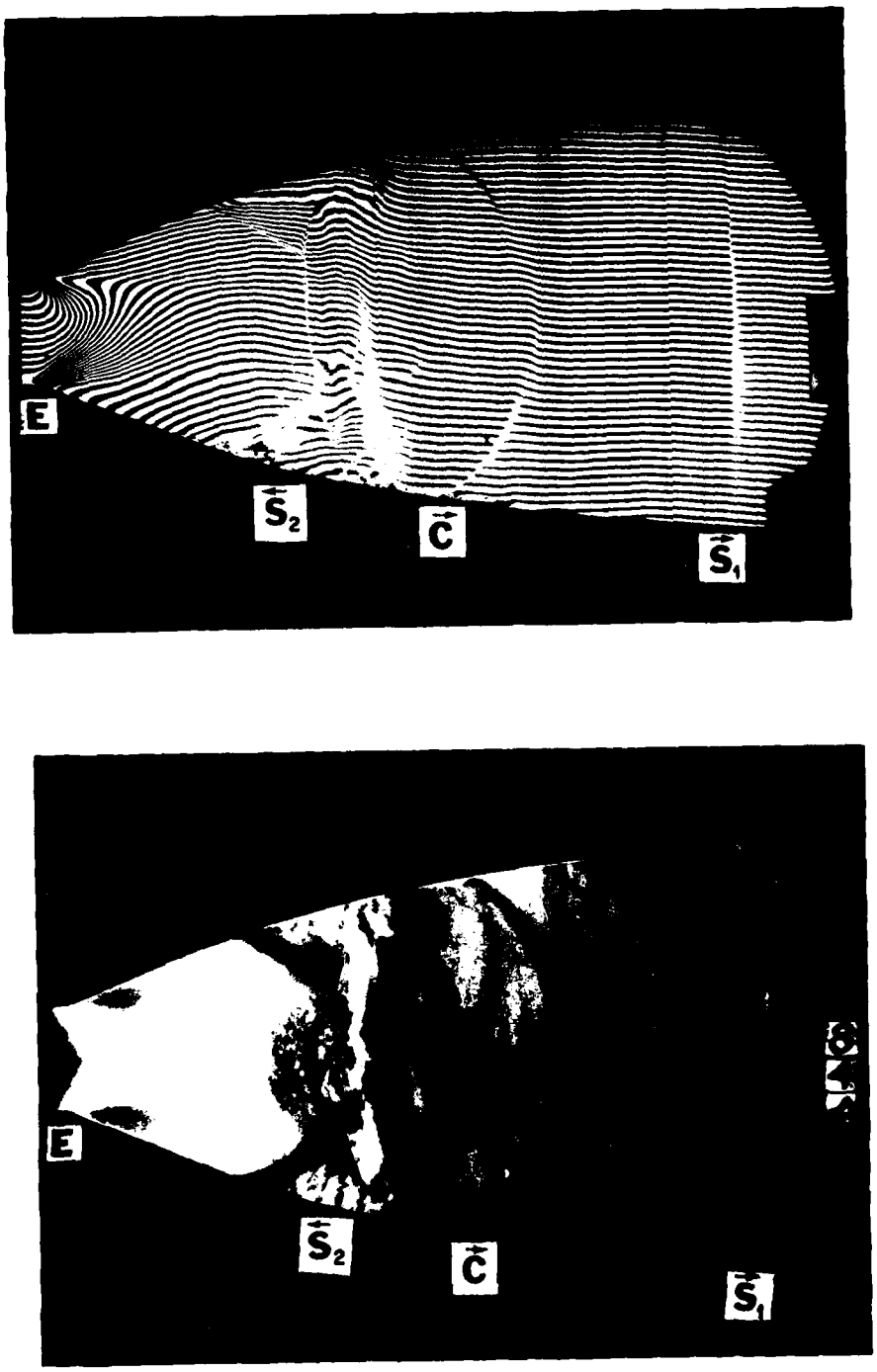

FIG. 9 STARTING FLOW IN A SUPERSONIC NOZZLE IN A SHOCK-TUBE CHANNEL.

The interferogram and schlieren photograph show how a planar moving shock wave S_1 is used to induce a supersonic flow in a two-dimensional nozzle past the expansion waves E, at the throat, for short-duration (microseconds or milliseconds) aerodynamic tests. In the process of starting this flow, contact surface C, and second shock wave S_2, are also generated and swept away to give a uniform supersonic stream. The shock S_2 becomes bifurcated as it separates the nozzle and wall boundary layers. The schlieren photograph provides a good picture of the wave system, whereas the interferogram makes it possible to determine the density through the nozzle flow.

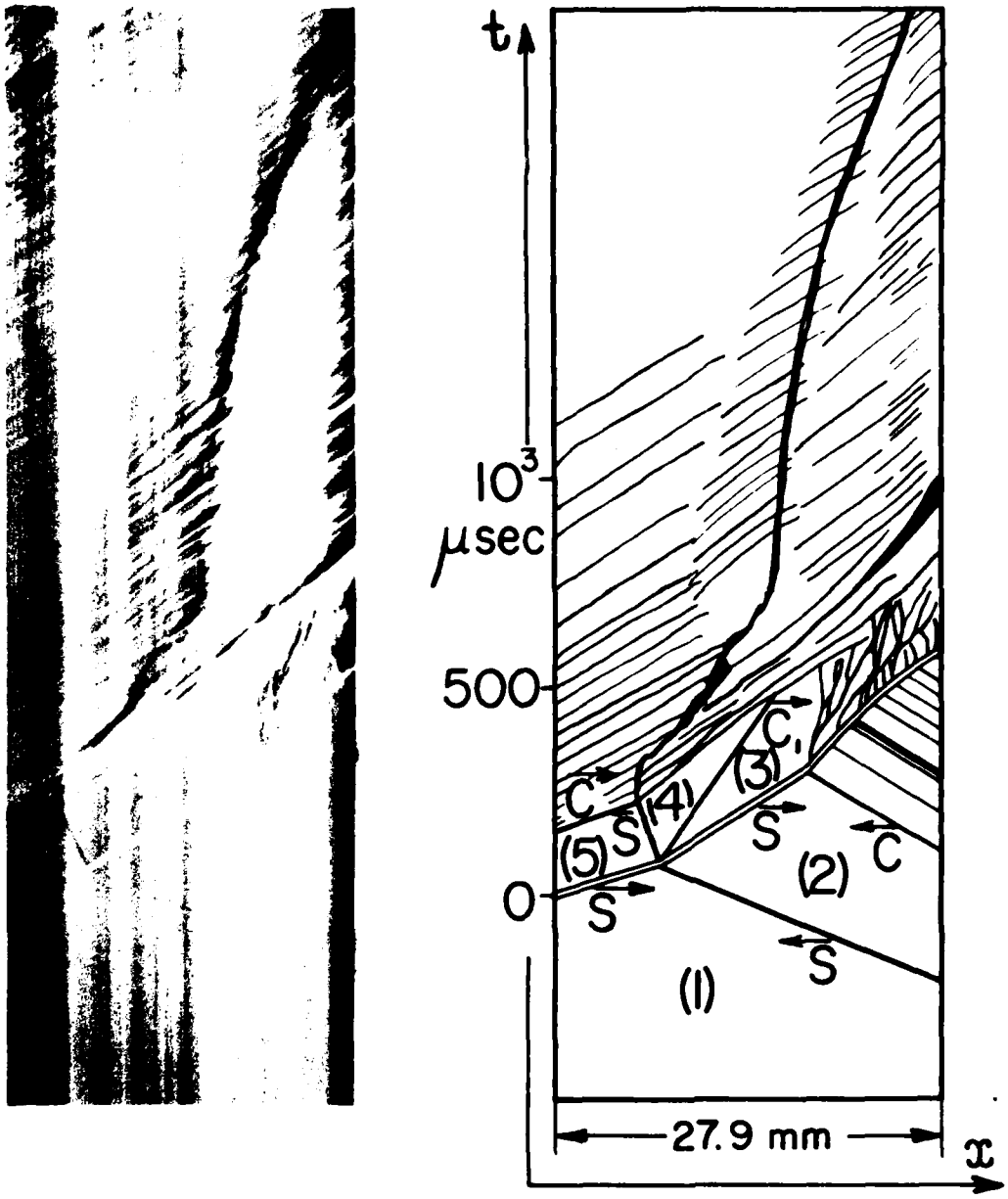

FIG. 10 HEAD-ON COLLISION OF TWO UNEQUAL SHOCK WAVES IN AIR.

This interaction was produced in the 3 in x 3 in Wave-Interaction Tube by using two drivers and a common channel. The schlieren photograph of the (x,t)-plane shows the left shock wave moving at a Mach number of 4.12 from state (5) into state (1) at room temperature and at a pressure of 1.5 torr; while the right shock is moving from (2) into state (1) at a Mach number of 2.17. After the collision the shock waves slow down but the pressure ($p_4 = p_3$) is very much increased. A perfect stable contact surface C_1 is also formed between the two new states (4) and (3).

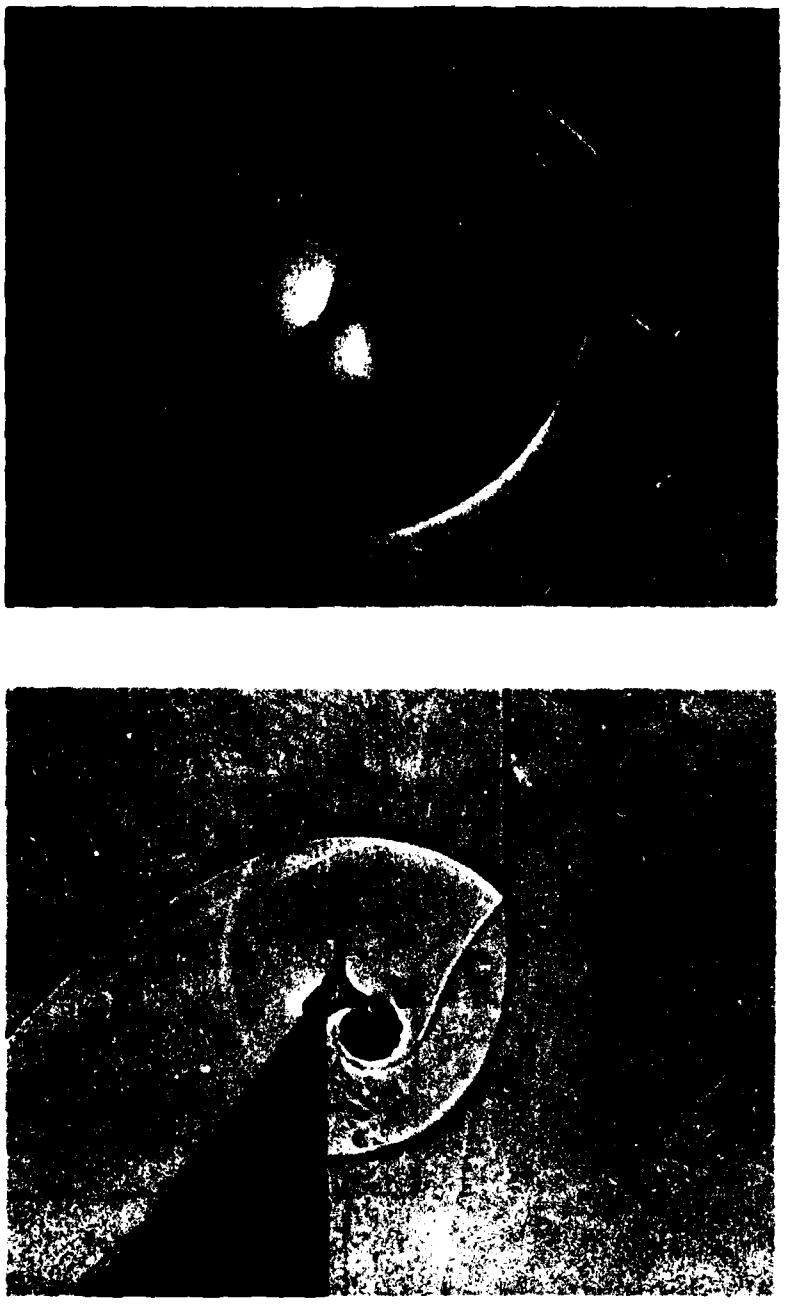

FIG. 11 SCHLIEREN PHOTOGRAPH AND SHADOWGRAM OF PLANAR SHOCK WAVE REFLECTION AND DIFFRACTION PRODUCING A SPIRAL VORTEX.

The incident shock wave S_1 and reflected shock wave S_2 produce a contact surface C. The boundary layer induced by S_1 along the wedge leaves at the apex and rolls up into a vortex-like form V. It is especially clear in the shadowgraph.

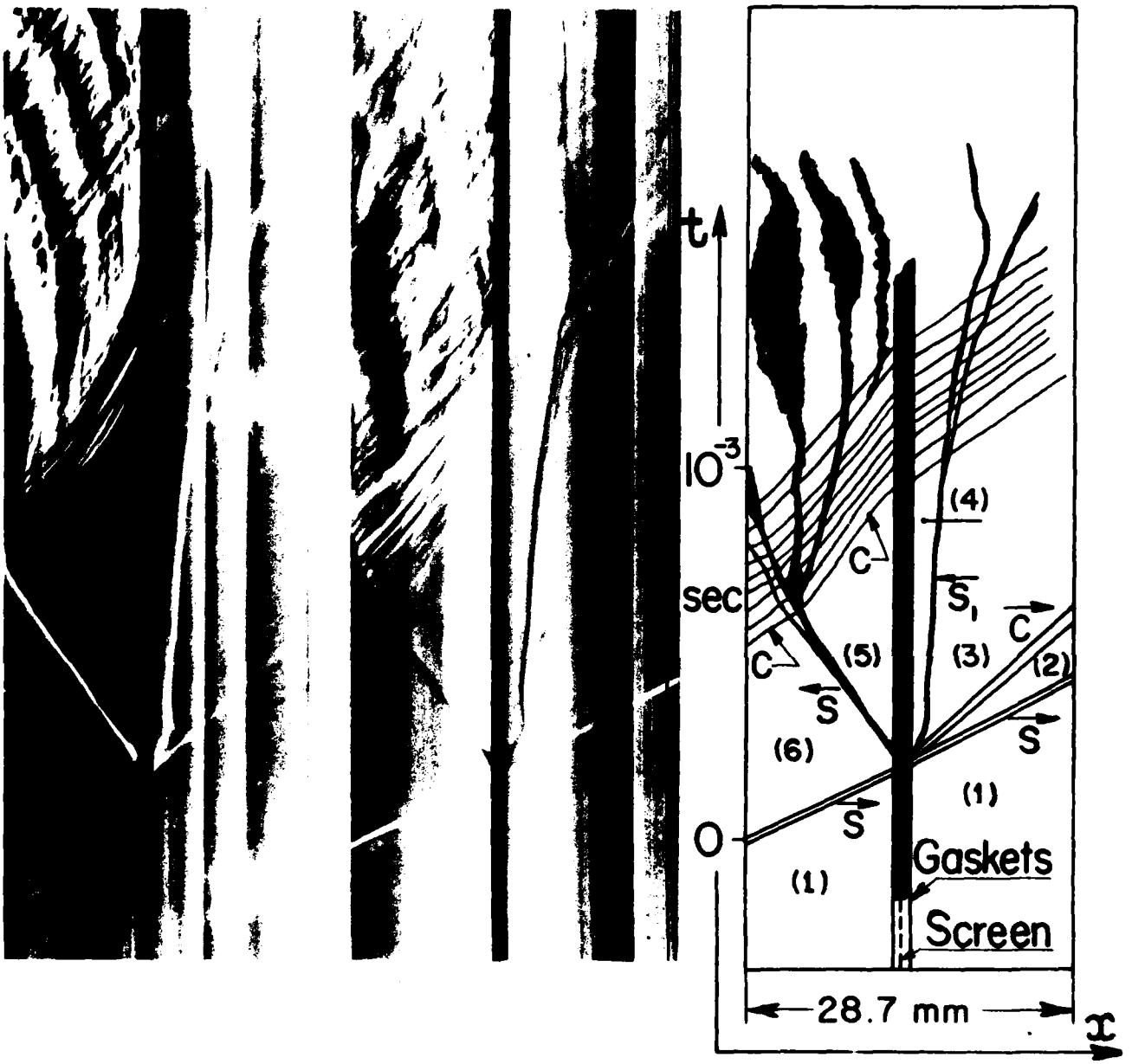

FIG. 12 INTERACTION OF A PLANE SHOCK WAVE WITH A PLANE WIRE SCREEN IN THE (x,t)-PLANE.

The schlieren photograph of the (x,t)-plane shows the shock wave moving from state (6) into state (1) at a Mach number of 1.98 in air at p_1 = 16.1 torr and a_1 = 1138 ft/s. It encounters a 90-mesh screen and is slowed down to M_s = 1.82, thereby producing a new contact surface C, between states (2) and (3) and a reflected shock moving into state (6). The flow through the screen is choked and gives rise to an auxiliary (or second) shock wave S_1 which is swept down by the flow into state (3). The flow Mach numbers in the various states are M_2 = 0.85, M_5 = 0.25, M_6 = 0.96. This flow may be compared with the nozzle flow of Fig. 9.

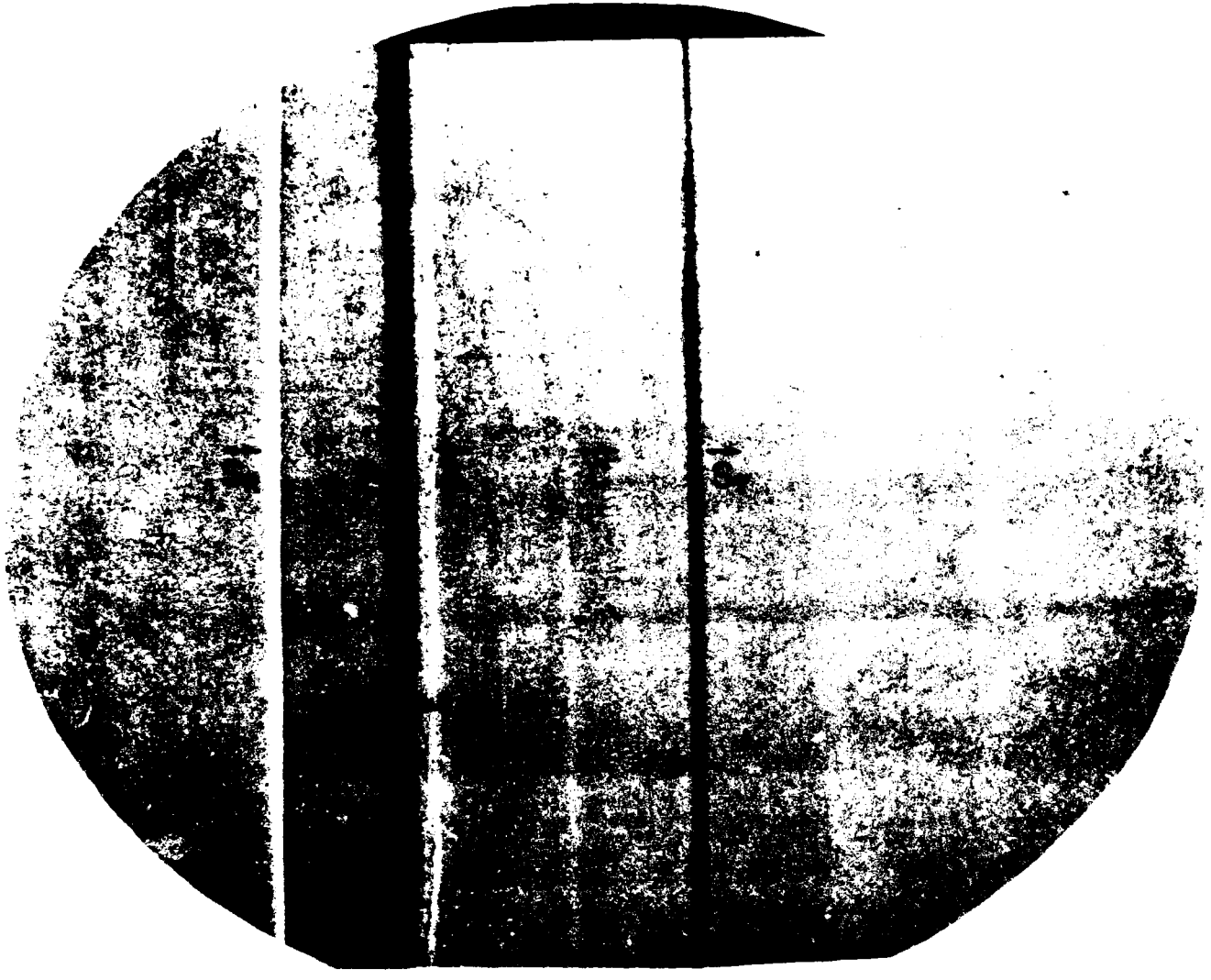

FIG. 13 INTERACTION OF A PLANE SHOCK WAVE WITH A PLANE PERFORATED PLATE IN THE (x,y)-PLANE.

This schlieren record shows a plane shock wave at an initial Mach number of 2.04 moving into air at 20 torr at room temperature and colliding with the perforated plate P, with 50% blockage. The interaction generates a transmitted shock wave S_T, followed by a contact surface C, a reflected shock wave S_R and an auxiliary shock wave S, resulting from the choked flow, which will be swept downstream.

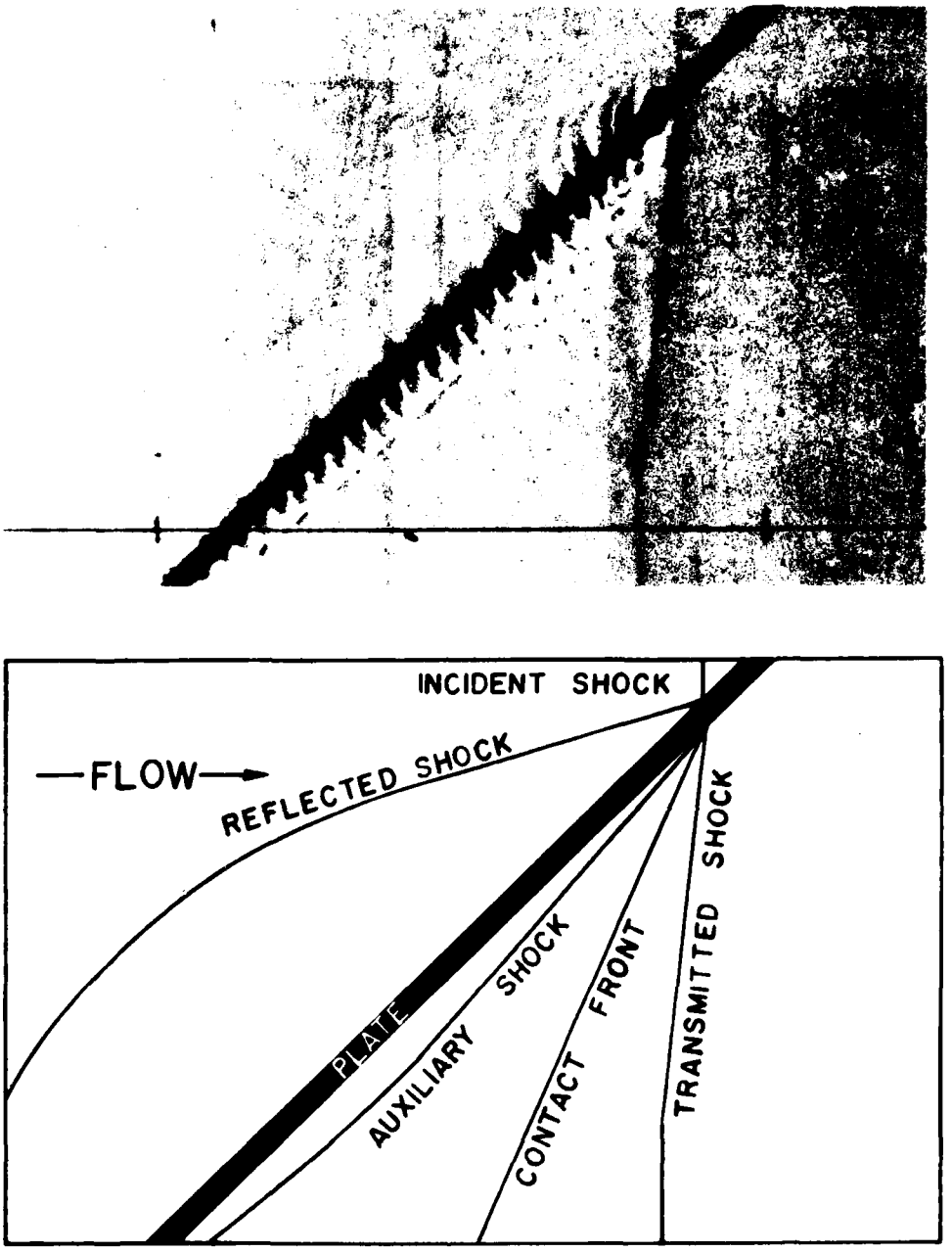

FIG. 14 INTERACTION OF A PLANE SHOCK WAVE WITH AN OBLIQUE PERFORATED PLATE IN THE (x,y)-PLANE.

The schlieren photograph shows a shock wave initially moving at a Mach number of 1.3 choking the inclined (45°) perforated (50% blockage) plate. This produced transmitted and reflected shock waves, a contact front and an auxiliary shock wave from the choked flow. The transverse waves can be reconstructed from an elemental consideration of Fig. 11. The transmitted shock has become perpendicular to the wall as a result of Mach reflection.

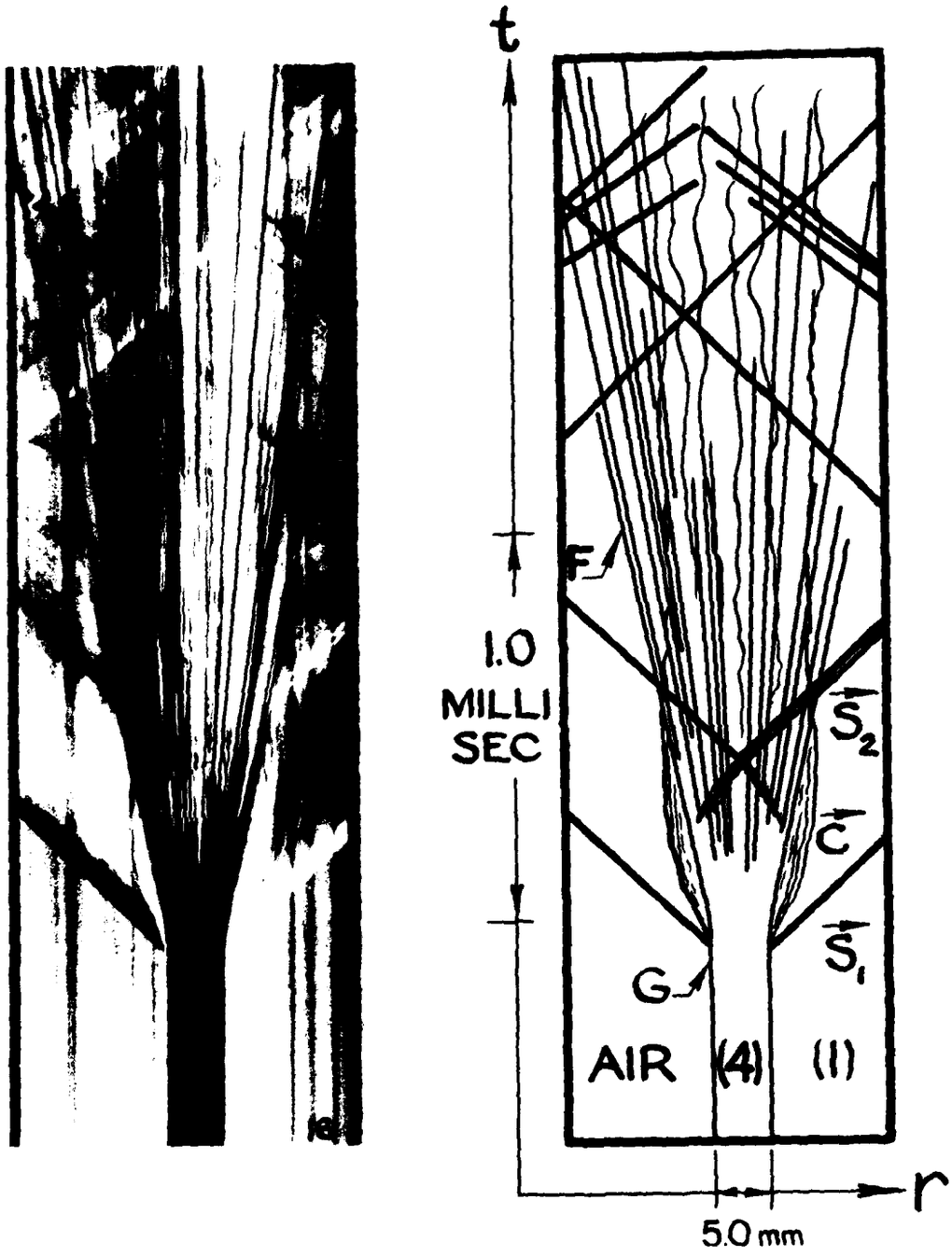

FIG. 15 EXPLODING GLASS SPHERE IN THE (r,t)-PLANE.

A schlieren record and explanatory sketch of the wave system in the distance-time plane produced by rupturing a 2-in dia pressurized glass sphere shows: G, glass sphere still intact; F, shattered sphere fragments; S_1, main shock wave; S_2, second shock wave resulting from the reflected implosion wave; air pressure p_4 = 22 atm, air pressure p_1 = 1.0 atm, temperature $T_1 = T_4$ = 26°C.

FIG. 1b EXPLODING GLASS SPHERE IN THE (x,y)-PLANE.

The explosion was generated in atmospheric air by bursting a 2-in dia glass sphere pressurized with air to 37 atm. The photograph, with a 2-microsecond exposure, was taken 150 microseconds after rupture through overpressure. G = broken glass sphere, C = turbulent contact front, S = shock wave.

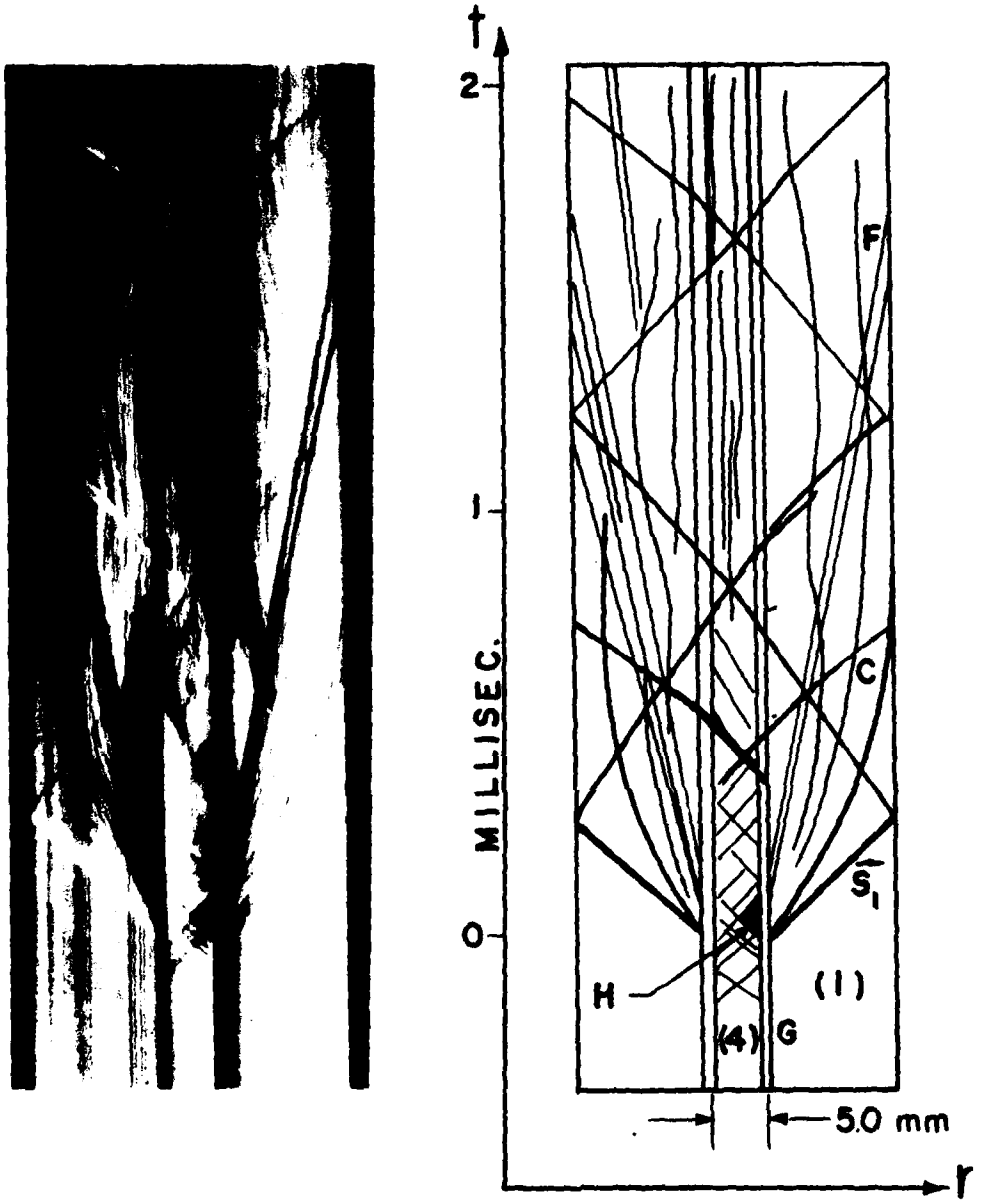

FIG. 17 EXPLODING GLASS CYLINDER IN THE (r,t)-PLANE.

A schlieren record and explanatory sketch of the wave system produced in the distance-time plane by rupturing a pressurized glass cylinder 2-inches in diameter and 2.5 inches long, shows: G, intact glass cylinder to be ruptured mechanically; F, glass fragments; H, head of rarefaction wave; S_1, main shock wave; C, contact surface; air pressure p_4 = 24 atm; air pressure p_1 = 1.0; temperatures $T_1 = T_4 = 27°C$.

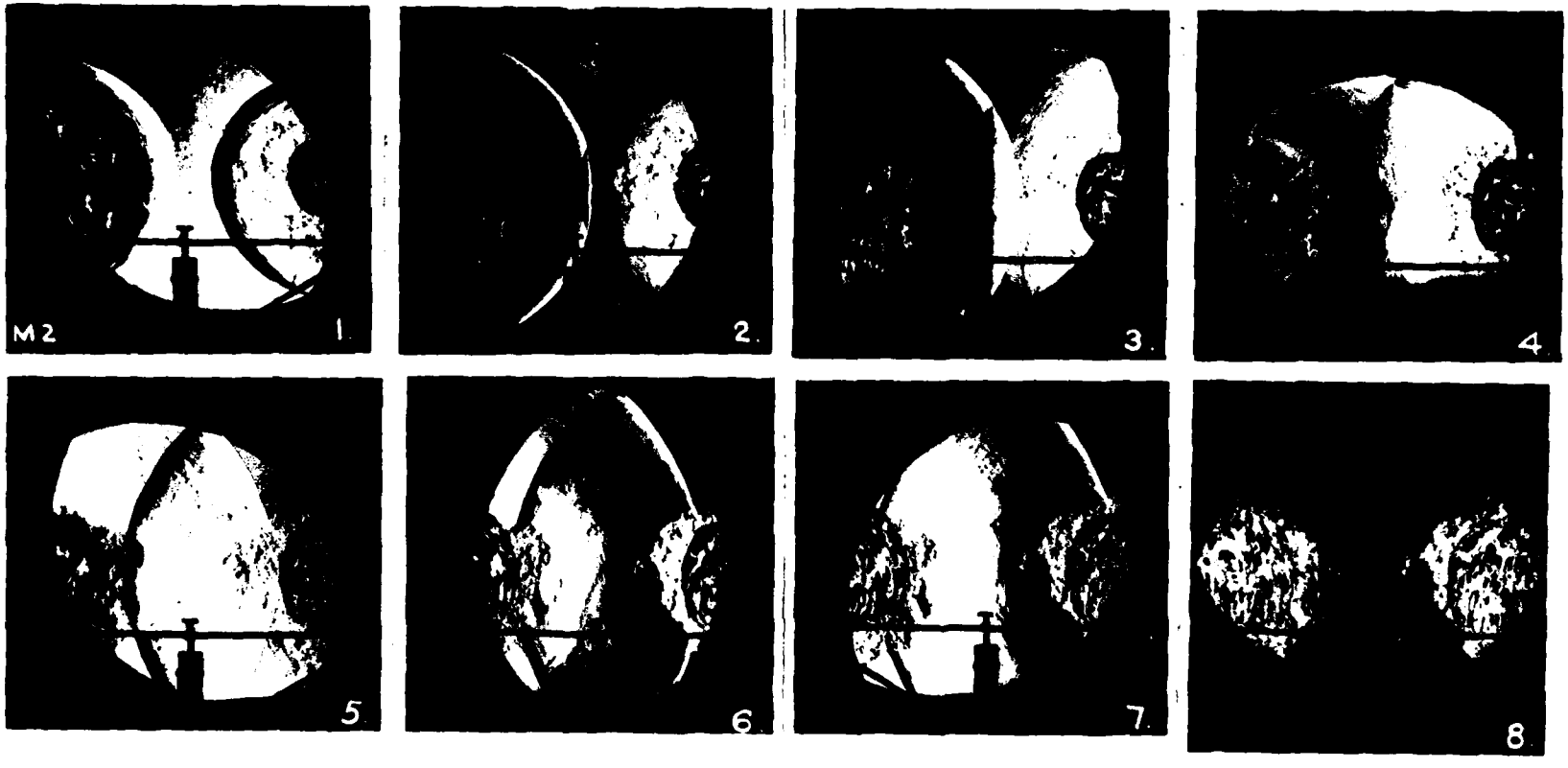

FIG. 18 COLLISION OF TWO SPHERICAL SHOCK WAVES IN THE (x,y)-PLANE.

Schlieren records from a high-speed multiple-spark camera show two ruptured 2-in dia glass spheres with their centres 9-in apart initially filled with helium at 22 atm and 22°C. The approach of the two shock waves shown in frame 1 was taken 250 μs after impact by the breaker. The remaining frames, at 50-μs intervals, record the collision and penetration of the first S_1, and second S_2, shock waves.

FIG. 19 COLLISION OF TWO SPHERICAL SHOCK WAVES IN THE (r,t)-PLANE.

A continuous schlieren photograph complementing Fig. 18, with the same initial conditions. The time and distance scales appear on the photograph. Note that the sphere on the right ruptured 160 μs later than the left sphere and gave rise to a collision of two spherical shock waves of unequal strength.

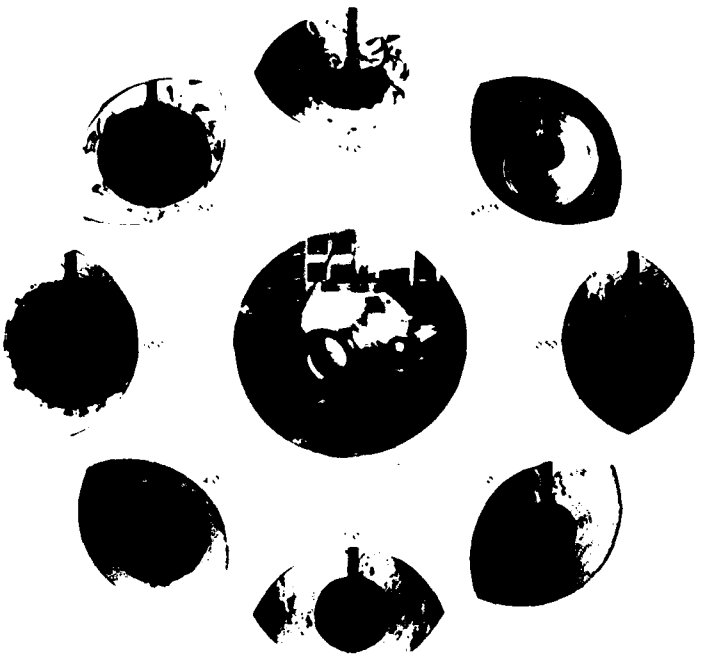

FIG. 20 UNDERWATER EXPLOSION.

A spherical underwater explosion is shown in some detail through schlieren photographs obtained from a high-speed multiple-spark camera with a variable framing rate of from 250 μs to 24 ms with an exposure time of 2 μs. The explosion was generated by bursting a 2-in dia glass sphere filled with carbon-dioxide at 20 atm at a depth of 13 in in a 3-ft dia steel sphere. The water was at 1 atm and 20°C. The times for each frame are given in ms. The central frame shows the intact glass sphere in the water-filled steel sphere prior to the blast. The first frame (upper right) shows the spherical shock wave in water. The remaining frames show the growth and collapse of the oscillating gas bubble as well as the glass fragments.

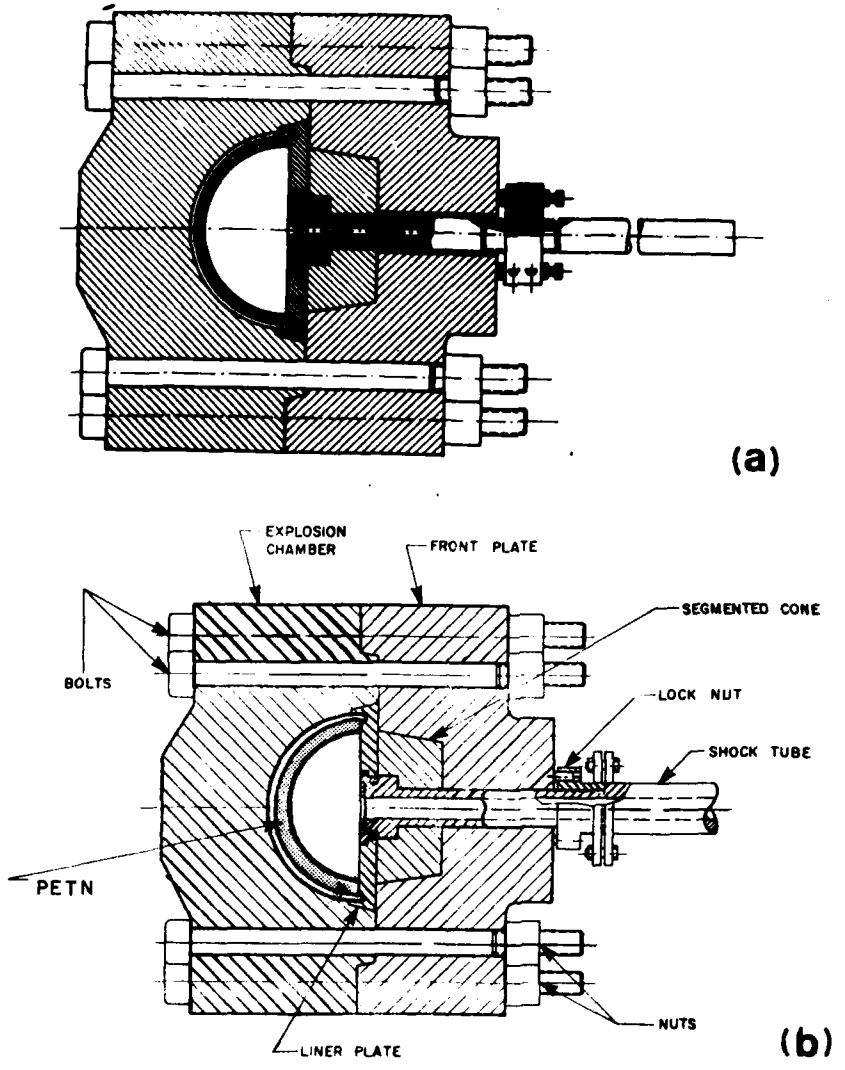

FIG. 21 UTIAS EXPLOSIVE-DRIVEN IMPLOSION CHAMBER IN THE LAUNCHER AND SHOCK-TUBE MODES.

The 8-in (20 cm) dia implosion chamber is shown with an 8-mm dia gun barrel in place in (a) and a 25-mm dia shock tube in (b). An exploded view of a proposed scaled version with a 60-cm dia cavity and a 25-cm dia x 4m long barrel is shown in (c). It is included as it illustrates the construction very well. Basically the implosion chamber consists of a rear large plate containing a hemispherical cavity. A hemispherical copper shell carrying an explosive PETN shell fits into this cavity. Another plate contains the gun barrel or shock tube, an exploding wire assembly, and an admission port for stoichiometric hydrogen-oxygen. The two plates are held by 32 large bolts. The gas is detonated by the exploding wire (d). The resulting detonation wave races to the PETN shell, impacts and detonates the explosive. The reflected gaseous and solid-explosive detonations overtake to form a single implosion, which reflects at the centre of the hemisphere major diameter thereby generating a pocket of plasma at extreme temperatures and pressures, which can be used for many applications.

FIG. 21 - CONTINUED

24 IN DIA HEMISPHERICAL IMPLOSION CHAMBER

1 IN DIA X 13 FT LONG BARREL

OVERALL WEIGHT 32,600 LB.

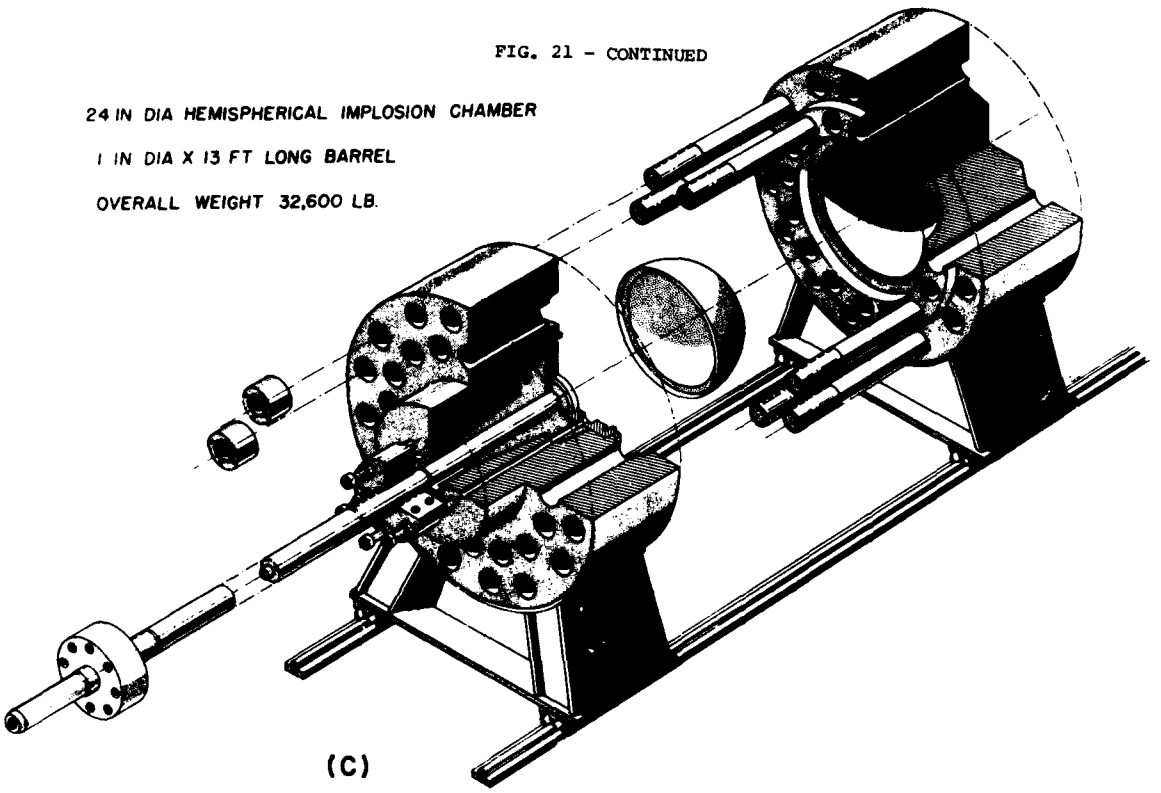

(C)

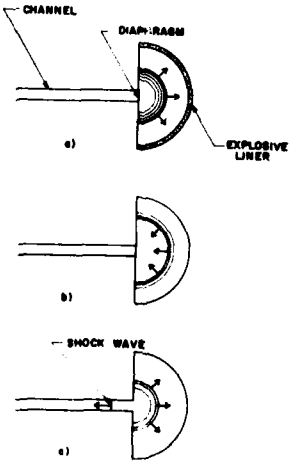

d, Schematic diagram illustrating the principle of operation of the (TIAS implosion-driven shock tube : a) ignition and detonation ; b) implosion phase ; c) reflection and generation of shock wave in the channel.

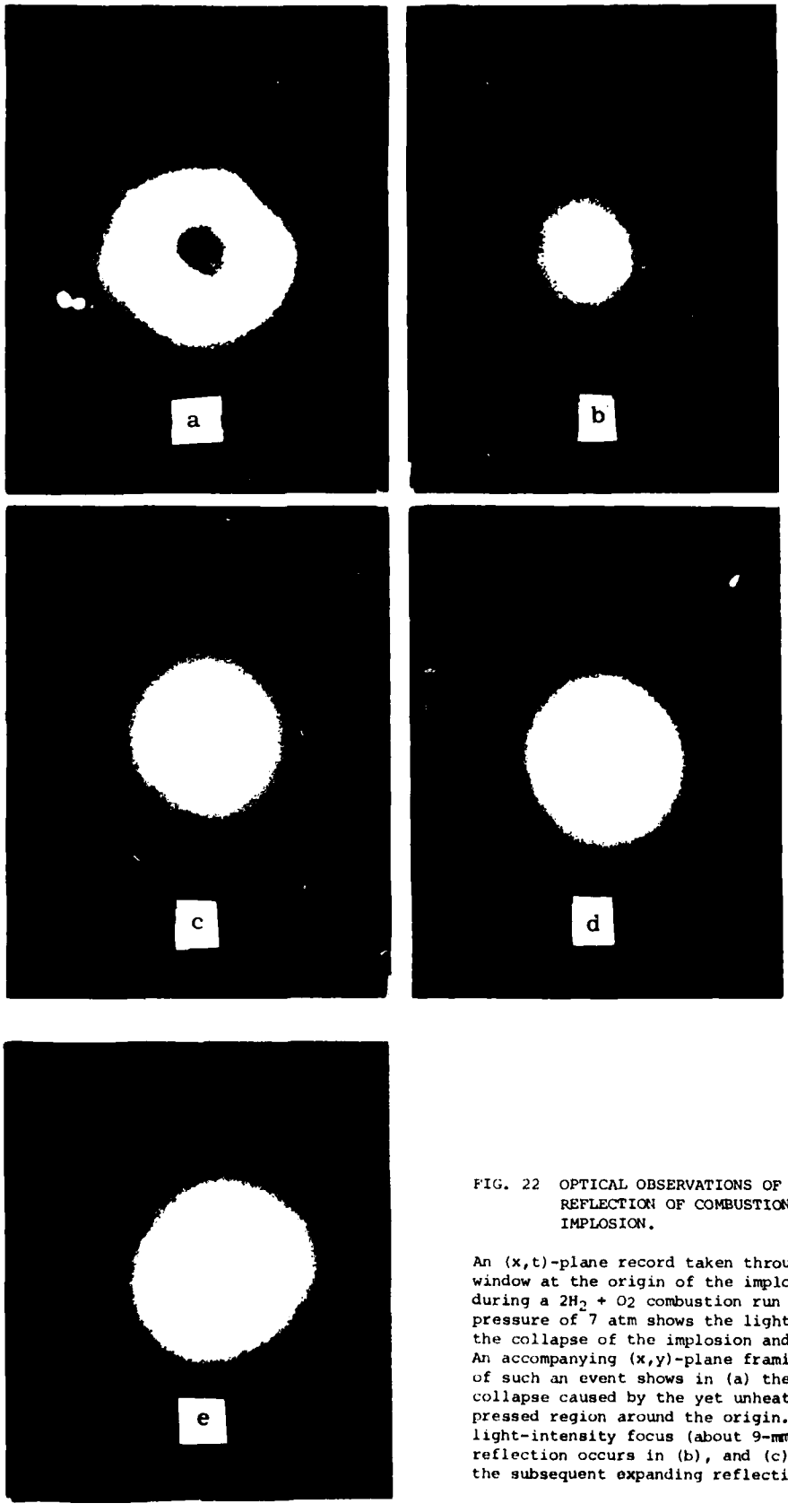

FIG. 22 OPTICAL OBSERVATIONS OF COLLAPSE AND REFLECTION OF COMBUSTION-DRIVEN IMPLOSION.

An (x,t)-plane record taken through a 19-mm dia window at the origin of the implosion chamber during a $2H_2 + O_2$ combustion run at an initial pressure of 7 atm shows the light intensity of the collapse of the implosion and its reflection. An accompanying (x,y)-plane framing-camera record of such an event shows in (a) the doughnut-like collapse caused by the yet unheated and uncompressed region around the origin. The complete light-intensity focus (about 9-mm dia) and its reflection occurs in (b), and (c) to (e) show the subsequent expanding reflection.

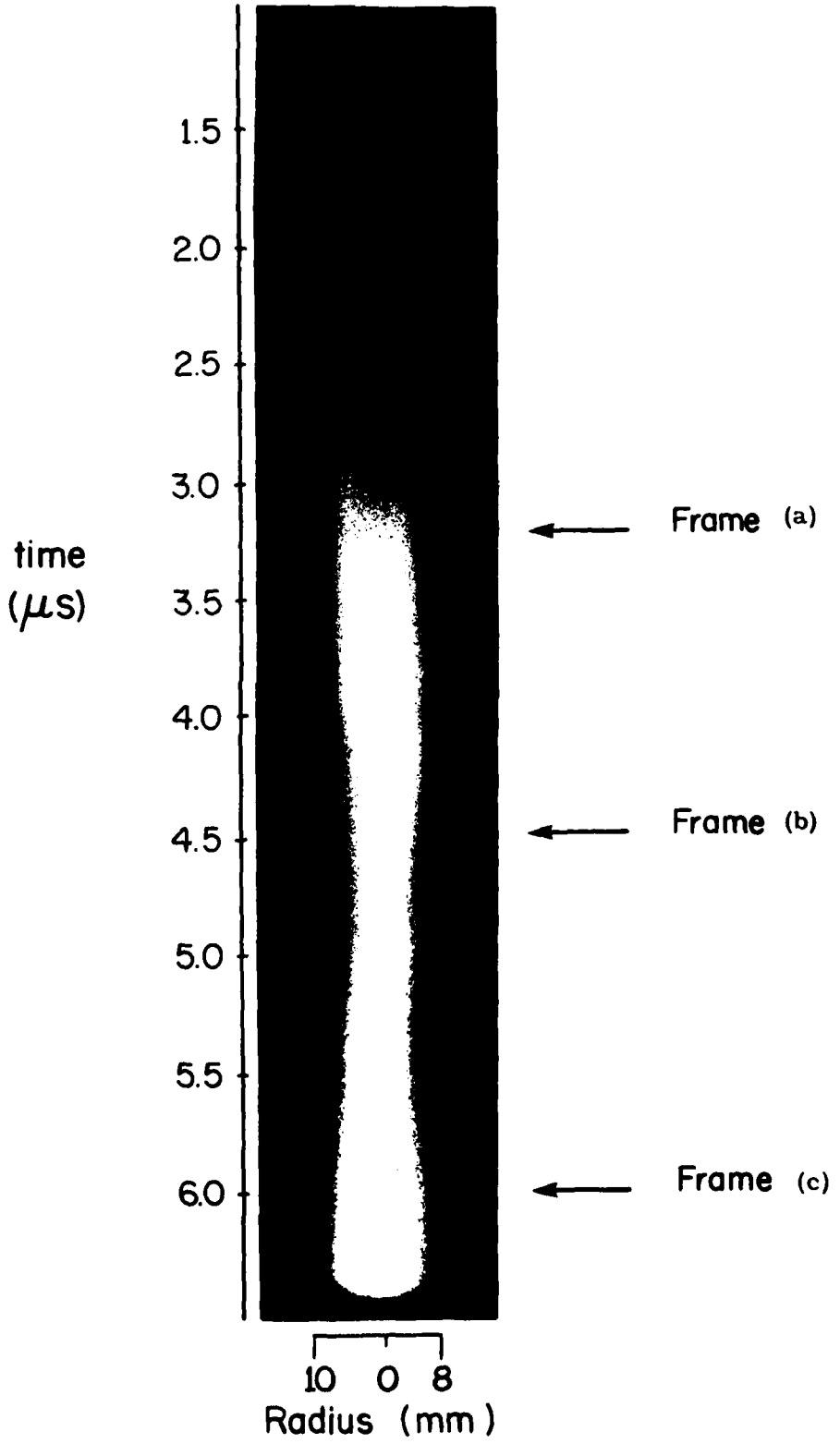

FIG. 22 - CONTINUED

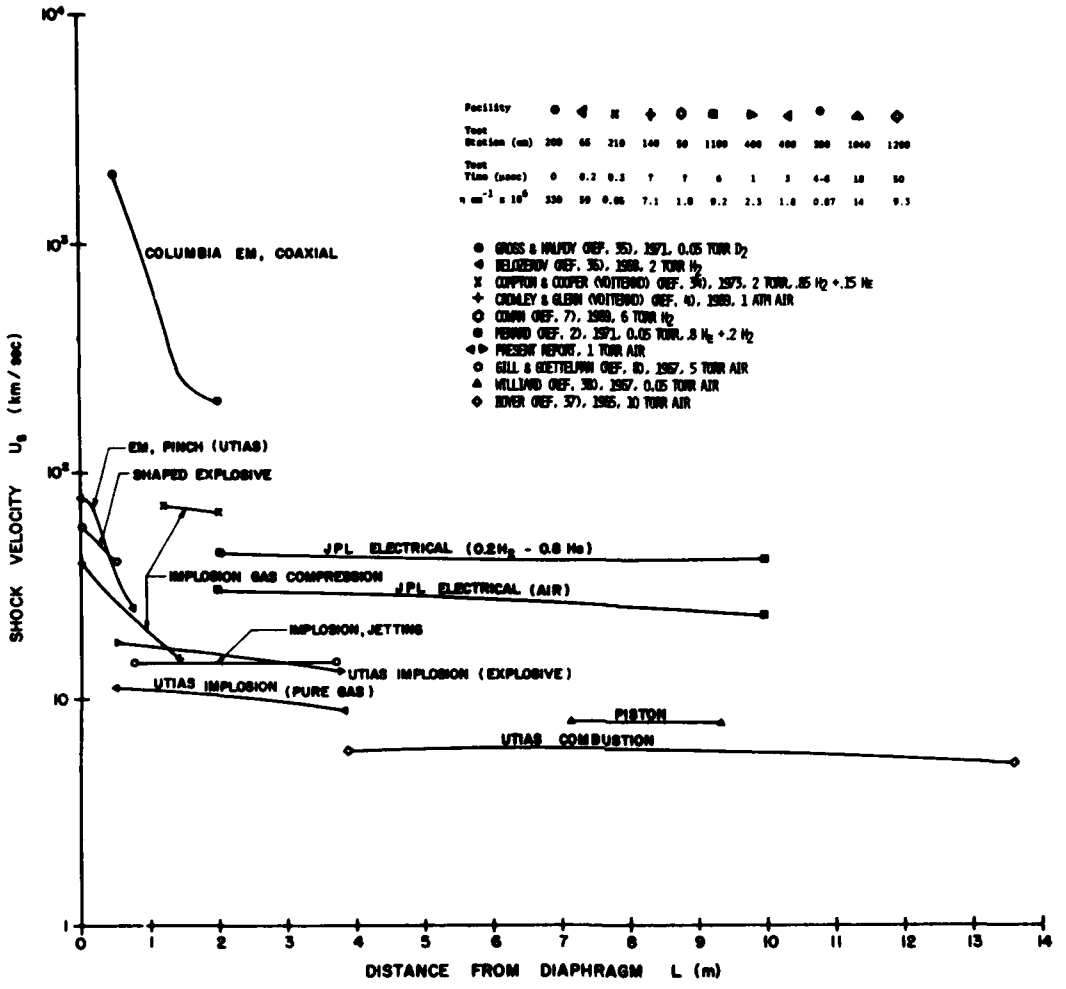

FIG. 23 COMPARISON OF HYPERVELOCITY SHOCK WAVES PRODUCED BY EXPLOSIVE-DRIVEN IMPLOSIONS WITH OTHER FACILITIES.

A comparison is shown of shock-tube performance using a variety of combustion, explosive and electro-magnetic drivers and various channel gases at different initial pressures. The highest velocity of about 2000 km/s achieved by Gross and Hamoy was a significant fraction of the speed of light but with catastrophic attenuation and zero test time. The Voitenko-type driver used by Compton and Cooper provided velocities up to 70 km/s with a 2 cm test length (0.3 μs) of uncontaminated gas behind the shock wave. The electrical drivers of Menard gave excellent shock-wave velocities with very little attenuation. The UTIAS explosive-driven implosion driver provided good shock velocities with moderate attenuation. (References noted in the figure may be found in the present Ref. 83.)

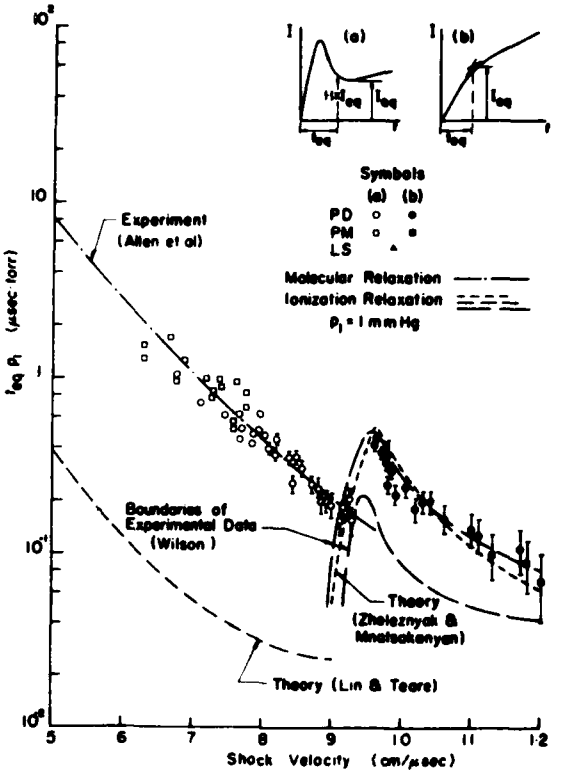

FIG. 24 RADIATIVE RELAXATION EFFECTS IN INTENSE SHOCK WAVES IN AIR.

The product of the relaxation time and initial pressure ($t_{eq} \cdot p_1$) is plotted against shock velocity in cm/μs. Our experimental data from photodiodes (PD), photomultiplier (PM) and laser schlieren (LS) sensors overlap and extend the results by Allen et al (see present Ref. 84). Two types of light intensity (I) vs time (t) records were obtained as shown in inserts (a) and (b). The equilibrium relaxation times (t_{eq}) and intensity (I_{eq}) are also defined. In (a), at lower shock velocities (< 0.95 cm/μs), the intensity in the shock front overshoots the equilibrium value whereas in (b) at higher shock velocities it vanishes. The reason being that initially the electrons are heated intensely by their interactions with the vibrationally excited nitrogen molecules. Consequently, a local overheating of the electron temperature takes place, which exceeds the equilibrium temperature. Subsequently, the emission in the spectral lines and molecular bands overshoot their equilibrium values. As the shock velocity increases more of the nitrogen molecules dissociate and this emission decreases and ultimately vanishes. The steep increase in ionization relaxation between 0.85 and 0.95 cm/μs results from about a 10-fold increase in electron-number density in this range requiring a longer relaxation time.

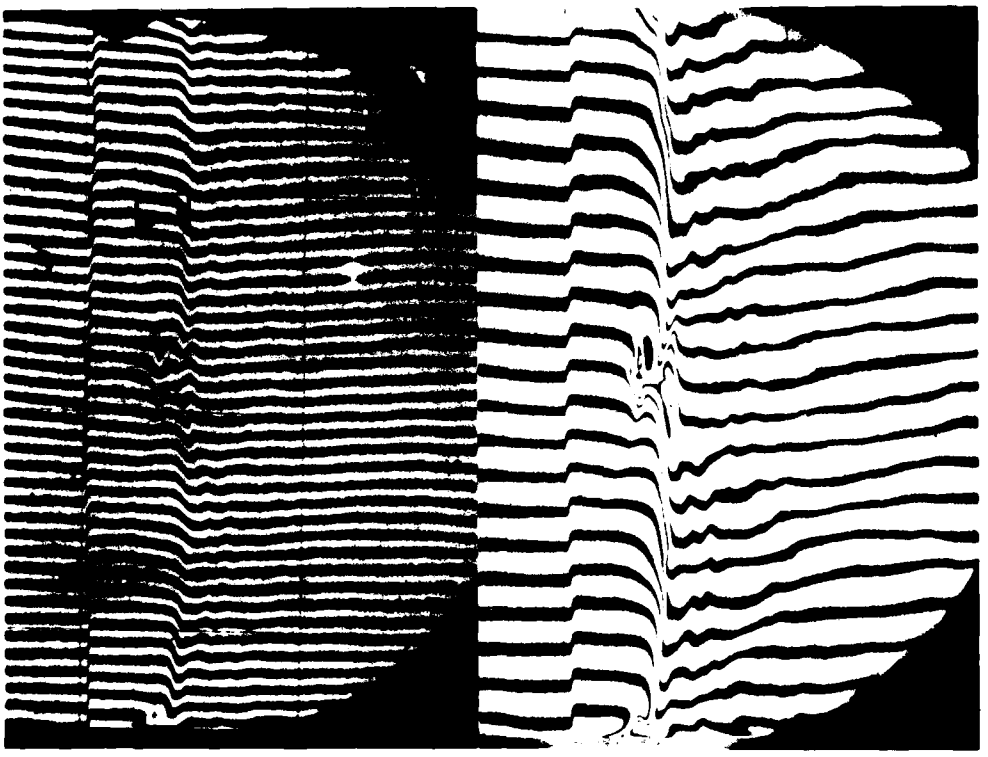

FIG. 25 PLANAR SHOCK-WAVE STRUCTURE IN ARGON.

Two laser interferograms, taken simultaneously at wavelengths λ of 3471 Å (left) and 6943 Å (right), of a shock wave S, moving left at M_S = 17.5 into argon at an initial pressure p = 2.3 torr. A sudden rise is seen in the fringes corresponding to the shock fronts, where the 3 translational degrees of the atom are excited. The fringes drop gradually due to the formation of electrons by atomic collisions and suddenly due to an avalanche of electrons from electron-electron impact (very prominent for the longer wavelength, right, which is more sensitive to the electron refractive index). From these two photographs it is possible to measure the electron number density and the total density of the plasma as well as the ionization relaxation length L, or time.

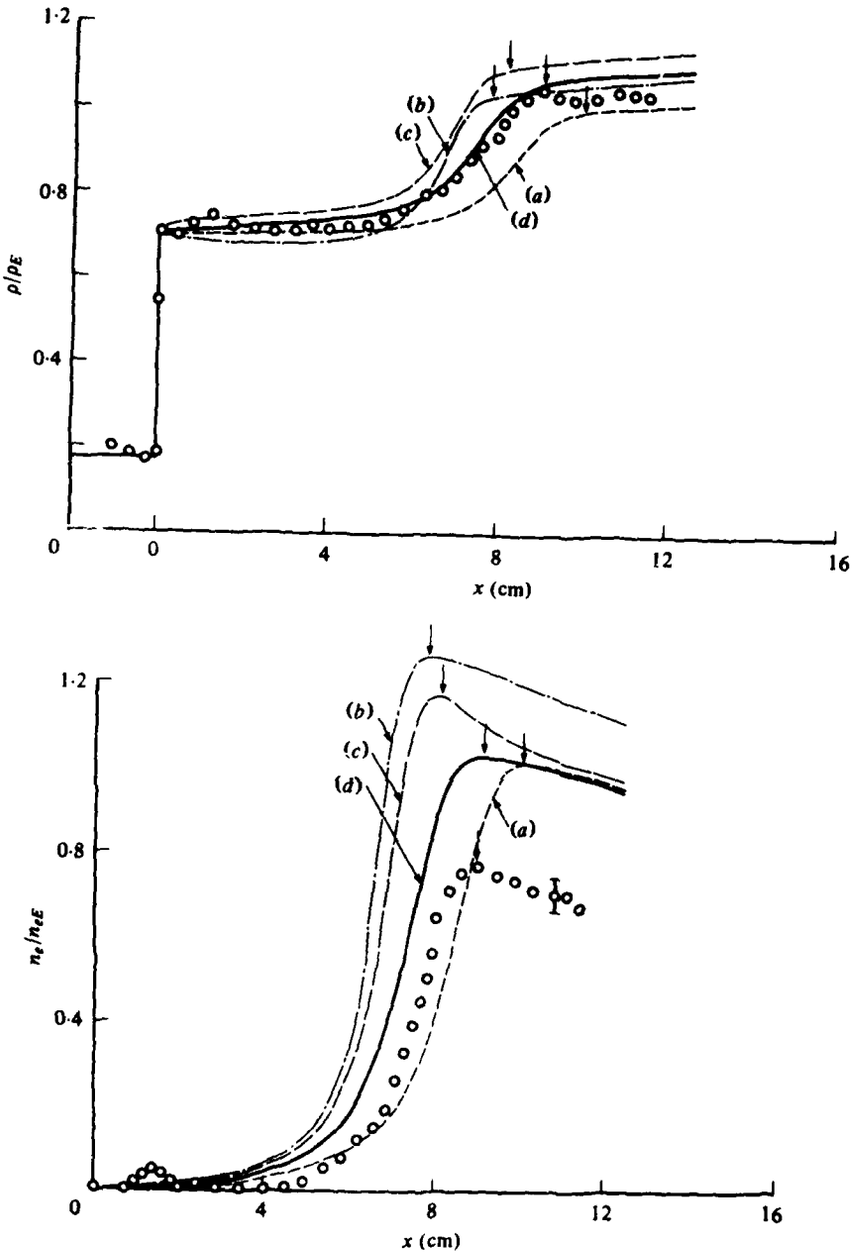

FIG. 26 TOTAL PLASMA DENSITY AND ELECTRON-NUMBER DENSITY IN AN IONIZING SHOCK-WAVE STRUCTURE IN ARGON.

The variation of the normalized total plasma density ρ/ρ_E with distance x is shown in (a) for M_s = 13.1, and initial pressure p = 5.16 torr and temperature 300K; ρ_E is the final equilibrium value. In (b) is shown the normalized electron number density. The solid line represents the best analysis done at UTIAS to date. The other lines represent less stringent models. The agreement of the total density profile with the interferometric measurements (see Fig. 25) is very good, but not so fair for the electron number density. The arrows indicate the equilibrium values for each model and experiment.

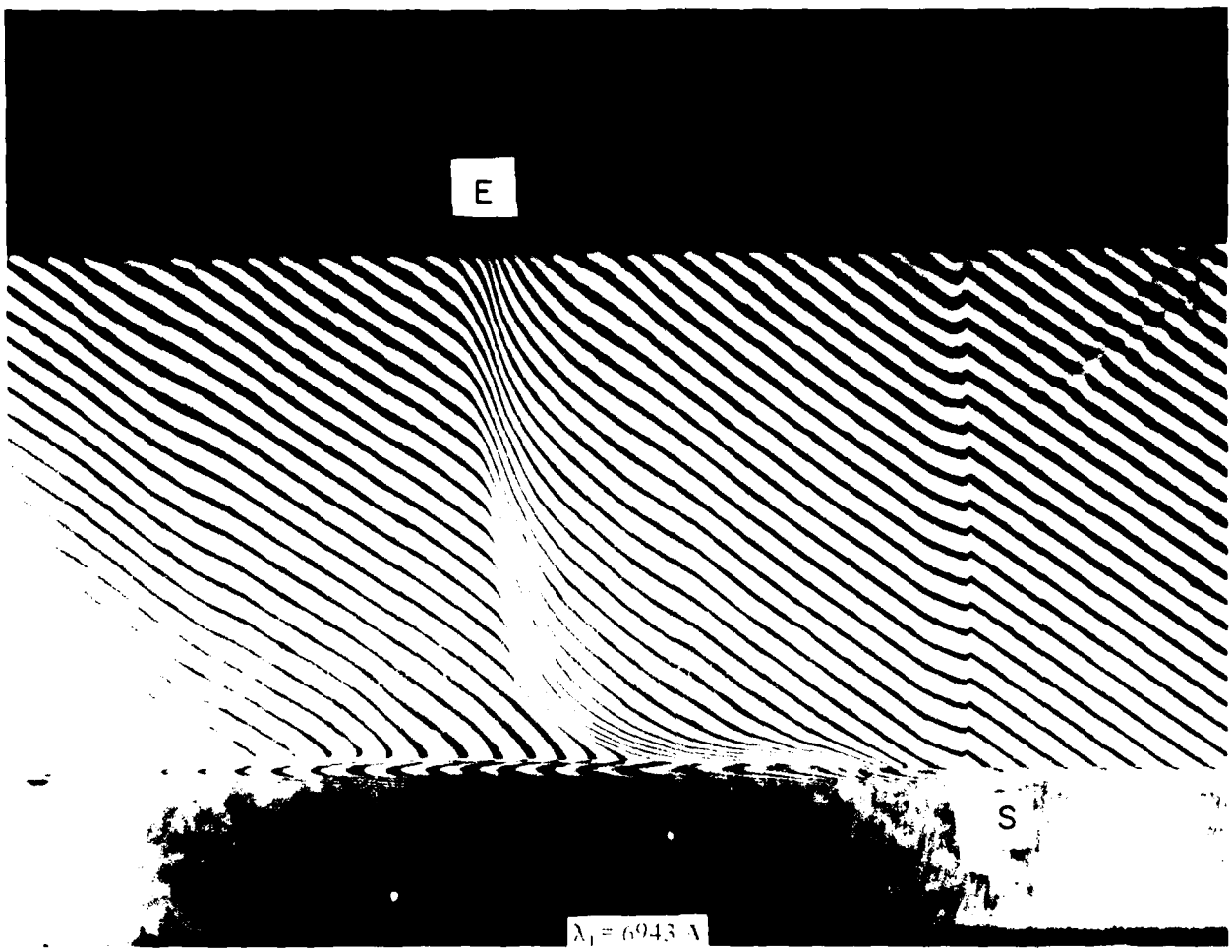

FIG. 27 APPROACH OF THE ELECTRON-CASCADE FRONT AND THE TRANSLATIONAL SHOCK WAVE NEAR THE WALL IN IONIZING ARGON.

An interferogram taken at λ_1 = 6943 Å of a shock wave moving to the right into argon. M_s = 15.9, p_o = 5.1 torr and T = 298 K. The translational shock-wave front S and the electron-cascade front E are clearly shown; the distance between them is the relaxation zone x_E = 2.1 cm; cross wires (+) are at 1.0 cm. Note how E approaches S near the wall and the build up of the side-wall boundary layer from S to the left.

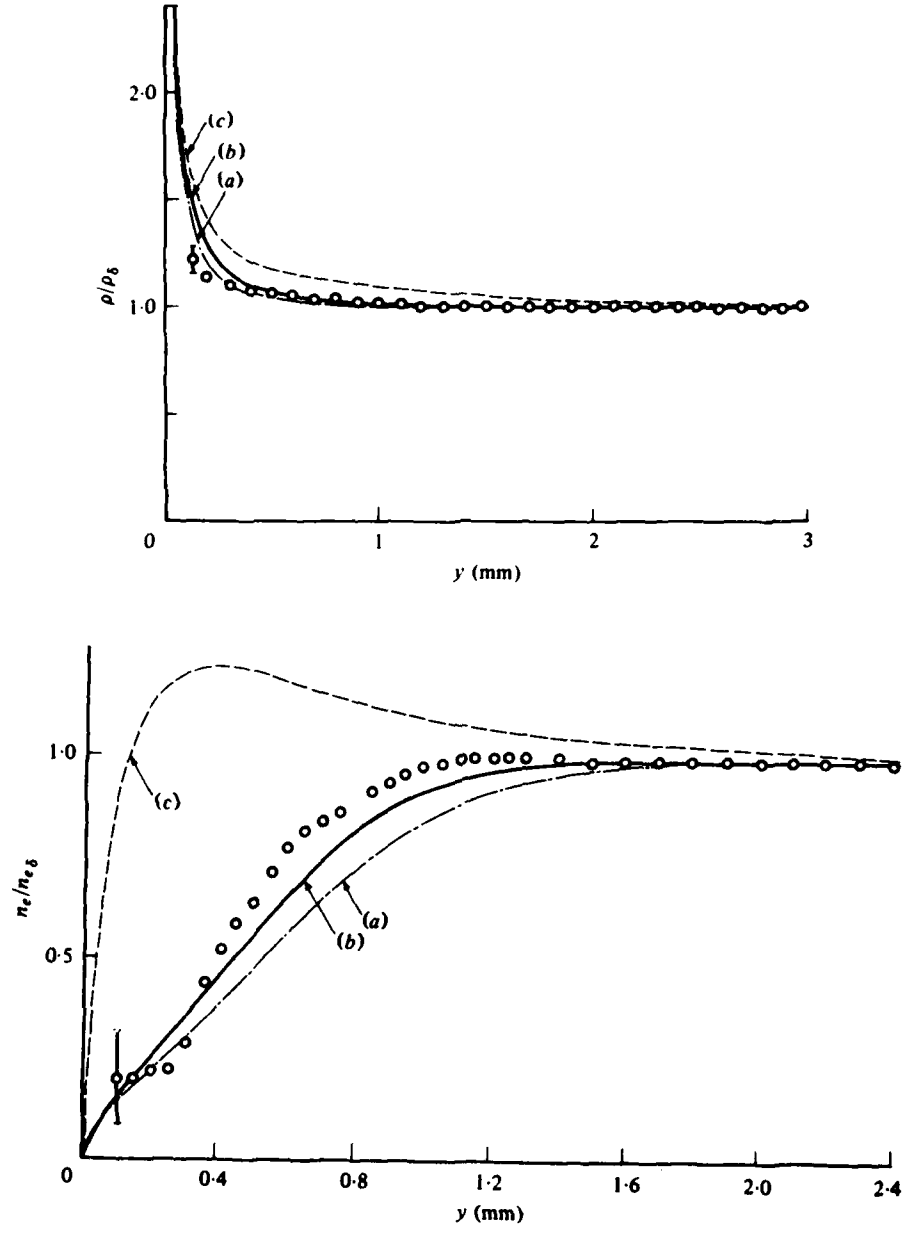

FIG. 28 TOTAL-PLASMA-DENSITY AND ELECTRON-NUMBER-DENSITY PROFILES OF LAMINAR SIDE-WALL BOUNDARY LAYER IN IONIZING ARGON.

A comparison of analytical and interferometric results of the normalized total density ρ/ρ_δ with distance from the wall y is shown in (a) and of the electron-number density $n_e/n_{e\delta}$ in (b), at a distance behind the shock wave of 9.5 cm, for M_s = 13.1, p = 5.16 torr, T = 300 K. The analytical curves are: (a) first-order result, (b) best analysis, (c) frozen solution; δ signifies conditions at the boundary-layer edge. The agreement with model (b) is very satisfactory.

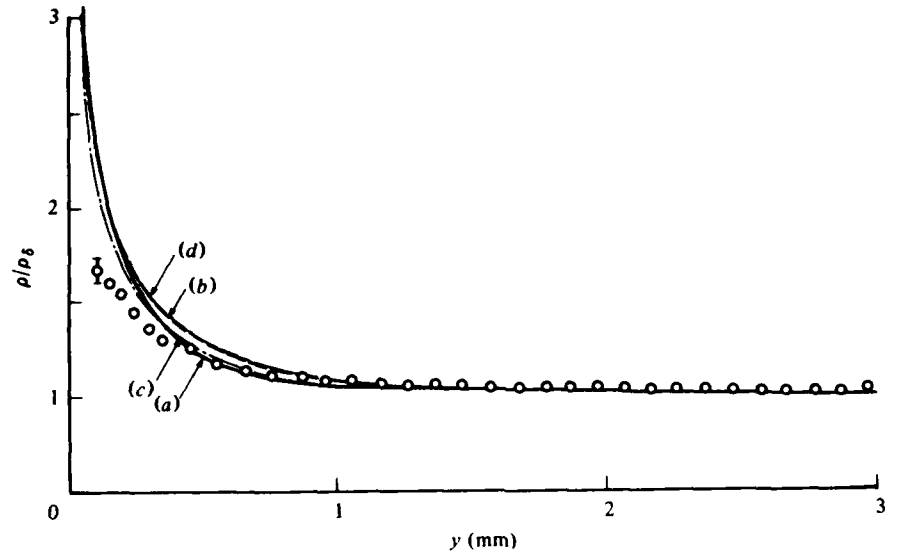

(a)

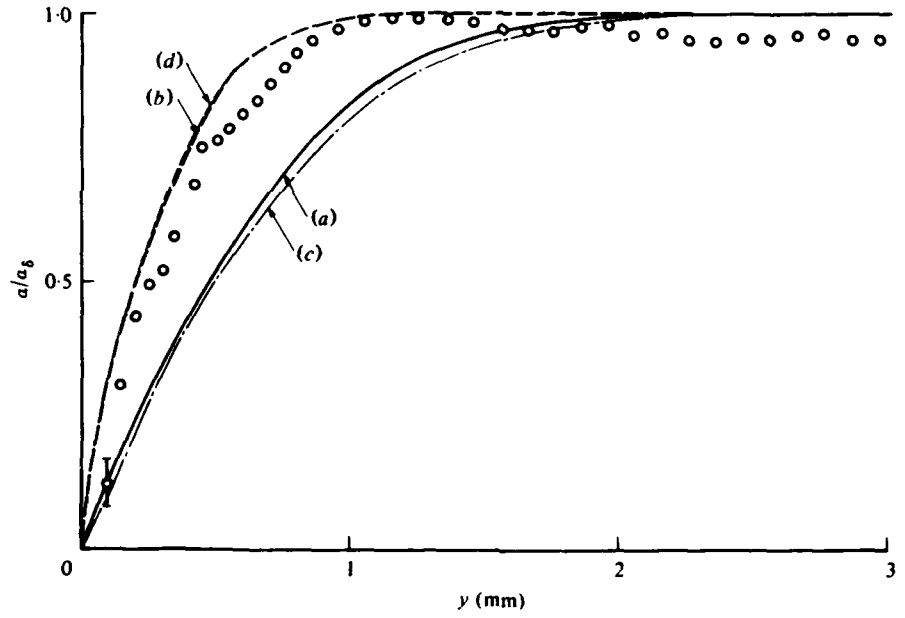

(b)

FIG. 29 TOTAL-PLASMA-DENSITY AND DEGREE OF IONIZATION PROFILES OF A LAMINAR FLAT-PLATE BOUNDARY LAYER IN IONIZING ARGON.

A comparison of analytical and experimental results of the normalized total density ρ/ρ_δ with distance from the wall y is shown in (a) and of the electron number density $\alpha/\alpha_{e\delta}$ in (b) at a distance from the leading edge x = 14.0 cm for M_s = 12.8, p = 5.01 torr and T = 297K. The analytical curves are: (a) nonequilibrium, (b) frozen, (c) first-order nonequilibrium, (d) first-order frozen. The total-plasma-density models are not significantly different for the experimental data to differentiate between them. However, the electron number density models are sensitive and the interferometric data is in better agreement with the frozen flow solutions.

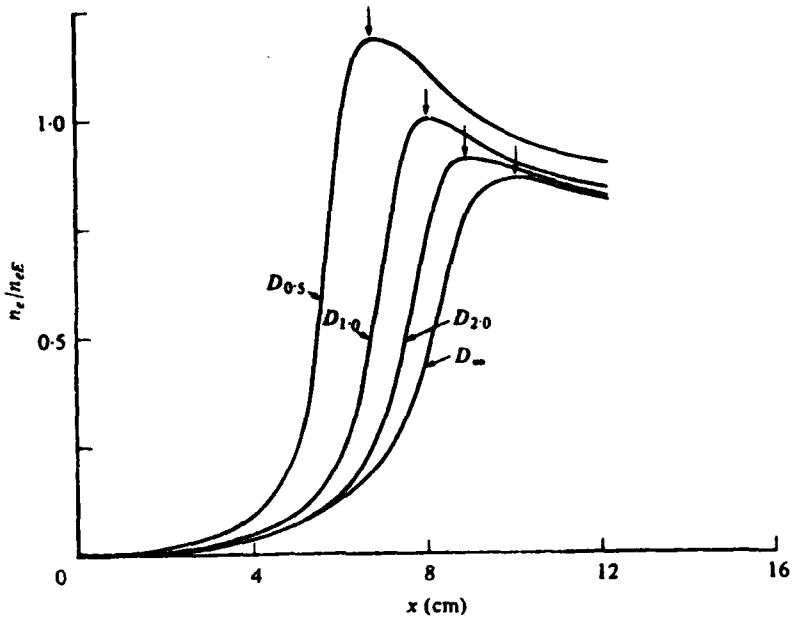

FIG. 30 EFFECT OF SHOCK-TUBE DIAMETER ON SHOCK-WAVE STRUCTURE IN IONIZING ARGON.

The variation of the normalized electron-number-density profiles n_e/n_{eE} with distance x for various shock-tube hydraulic diameters D, indicate how important this quantity is in determining the shape and size of the profile. The case illustrated in Fig. 26 was chosen as an example for M_s = 13.1, p_1 = 5.16 torr and T = 300 K. For the present tube, 10 cm x 18 cm, D_1 = 12.9; other D's are in proportion. It is seen that the relaxation lengths (from 0 to arrow) decrease and the electron number density increases as the shock-tube diameter decreases. Consequently, the effects of the sidewall boundary layer on shock structure increases with decreasing tube diameter.

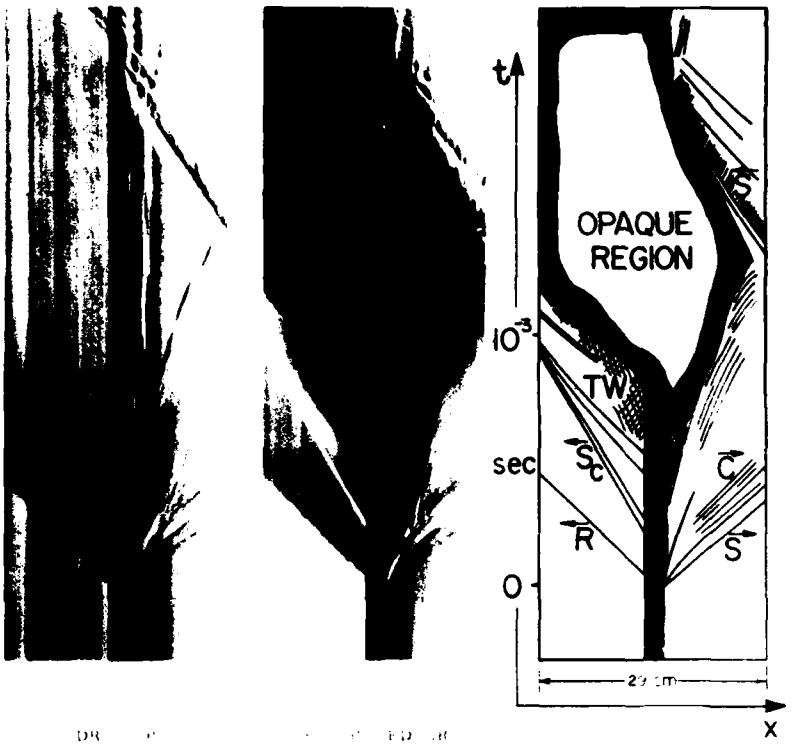

FIG. 31 CONDENSATION SHOCK WAVES IN THE (x,t)-PLANE.

If a moist gas is used in the driver gas, then on breaking the diaphragm the rapid cooling in the rarefaction wave R, with the consequent release of the latent heat of vaporization, results in a condensation shock wave S_c. Its path is clearly shown on the schlieren record for saturated air in a 7.6 cm x 7.6 cm shock tube. The opaque region is one of condensation. The condensation shock-wave birth-point occurs at the tail of the rarefaction wave to the right of the t-axis and is masked by the rupturing diaphragm. The saturated air in the driver was at 1 atm and 297 K with air in the channel at 30 torr, at a diaphragm pressure ratio of 25.

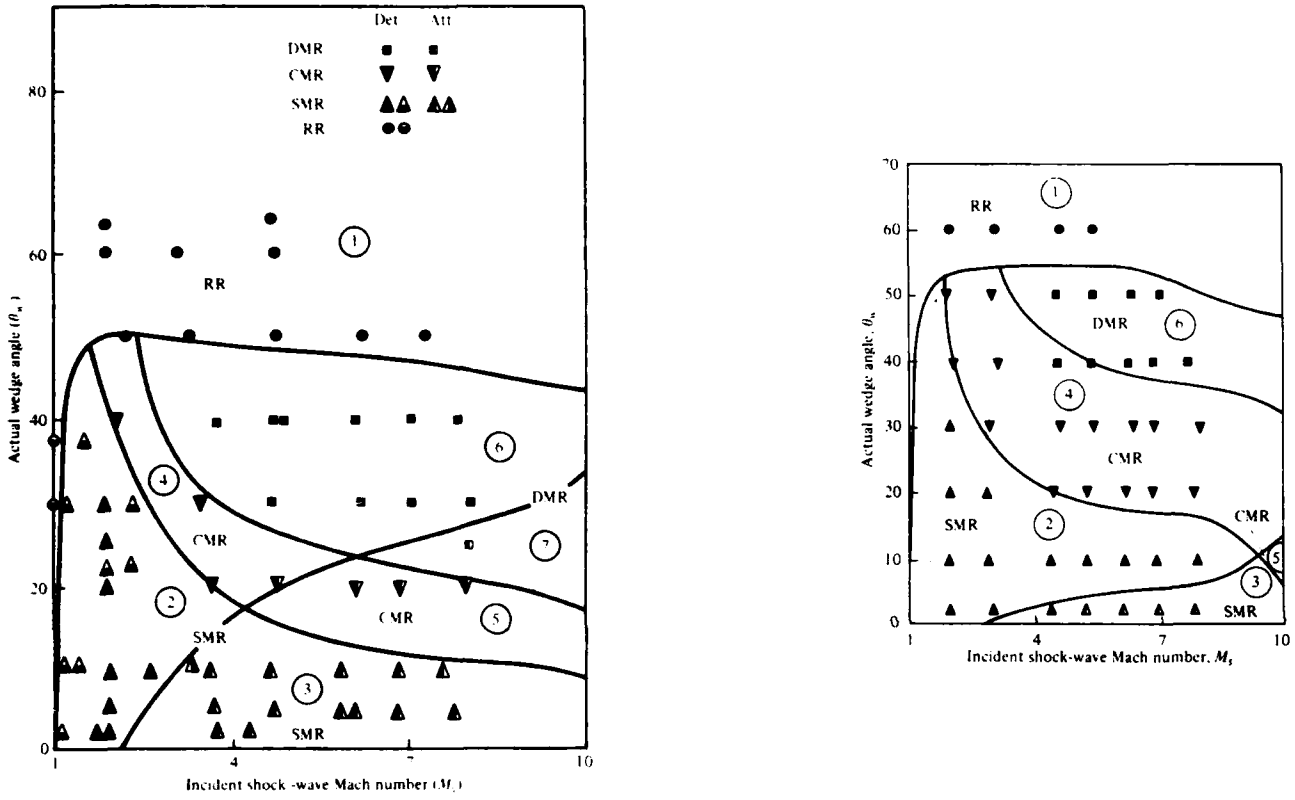

FIG. 32 COMPARISON OF ANALYSIS AND EXPERIMENT ON THE REGIONS AND THEIR TRANSITION BOUNDARIES OF REGULAR (RR), SINGLE MACH (SMR), COMPLEX MACH (CMR) AND DOUBLE MACH (DMR) REFLECTIONS IN THE MACH-NUMBER WEDGE-ANGLE (M_S, θ_W)-PLANE.

(a) Diatomic gas; note the upper area from the right-running upward line is for detached shock waves at the wedge angle and the lower area for attached waves. ⊖, ⧋, ⧊, air (data from White 1951); ●, ■, ◘, ▼, ▽, ▲, △, nitrogen (Ben-Dor & Glass 1978); ———, imperfect nitrogen, P_O = 15 torr, T_O = 300 K.

(b) Monatomic gas, imperfect argon, P_O = 15 torr, T_O = 300 K. Detached shock wave: ■, DMR; ▼, CMR; ▲, SMR; ●, RR. Attached shock wave: △, SMR.

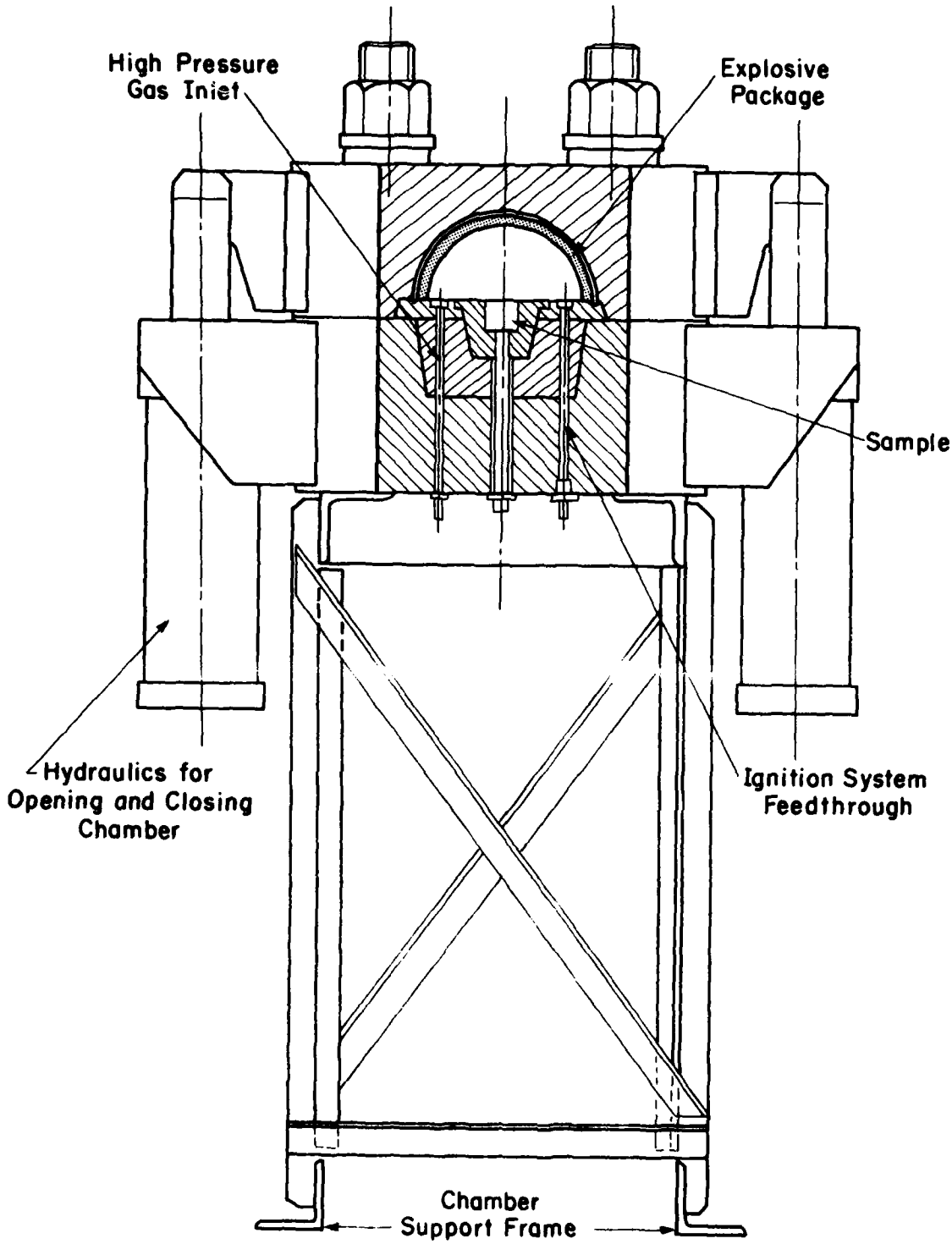

FIG. 33 MECHANIZED NEW IMPLOSION CHAMBER.

This new 20-cm dia implosion chamber is being used by 3M Canada Inc. at UTIAS under the direction of Dr. N. Salansky. The basic design is unchanged. The four hydraulic jacks can rapidly open and close the chamber once the 4 large nuts have been unfastened, rather than the 32 nuts used in the older design. The fact that the major diameter is horizontal (rather than vertical as in the older design) has much improved the focussing of the implosions.

X-RAY DIFFRACTION PATTERN OF A GRAPHITE - IRON MIXTURE AFTER AN EXPERIMENT AND SEPARATION (Diamond X-Ray Pattern is given below for comparison)

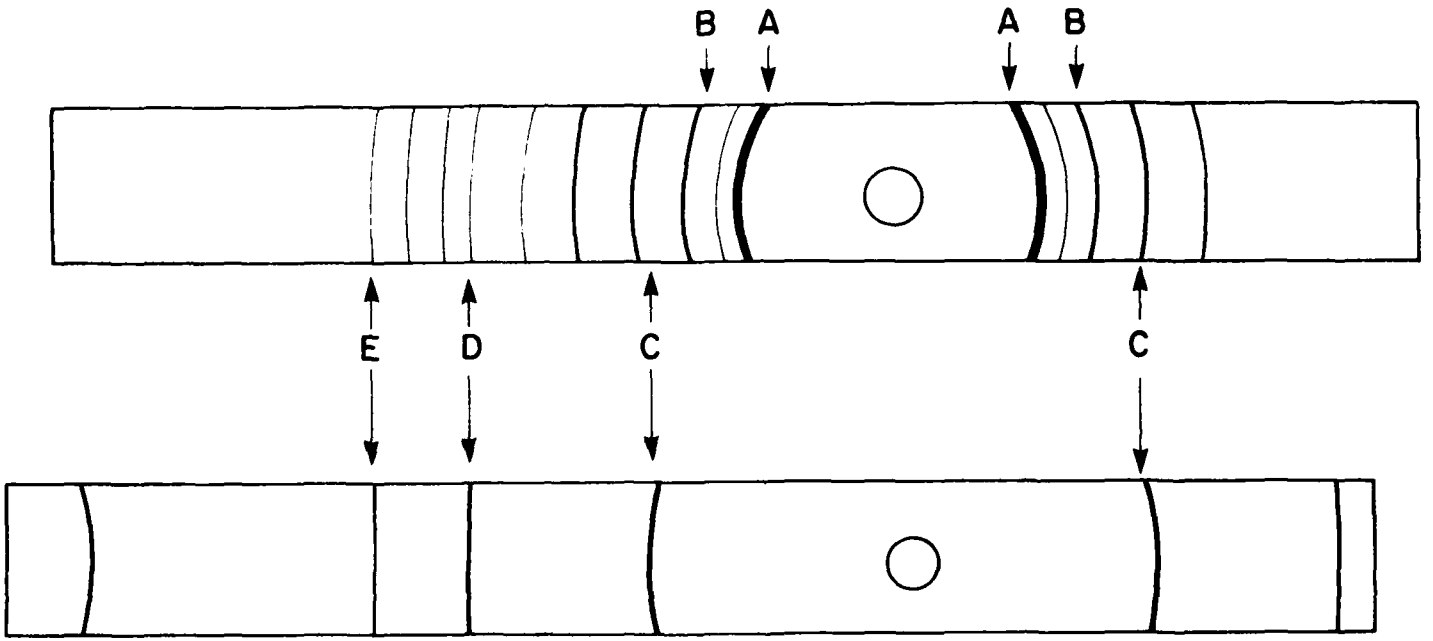

A - Graphite Line (d=3.35 Å)
B - Iron Oxide Line (d = 2.52 Å) due to Separation
C, D, E - Diamond Lines (d = 2.06 Å , d = 1.26 Å , d = 1.08 Å)

(a)

FIG. 34 X-RAY AND ELECTRON DIFFRACTION AND PHOTOMICROGRAPHS OF GRAPHITE AND DIAMONDS.

(a) X-ray diffraction pattern of a graphite-iron mixture after an experiment and separation (diamond X-ray pattern is given below for comparison). A - graphite line (d = 3.35 Å); B - iron oxide line (d = 2.52 Å) due to separation; C, D, E - diamond lines (d = 2.06 Å, d = 1.26 Å, d = 1.08 Å).

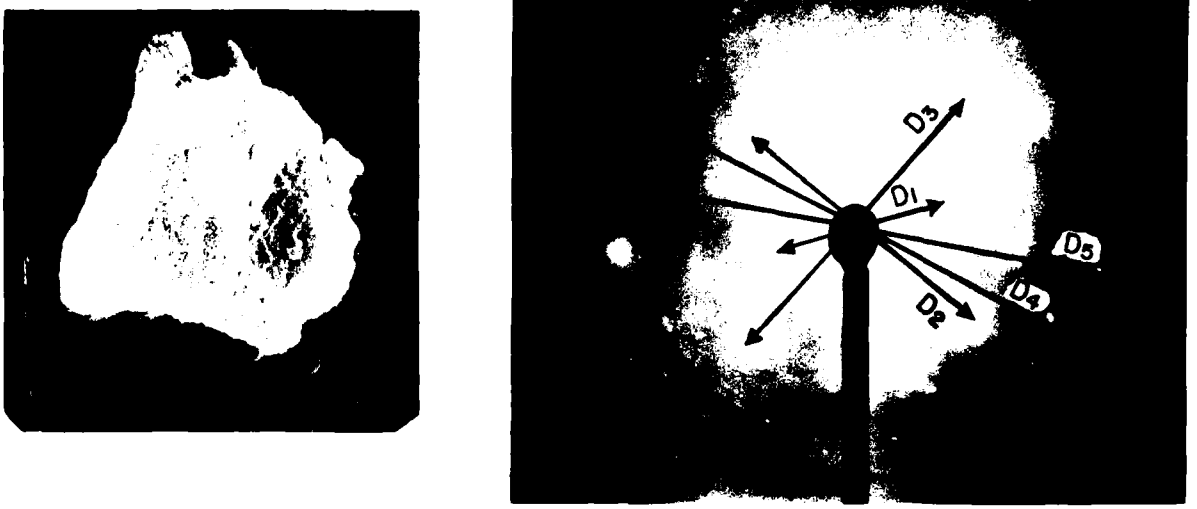

(b)

FIG. 34 - CONTINUED

(b) (i) Electron diffraction of a shocked graphite particle showing the diamond reflection rings D_1 to D_{11}.
(ii) Electron scanning micrograph of a shocked graphite diamond particle magnitified by 4000.

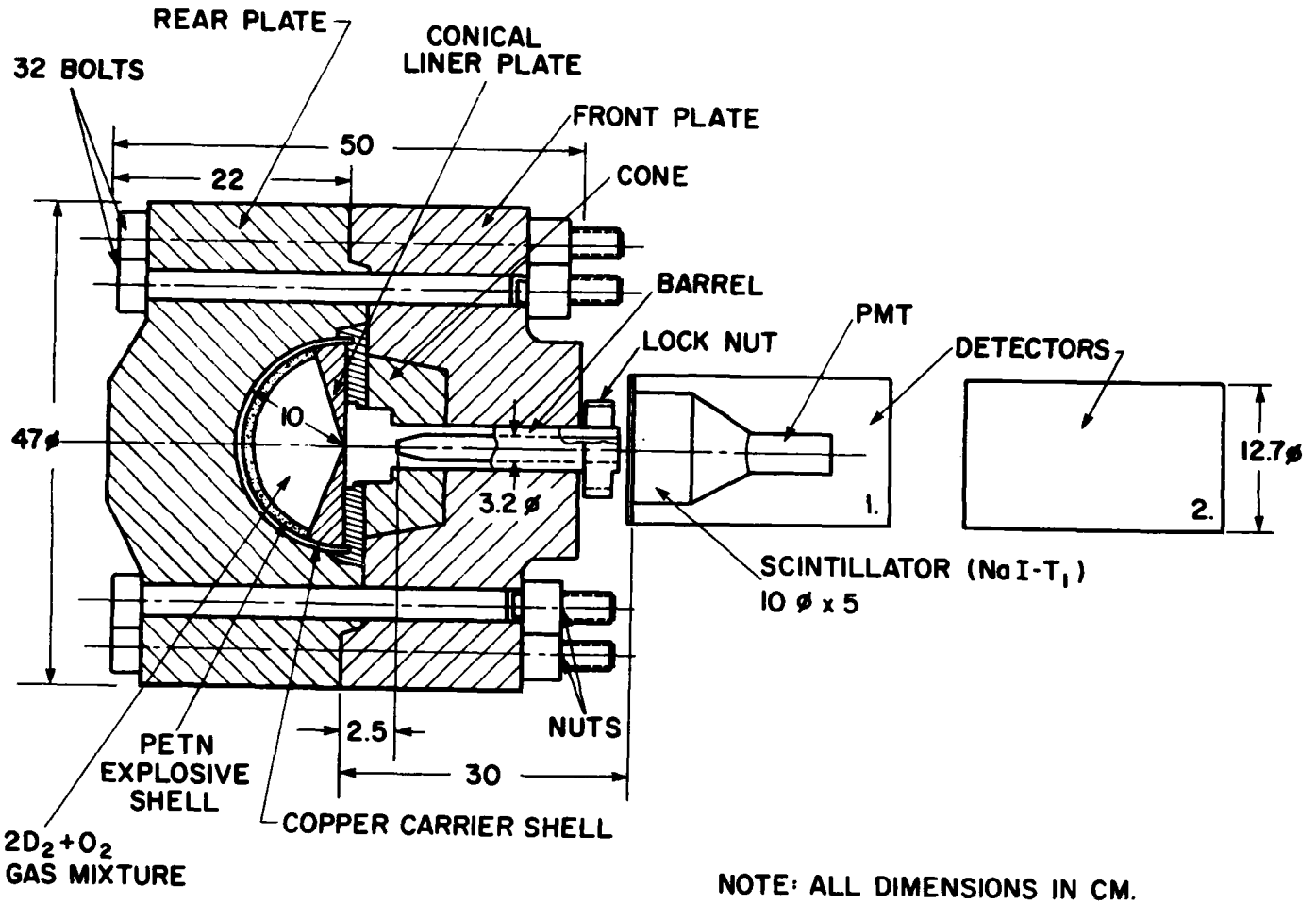

UTIAS IMPLOSION CHAMBER FACILITY AND SCINTILLATOR DETECTORS

FIG. 35 NEUTRON AND γ-RAY SCINTILLATOR SIGNALS FROM D-D REACTIONS AT AN IMPLOSION FOCUS.

(i) Schematic diagram of experimental setup.

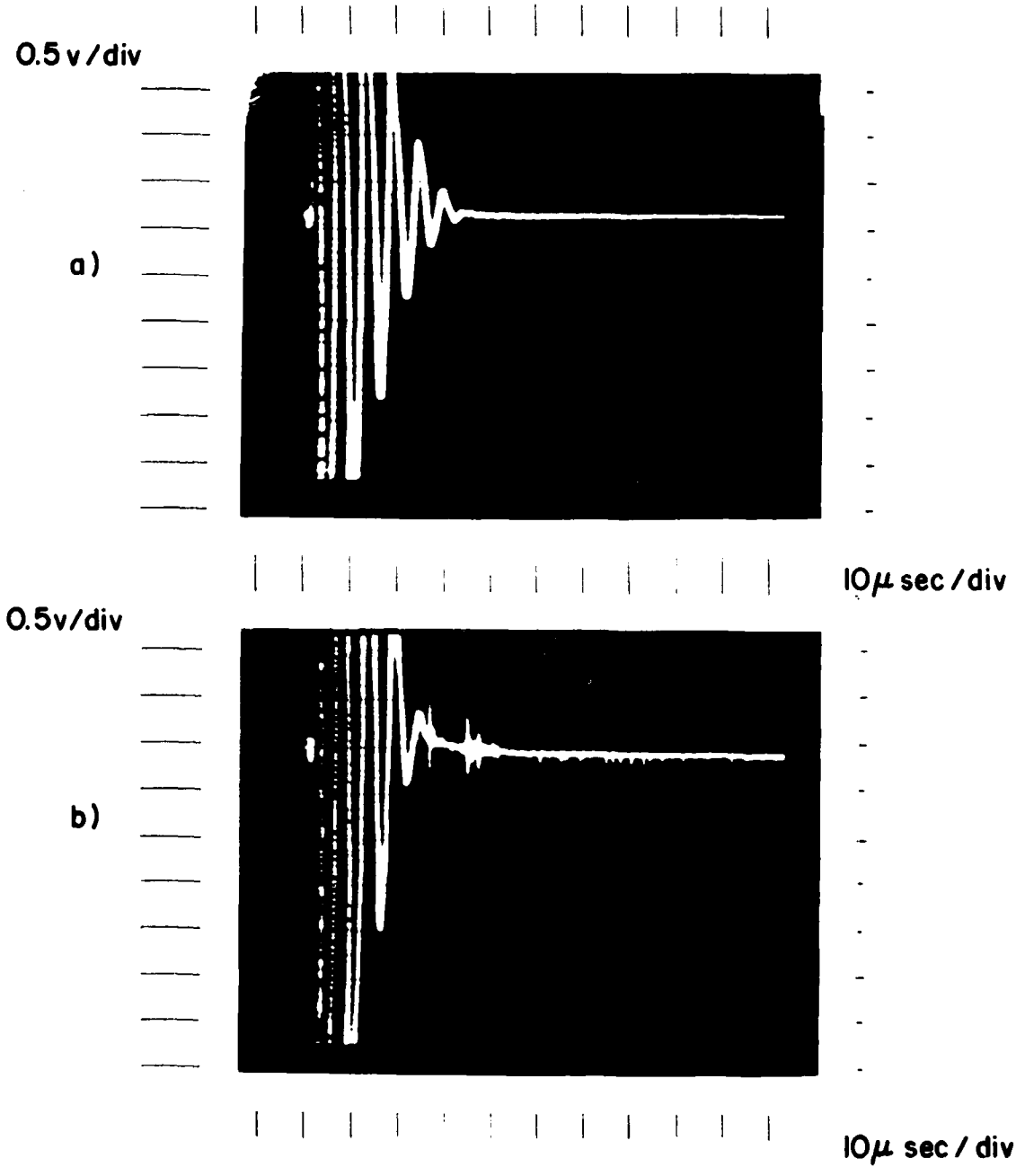

DISPLAY OF DETECTOR I, WITHOUT a) AND WITH FUSION b)

(ii) Voltage vs time record showing the oscillations produced by the exploding wire discharge, and the individual events from neutron or γ-ray encounters with the scintillator as a result of the neutron interactions with the steel implosion chamber.

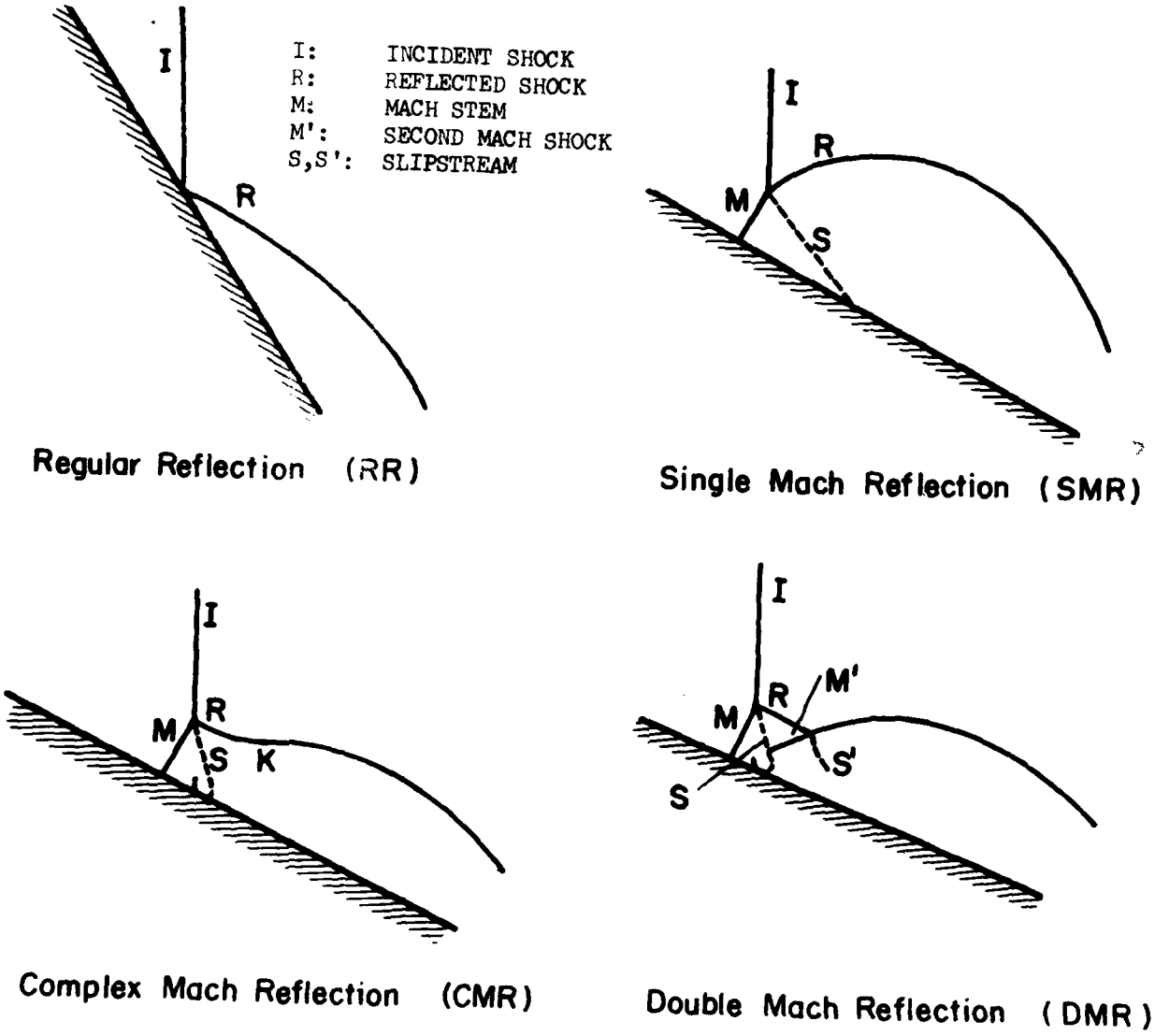

FIG. 36 INFINITE-FRINGE INTERFEROGRAMS OF THE FOUR TYPES OF NONSTATIONARY OBLIQUE-SHOCK-WAVE REFLECTIONS IN CARBON DIOXIDE AND EXPLANATORY SKETCH.

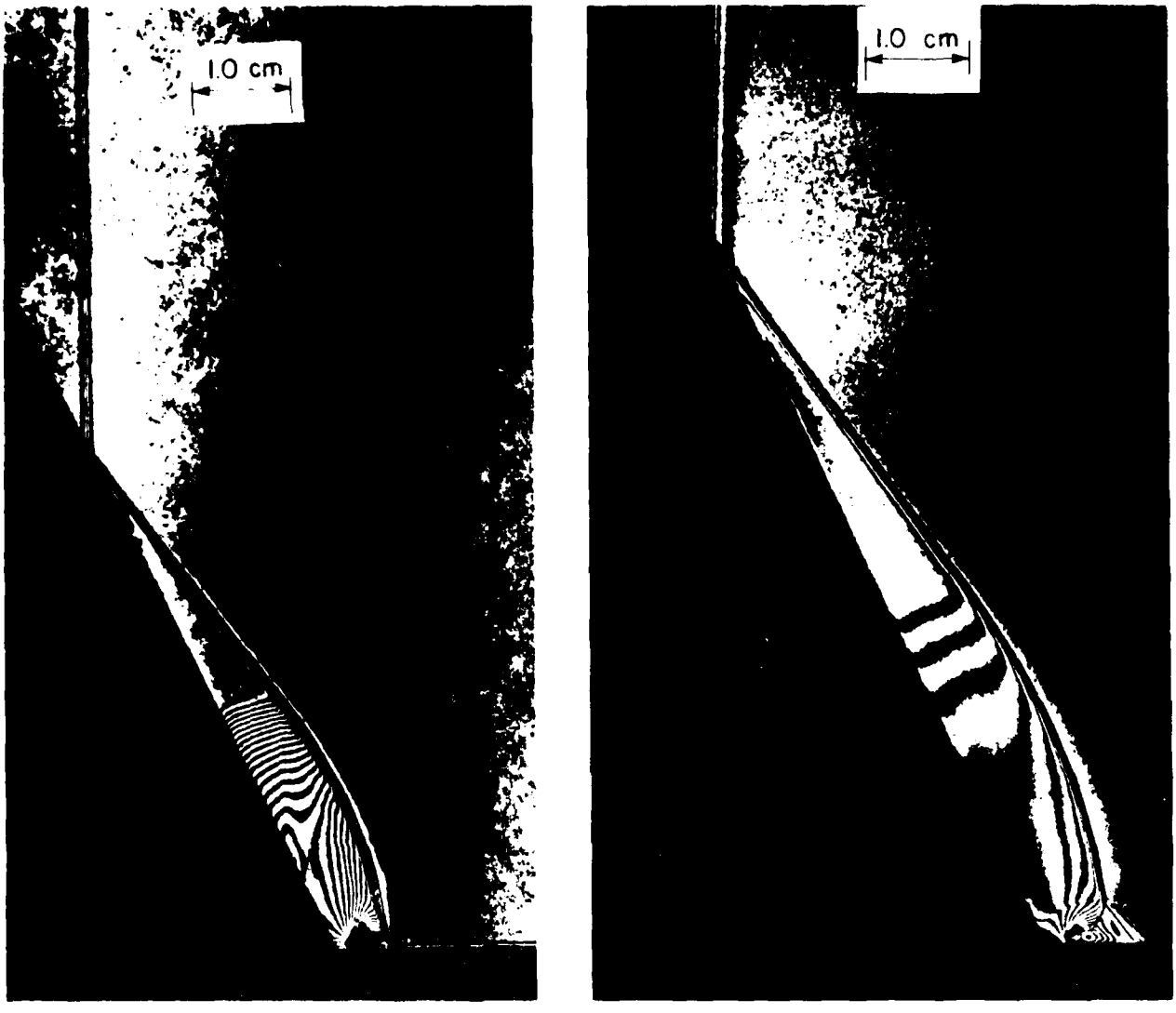

FIG. 36

(1) Regular reflection (RR); the effects of a decreased pressure on the isopycnic distribution and vibrational relaxation lengths (ℓ_v) are noted in (a) and (b).

(a) M_s = 2.4, θ_w = 63.4°, P_o = 200 torr, T_o = 298.4°K, ℓ_v = 0.5 mm, λ = 6943Å.

(b) M_s = 2.4, θ_w = 63.4°, P_o = 40 torr, T_o = 298.7°K, ℓ_v = 2.6 mm, λ = 6943Å.

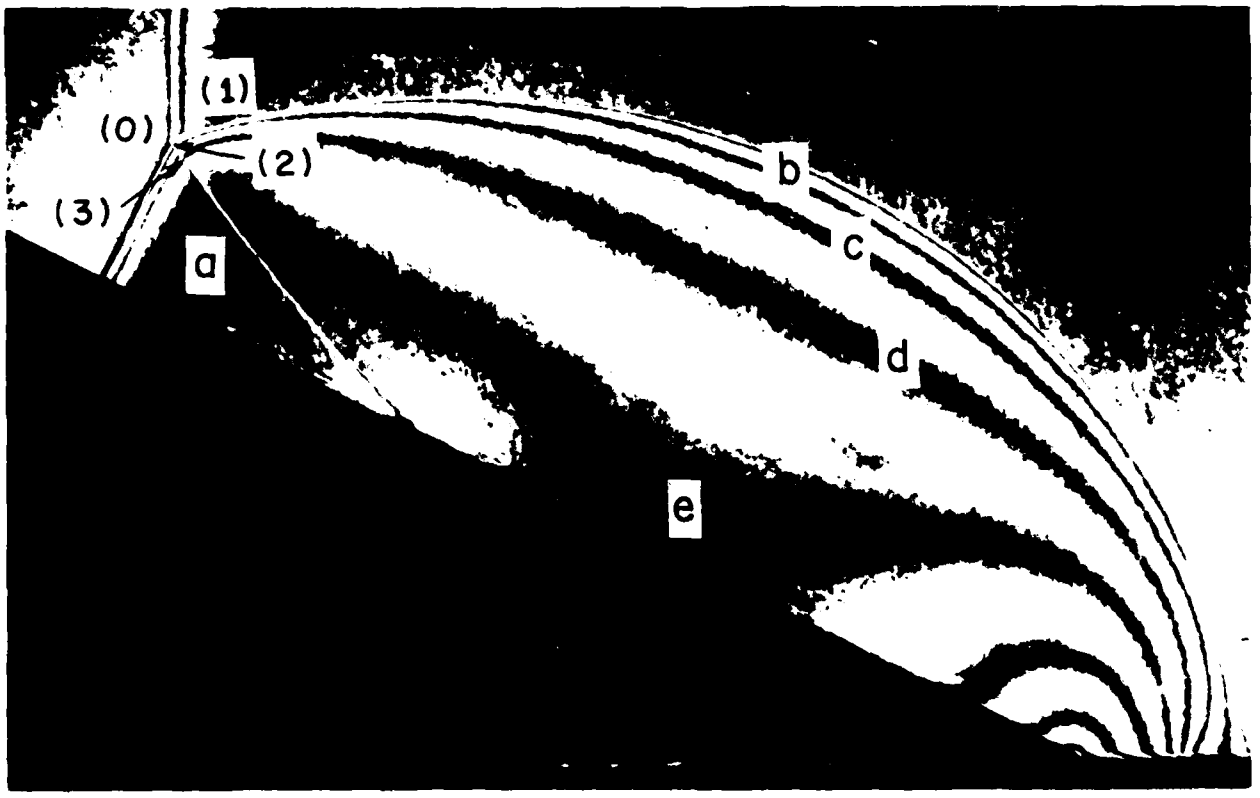

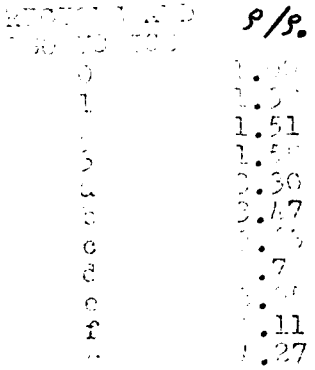

(11) Single Mach reflection (SMR); the three-wave elements (incident I, reflected R, and Mach M, shocks) and the slipstream S, are well illustrated.
M_S = 1.78, θ_w = 27°, P_0 = 80 torr, T_0 = 298.4K, λ = 6943Å.

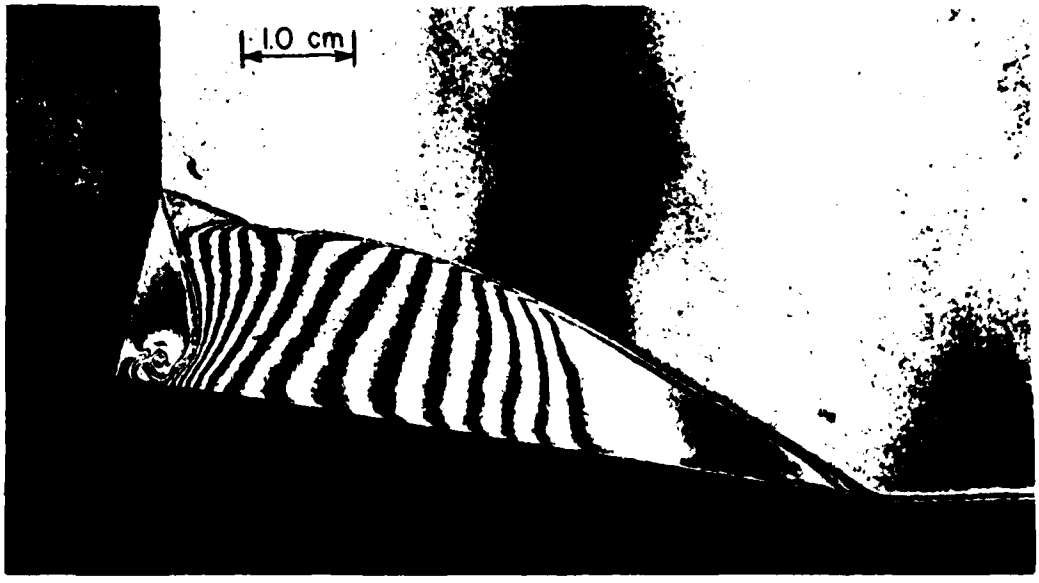

(a)

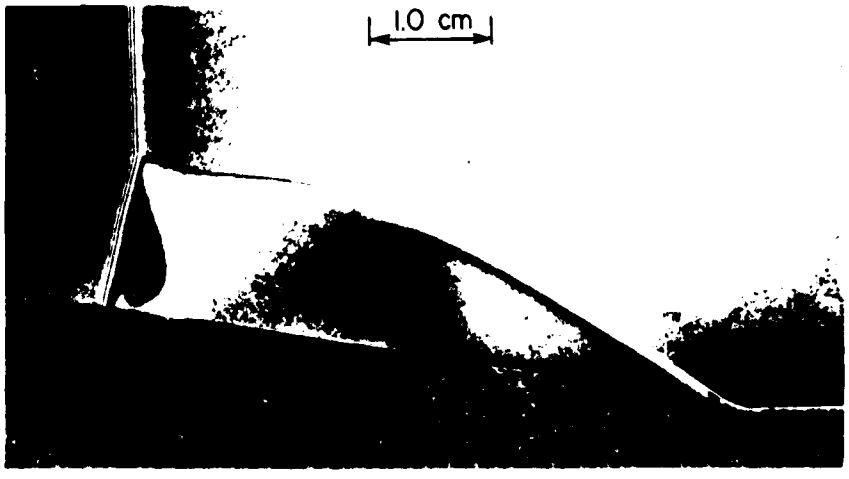

(b)

(iii) Complex Mach reflection (CMR) - perhaps transitional (TMR) would be a better term, as there is nothing complex about this reflection, since it occurs between single and double Mach reflection; the influence of initial pressure on the number of isopycnics and the resulting vibrational relaxation lengths (ℓ_v) are shown in (a) and (b)

(a) $M_s = 6.0$, $\theta_w = 10.1°$, $P_o = 45$ torr, $T_o = 297.9$ K, $\ell_v = 0.2$ mm.

(b) $M_s = 6.0$, $\theta_w = 10.1°$, $P_o = 5$ torr, $T_o = 299.1°$K, $\ell_v = 2.1$ mm.

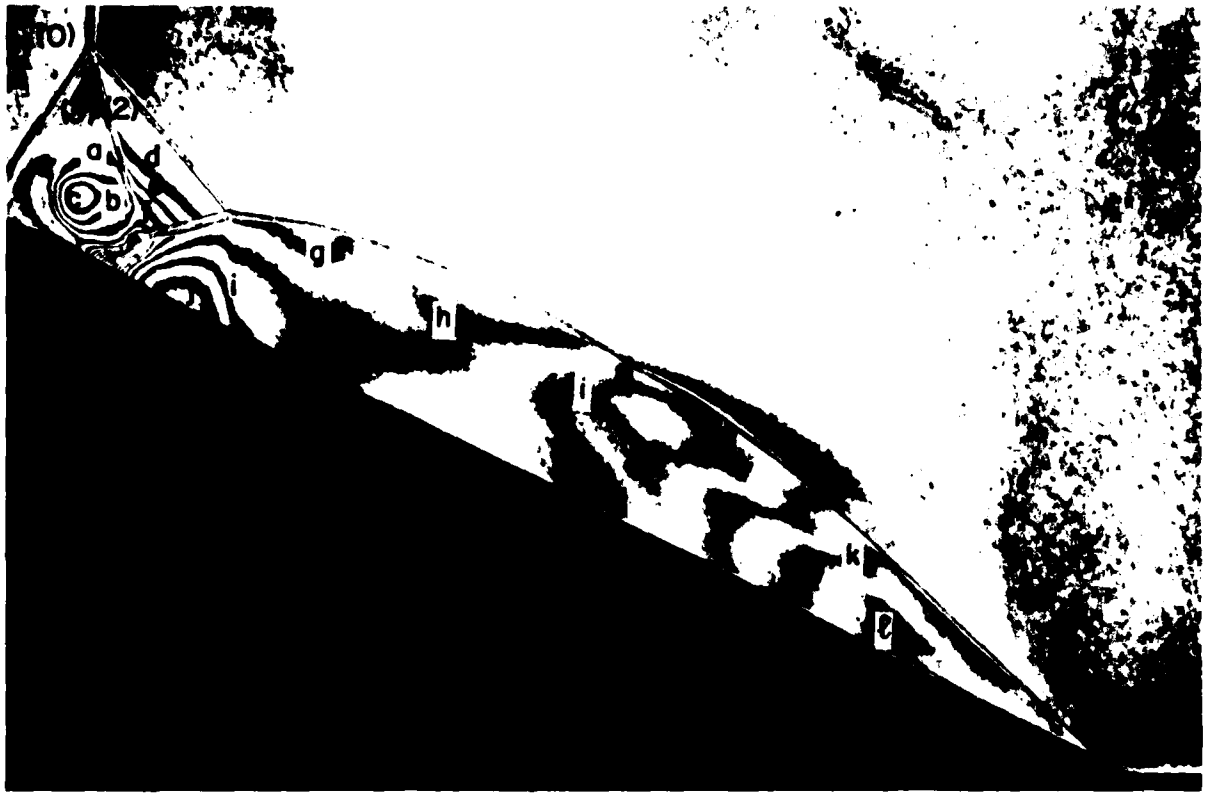

	ρ/ρ_0
0	1.00
1	2.15
2	[illegible]
3	[illegible]
4	[illegible]
b	[illegible]
c	11.1
d	10.3
e	[illegible]
f	[illegible]
[illegible]	23.6
[illegible]	[illegible]
[illegible]	25.1
j	[illegible]
[illegible]	[illegible]
l	29.9

(iv) A double Mach reflection shows the new Mach shock M' and its interaction with the slipstream and the wall. The new slipstream S' is very weak in this case but can be noted in isopycnic sharp changes near the new triple point T'.
M_S = 8.16, θ_W = 27°, P_0 = 10.2, T_0 = 299.1K, λ = 6943Å.

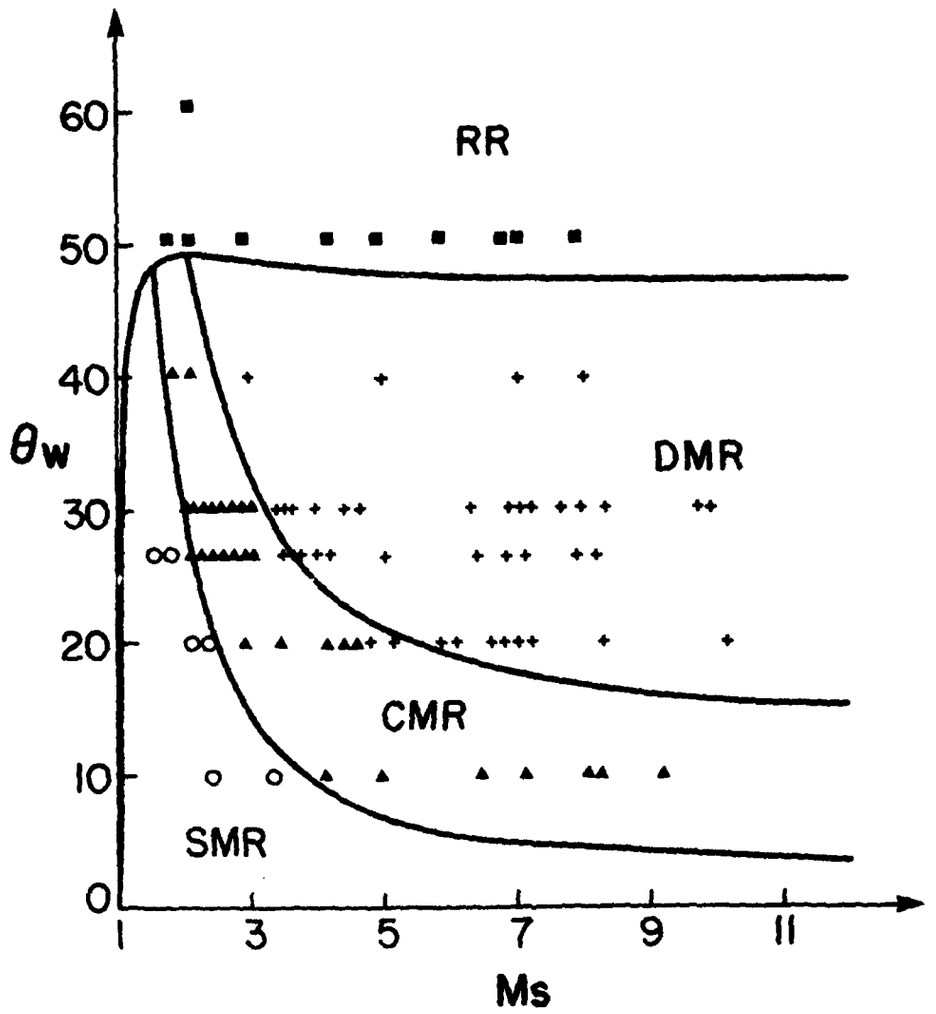

FIG. 37 *COMPARISON OF PREDICTED REGIONS OF PSEUDOSTATIONARY OBLIQUE-SHOCK-WAVE REFLECTIONS AND EXPERIMENTAL RESULTS FOR PERFECT* CO_2, $\gamma = 1.290$.

Types of reflection: ■ = RR; o = SMR; ▲ = CMR; + = DMR.

FIG. 38 COMPLEX-MACH REFLECTION IN AIR SHOWING OXYGEN DISSOCIATION.

The dissociation behind the incident shock wave and Mach stem are clearly shown by crowded isopycnics at the shock front. A reasonable indication of the dissociational relaxation length ℓ_d, can be obtained by measuring the true distance between the front of the shock to the end of the last (5th) fringe.
$M_S = 10.0$, $\omega = 10°$, $P_o = 15$ torr, $T_o = 23.4°C$, $\lambda = 3471.5\text{Å}$, $\ell_d = 2.2$ mm.

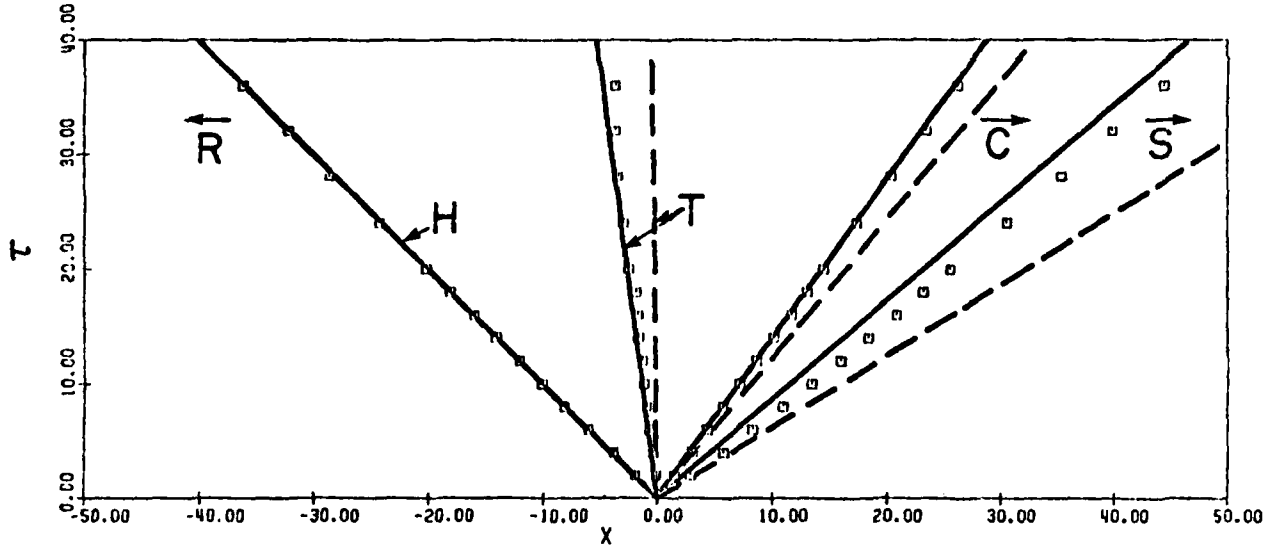

FIG. 39 FLOW IN A DUSTY-GAS SHOCK TUBE.

(i) Wave diagram of time-distance plane after diaphragm rupture [$X = x/\ell$, $\tau = t/(\ell/a_{1f})$]. □ present results, ——— equilibrium flow, ------ frozen flow. R = rarefaction wave, H = head, T = tail, C = contact surface, S = shock front. The dashed lines show the classical shock tube problem in the (x,t)-plane for a diaphragm pressure ratio of 10. The solid lines show the final equilibrium values for a dust particle density of 2.5 g/cm^3 (typical of crown glass) and an air density of 1.23 x 10^{-3} g/cm^3 and the gas sound (frozen) speed a_{1f} = 350 m/sec, for the gas plus particle equilibrium sound speed a_{1e} = 229 m/sec. For 10 μm particles, the reference length ℓ = 2.72 cm; the mass concentration α = 1 and the particle number density $n_p = 0.94 \times 10^6$. The square points show the numerical results from the random-choice method of how the initially frozen gas shock wave approaches equilibrium in the dusty gas.

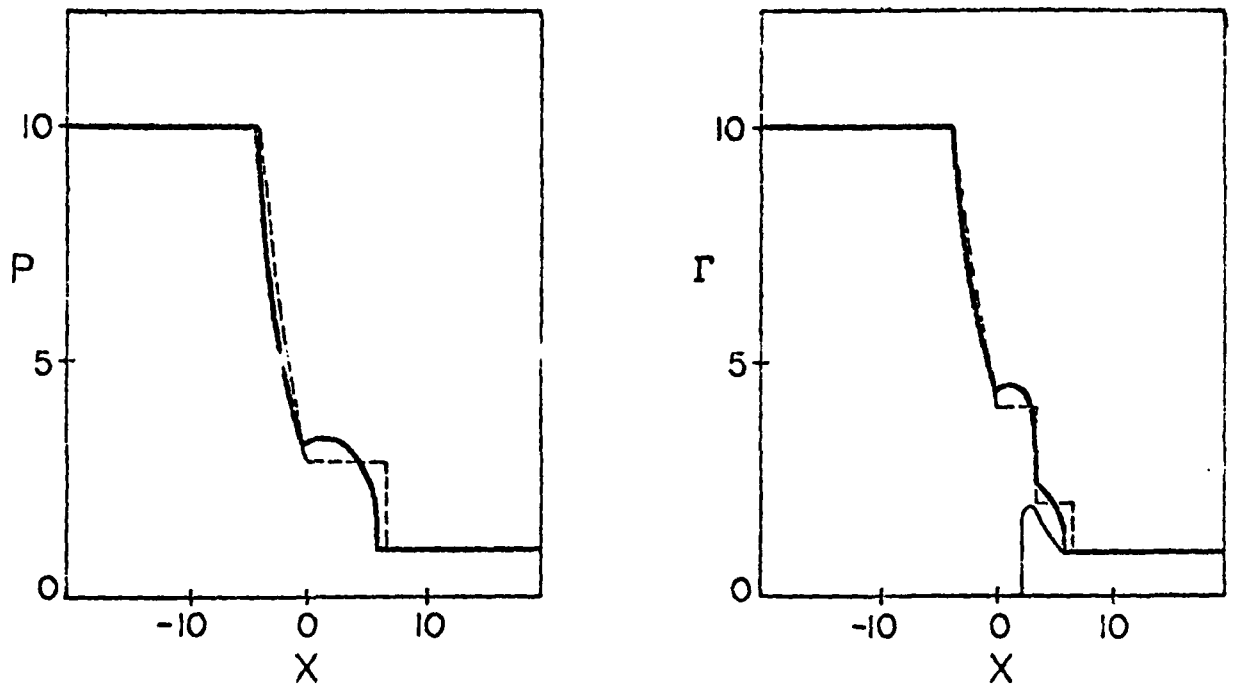

FIG. 39 - CONTINUED.

(ii) Flow quantities at $t = 3.1 \times 10^{-4}$ sec. ——— gas, ——— particles, ------ frozen flow. $P = p/p_1$, $\Gamma = \rho/\rho_1$ or σ/σ_1, $X = x/\ell$, $T = T/T_1$ or Θ/T_1, $U = u/a_{1_f}$ or v/a_{1_f}. The nonequilibrium transitions through the shock wave and contact front show the pressure, mass concentration, gas and particle velocities and temperatures. It is seen that the shock transition consists of a frozen viscous shock followed by an approach to equilibrium for the given time (3.1×10^{-4} sec). The pressure and the density at equilibrium are greater than for the classical case, owing to the drag by and heat transfer to the particles. The dust concentration reaches a maximum in the contact front and then drops abruptly shortly after, even though the gas temperature in the rear of the contact front still continues to drop below that of the particles. At this short time the gas and particles are still not in equilibrium although they become so later. Both temperatures are, of course, lower than the classical gas temperature. The same remarks apply to the particle velocities.

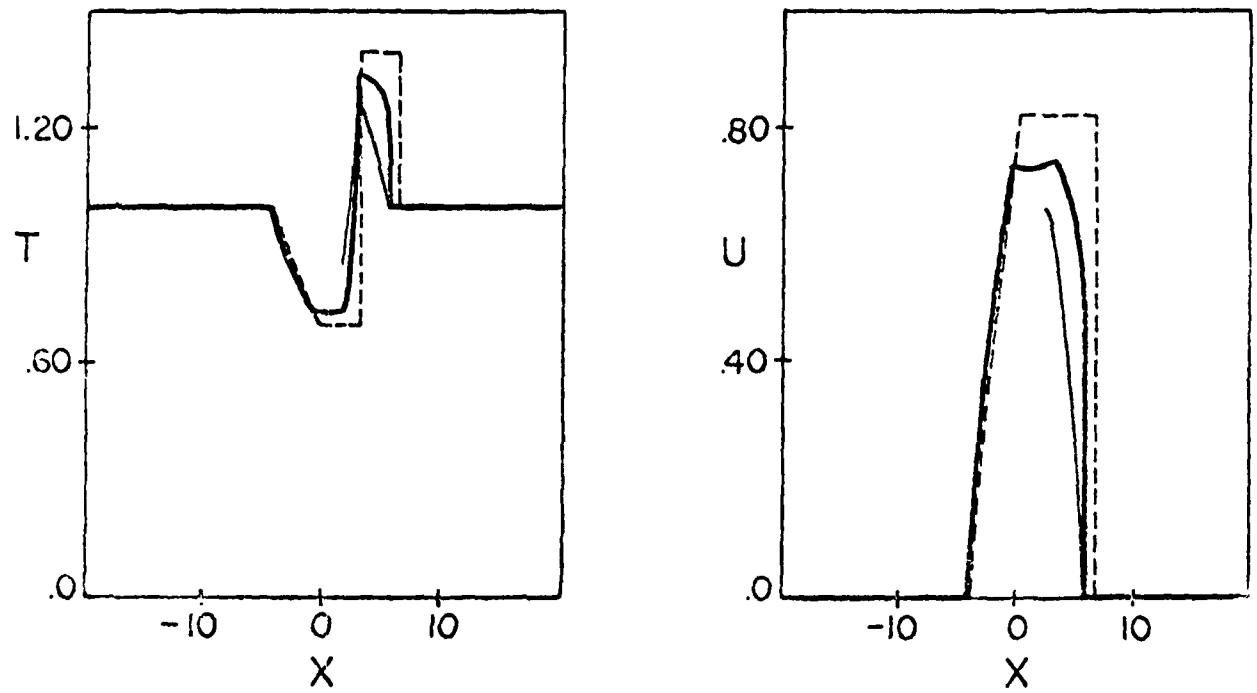

FIG. 39 - CONCLUDED.

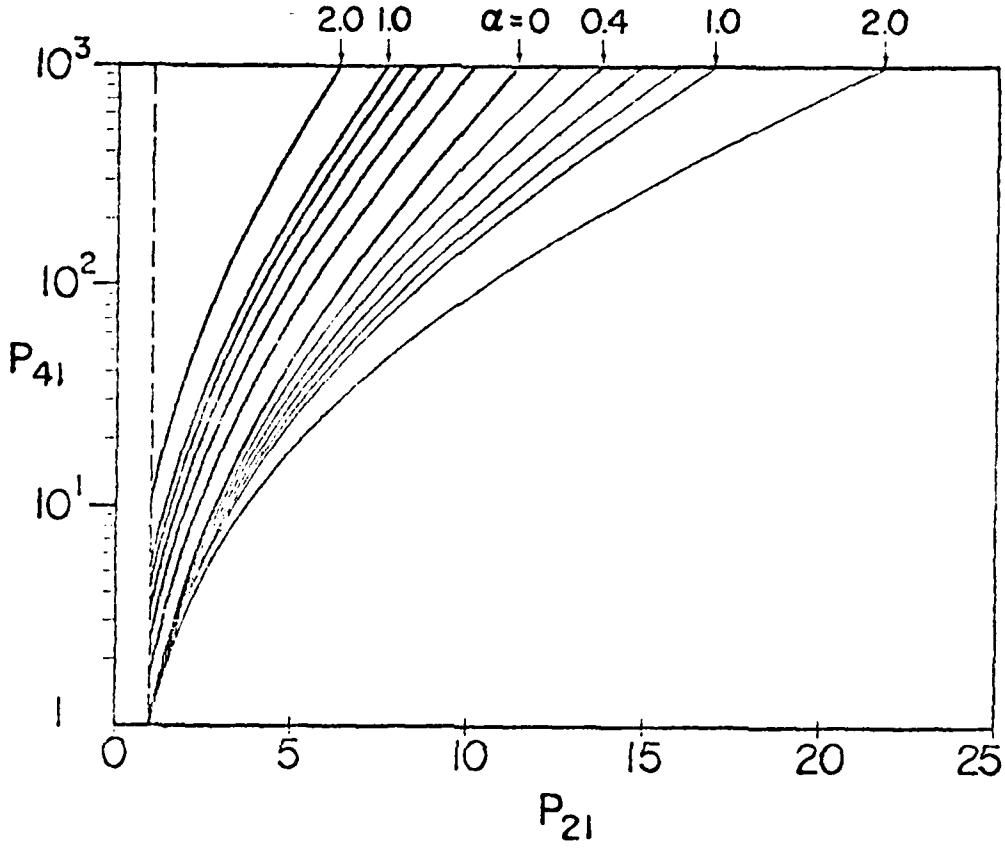

(a)

FIG. 40 VARIATIONS OF THE FROZEN AND EQUILIBRIUM SHOCK-WAVE PRESSURE RATIO P_{21} AND SHOCK-WAVE MACH NUMBER M_s, WITH THE SHOCK-TUBE DIAPHRAGM PRESSURE RATIO P_{41}, AND PARTICLE CONCENTRATION α.

The above appear in (a) and (b), respectively. The dashed lines at $P_{21} = 1$ and $M_s = 1$ show the regions of fully-dispersed shock waves, that is, the frozen front has vanished and only a transition to equilibrium is possible. The case $\alpha = 0$ is for the classical shock-tube problem; the particle number density n_p increases linearly with α. Note that a larger diaphragm pressure ratio P_{41} is required in order to produce the same shock Mach number M_s, as the dust concentration α increases, as expected.

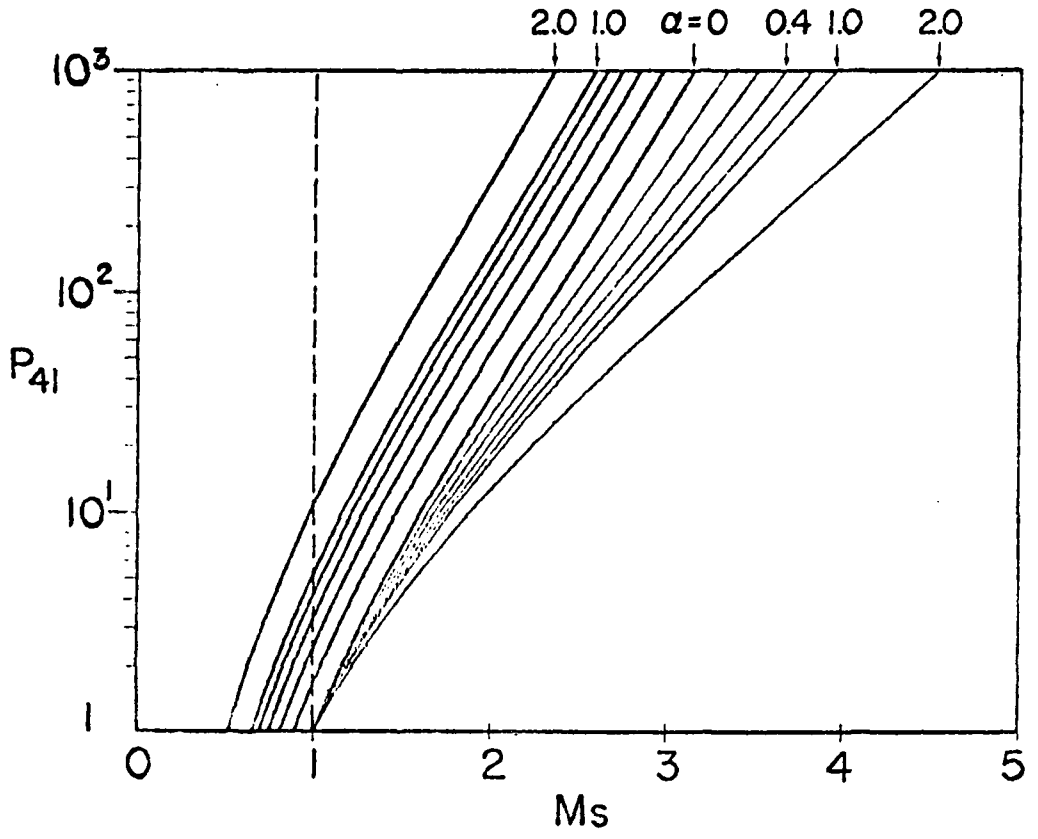

FIG. 40(b)

UTIAS Review No. 45

Institute for Aerospace Studies, University of Toronto (UTIAS)
4925 Dufferin Street, Downsview, Ontario, Canada, M3H 5T6

BEYOND THREE DECADES OF CONTINUOUS RESEARCH AT UTIAS ON SHOCK TUBES AND WAVES

Glass, I. I. Approx. 65 pages 40 figures

1. Shock tubes
2. Shock-wave dynamics
3. Implosion dynamics
4. Hypervelocity launchers
5. Rarefaction waves
6. Condensation and nucleation
7. Wave interactions
8. Ionizing shock-wave structure and boundary layers
9. Sonic-boom effects
10. Oblique-shock-wave reflections
11. Shock waves in dusty gases
12. Thermonuclear fusion
13. Numerical methods
14. Optical techniques

I. Glass, I. I. II. UTIAS Review No. 45

Analytical and experimental research on nonstationary shock waves, rarefaction waves and contact surfaces has been conducted continuously at UTIAS since its inception in 1948. Some unique facilities were used to study the properties of planar, cylindrical and spherical shock waves and their interactions. Investigations were also performed on shock-wave structure and boundary layers in ionizing argon, water-vapour condensation in rarefaction waves, magnetogasdynamic flows, and the regions of regular and various types of Mach reflections of oblique shock waves. Explosively-driven implosions have been employed as drivers for projectile launchers and shock tubes, and as a means of producing industrial-type diamonds from graphite, and fusion plasmas in deuterium. The effects of sonic-boom on humans, animals and structures has also formed an important part of the investigations. More recently, interest has focussed on shock waves in dusty gases, the viscous and vibrational structure of weak spherical blast waves in air, and oblique shock-wave reflections. In all of these studies instrumentation and computational methods have played a very important role. A brief survey of this work is given with some perspectives on future research.

Available copies of this report are limited. Return this card to UTIAS, if you require a copy.

UTIAS Review No. 45

Institute for Aerospace Studies, University of Toronto (UTIAS)
4925 Dufferin Street, Downsview, Ontario, Canada, M3H 5T6

BEYOND THREE DECADES OF CONTINUOUS RESEARCH AT UTIAS ON SHOCK TUBES AND WAVES

Glass, I. I. Approx. 65 pages 40 figures

1. Shock tubes
2. Shock-wave dynamics
3. Implosion dynamics
4. Hypervelocity launchers
5. Rarefaction waves
6. Condensation and nucleation
7. Wave interactions
8. Ionizing shock-wave structure and boundary layers
9. Sonic-boom effects
10. Oblique-shock-wave reflections
11. Shock waves in dusty gases
12. Thermonuclear fusion
13. Numerical methods
14. Optical techniques

I. Glass, I. I. II. UTIAS Review No. 45

Analytical and experimental research on nonstationary shock waves, rarefaction waves and contact surfaces has been conducted continuously at UTIAS since its inception in 1948. Some unique facilities were used to study the properties of planar, cylindrical and spherical shock waves and their interactions. Investigations were also performed on shock-wave structure and boundary layers in ionizing argon, water-vapour condensation in rarefaction waves, magnetogasdynamic flows, and the regions of regular and various types of Mach reflections of oblique shock waves. Explosively-driven implosions have been employed as drivers for projectile launchers and shock tubes, and as a means of producing industrial-type diamonds from graphite, and fusion plasmas in deuterium. The effects of sonic-boom on humans, animals and structures has also formed an important part of the investigations. More recently, interest has focussed on shock waves in dusty gases, the viscous and vibrational structure of weak spherical blast waves in air, and oblique shock-wave reflections. In all of these studies instrumentation and computational methods have played a very important role. A brief survey of this work is given with some perspectives on future research.

Available copies of this report are limited. Return this card to UTIAS, if you require a copy.

UTIAS Review No. 45

Institute for Aerospace Studies, University of Toronto (UTIAS)
4925 Dufferin Street, Downsview, Ontario, Canada, M3H 5T6

BEYOND THREE DECADES OF CONTINUOUS RESEARCH AT UTIAS ON SHOCK TUBES AND WAVES

Glass, I. I. Approx. 65 pages 40 figures

1. Shock tubes
2. Shock-wave dynamics
3. Implosion dynamics
4. Hypervelocity launchers
5. Rarefaction waves
6. Condensation and nucleation
7. Wave interactions
8. Ionizing shock-wave structure and boundary layers
9. Sonic-boom effects
10. Oblique-shock-wave reflections
11. Shock waves in dusty gases
12. Thermonuclear fusion
13. Numerical methods
14. Optical techniques

I. Glass, I. I. II. UTIAS Review No. 45

Analytical and experimental research on nonstationary shock waves, rarefaction waves and contact surfaces has been conducted continuously at UTIAS since its inception in 1948. Some unique facilities were used to study the properties of planar, cylindrical and spherical shock waves and their interactions. Investigations were also performed on shock-wave structure and boundary layers in ionizing argon, water-vapour condensation in rarefaction waves, magnetogasdynamic flows, and the regions of regular and various types of Mach reflections of oblique shock waves. Explosively-driven implosions have been employed as drivers for projectile launchers and shock tubes, and as a means of producing industrial-type diamonds from graphite, and fusion plasmas in deuterium. The effects of sonic-boom on humans, animals and structures has also formed an important part of the investigations. More recently, interest has focussed on shock waves in dusty gases, the viscous and vibrational structure of weak spherical blast waves in air, and oblique shock-wave reflections. In all of these studies instrumentation and computational methods have played a very important role. A brief survey of this work is given with some perspectives on future research.

Available copies of this report are limited. Return this card to UTIAS, if you require a copy.

UTIAS Review No. 45

Institute for Aerospace Studies, University of Toronto (UTIAS)
4925 Dufferin Street, Downsview, Ontario, Canada, M3H 5T6

BEYOND THREE DECADES OF CONTINUOUS RESEARCH AT UTIAS ON SHOCK TUBES AND WAVES

Glass, I. I. Approx. 65 pages 40 figures

1. Shock tubes
2. Shock-wave dynamics
3. Implosion dynamics
4. Hypervelocity launchers
5. Rarefaction waves
6. Condensation and nucleation
7. Wave interactions
8. Ionizing shock-wave structure and boundary layers
9. Sonic-boom effects
10. Oblique-shock-wave reflections
11. Shock waves in dusty gases
12. Thermonuclear fusion
13. Numerical methods
14. Optical techniques

I. Glass, I. I. II. UTIAS Review No. 45

Analytical and experimental research on nonstationary shock waves, rarefaction waves and contact surfaces has been conducted continuously at UTIAS since its inception in 1948. Some unique facilities were used to study the properties of planar, cylindrical and spherical shock waves and their interactions. Investigations were also performed on shock-wave structure and boundary layers in ionizing argon, water-vapour condensation in rarefaction waves, magnetogasdynamic flows, and the regions of regular and various types of Mach reflections of oblique shock waves. Explosively-driven implosions have been employed as drivers for projectile launchers and shock tubes, and as a means of producing industrial-type diamonds from graphite, and fusion plasmas in deuterium. The effects of sonic-boom on humans, animals and structures has also formed an important part of the investigations. More recently, interest has focussed on shock waves in dusty gases, the viscous and vibrational structure of weak spherical blast waves in air, and oblique shock-wave reflections. In all of these studies instrumentation and computational methods have played a very important role. A brief survey of this work is given with some perspectives on future research.

Available copies of this report are limited. Return this card to UTIAS, if you require a copy.

END

DATE
FILMED

1-82

DTIC